Republic of Iraq
Ministry of Higher Education
and Scientific Research
Al-Nahrain University
College of Science
Department of Chemistry

Photobleaching of dye pollutants onto immobilized TiO_2 anatase nanocatalyst

A Thesis

Submitted to the college of science/Al-Nahrain University as partial fulfillment of the requirements for the Degree of Master of Science in Chemistry

By

Israa Nihad Esmaeel

B.Sc. chemistry / college of science / University of Al-Nahrain

Supervised by

Prof. Dr. Hilal S. Wahab

April 2016 Rajab 1473

بسم الله الرحمن الرحيم

نَرفَعُ دَرَجاتٍ مَن نَشاءُ وَفَوقَ كُلِّ ذي عِلمٍ

عَليمٌ ﴿٧٦﴾

صدق الله العظيم

سورة يوسف

اهداء

إلى من سعى وشقى لأنعم بالراحة والهناء الذي لم يبخل بشئ من أجل دفعي في طريق النجاح الذي علمني أن أرتقي سلم الحياة بحكمة وصبر

والدي الغالي

الى من نذرت عمرها في أداء رسالة صنعتها من أوراق الصبر وطرزتها في ظلام الدهر على سراج الأمل بلا فتور أو كلل

والدتي الحبيبة

الى من يحملون في عيونهم ذكريات طفولتي وشبابي الى القلوب الطاهرة والنفوس البريئة

اخواتي

الى الاخت التي لم تلدها امي الى صديقتي

الاء رزاق

ACKNOWLEDGEMENT

Above all else, I want to express my great thanks to Allah for his uncountable gifts and for helping me to present this thesis.

Special thanks are extended to my supervisor ***professor Dr. Hilal S. Wahab*** *for his considerable effort, great help and continuous scientific directing along this study.*

Special thanks to my parents and sisters for their full support, encouragement and patience that gave me the power all my life.

I am very grateful to ***staff*** *of department of chemistry, Al-Nahrain University, college of science for supporting and helping in this study.*

*My thanks and appreciation to my friends especially (****Ahmed A. Hussain, Hussain M. Hadi, Alaa R. Shaker****,* ***Alaa Adnan****).*

Table of Contents

List of Figures

List of Images

List of Tables

List of Abbreviations

SEM	Scanning Electron Microscopy
EDXS	Energy Dispersive X-Ray Spectroscopy
XRD	X-Ray Diffraction
TEM	Transmission Electron Microscopy
BET	Brunauer-Emmett-Teller
UV-VIS	Ultra Violet-Visible Spectrophotometer
$\mathbf{k_{app}}$	Apparent rate constant
AOP	Advanced Oxidation Process
EBT	Eriochrom Black T
MV	Methyl Violet
Eg	Band gap energy
HOMO	Highest Occupied Molecular Orbital
LUMO	Lowest Unoccupied Molecular Orbital
$\mathbf{Q_e}$	Adsorption capacity
$\mathbf{C_o}$	Initial concentration of solute
$\mathbf{C_e}$	Concentration of solute at equilibrium
$\mathbf{K_p}$	Thermodynamic equilibrium constant
$\mathbf{k_1}$	rate constant of the first-order model
pzc	Point of Zero Charge
$\mathbf{K_{ad}}$	Adsorption equilibrium coefficient
NFDW	Nano Filtered Deionized Water
$\mathbf{k_2}$	rate constant of the second-order model.
$\mathbf{Q_{max}}$	maximum adsorption capacity
$\mathbf{K_l}$	Langmuir constant
$\mathbf{K_f}$	Freundlich constant
n	Adsorption intensity
SCE	Saturated Calomel Electrode

C.B.	Conduction Band
V.B.	Valance Band
$\mathbf{h^+}$	hole
$\mathbf{e^-}$	electron

Abstract

In this research study, the photobleaching (photocatalytic degradation) of two dyes namely; Eriochrom Black T (EBT) as anionic dye and Methyl Violet (MV) as cationic dye have been investigated using laboratory synthesized anatase TiO_2 nanoparticle in aqueous solution. The nano TiO_2 photocatalysts has been characterized using several analytical instruments including; Scanning Electron Microscopy (SEM), Energy Dispersive X-Ray Spectroscopy (EDXS), X-Ray Diffraction (XRD), UV-VIS spectrometry (UV-VIS), Transmission Electron Microscopy (TEM), and Brunauer–Emmett–Teller (BET) methodology for specific surface area and porosity measurements. The impacts of several operational parameters of slurry photocatalysis, based on in situ sensitization (self sensitization) concept for the nano photocatalyst under visible light illumination have been investigated including, TiO_2 loading, solution pH, initial dye concentration and visible light intensity. At optimum experimental conditions for EBT including pH = 3, 80 mg/l TiO_2 loading, and 1.3 x 10^{-4} mol/l (60 mg/l) for EBT, the value of the apparent rate constant, k_{app}, obtained was 0.099 min^{-1} and the half life of the process, accordingly is equal to 7 min. Whereas, for MV dye implying pH = 7, 30 mg/l TiO_2 loading, and 1.016 x 10^{-5} mol/l (4 mg/l) for MV, the value of the apparent rate constant, k_{app} , obtained has been 0.077 min^{-1} and the half life of the process, accordingly is equal to 9 min. Kinetic studies for the photobleaching of EBT and MV revealed that the process follows the pseudo first order pattern regardless of reaction conditions. The main process thermodynamic parameters namely, Gibbs energy, enthalpy and entropy were also deduced following the computation of photocatalysis activation energy employing the well known Arrhenius relation. Also, many routes for the immobilization of

nano TiO_2 onto stainless steel plates like swirling, rotating and dipping have been investigated to be employed and optimized experimentally for best photodegradation of model pollutants. The photocatalytic decomposition rate increases with the number of loaded layers of TiO_2 up to five repetitions. Rotational coating of 5 layers (R_5) concluded to be the most stable recipe of immobilization of TiO_2 on st. st. slide and potentially most photocatalytically active. Accordingly, R_5 recipe was applied on st. st. plate in escalated procedure in the prototype assembly to be illuminated by means of solar energy which has shown better degradation rates.

CHAPTER ONE

INTRODUCTION

AND

LITERATURE REVIEW

1. Introduction

1.1 Advanced oxidation techniques for water treatment

Textile wastewater contains a great assortment of pigmentations and chemicals additions such as pharmaceutical yields, industrial chemicals and different organic compounds that are steady to light, oxidizing agent, and are reluctant to aerobic digestion that constrain a threat to the ambience which make the ecological defiance for textile industry not only as liquid waste but also in its chemical composition [1]. About 12% of synthetic textile dyes namely: Caramine, indigo red, Red 120, rhodamine B, methylene blue, Eriochrome Black-T (EBT)...etc. are applied every year [2]. Abstraction of dyes from the industrial effluents is a prime ecological concern because most of these dyes are carcinogenic, mutagenic, and teratogenic to humans and other organisms. That's why the removal of dyes from water and wastewater before blending with natural water resources is very important [3]. Traditional procedures to clear these pollutants include physical, chemical, and biological processes. Nevertheless, the individual implementation of these mechanics is mostly calibrated and can't degrade completely the organic matter [4]. The traditional procedures like separation, centrifugation,, filtration, and adsorption with activated coal…etc which are employed for water treatment stipulate certain operational conditions like removal of solids and emulsioned oil from the wastewater pretreatment [5]. Further, these techniques may not be very efficient, because they are either slow or non-destructive to some or most everlasting organic pollutants. Therefore it is fundamental to research the employment of efficient catalytic substances to abstract very toxic compounds from potential origins of drinking water. Semiconductor heterogeneous photocatalysis is a widespread technique that has the great potential to dominate the

organic contaminants in water or air [4,6]. This technique also known as "Advanced Oxidation Process (AOP)" or Advanced Oxidation Technique (AOT) which is a set of mechanisms that normally involve a strong oxidizing species such as •OH radicals produced *in situ*, which brings about a series of reactions subsequently to break down the macromolecule into smaller and less hurtful materials. In many situations the macromolecule is totally broken down to water and carbon dioxide [7]. The behavior of chemicals is safely altered after the treatment. The declination makes organic chemicals smaller and biodegradable [8]. In modern years hydrogen peroxide, ozone and /or Fenton reagents, with a source of UV light have been recorded to be helpful for the photo-oxidation of organic pollutants in waste waters [9]. These techniques are distributed under the definition of AOTs, Which are tabulated in table (1-1).

Table (1-1): List of examples of methods classified as AOTs systems [9]

Dark AOT	Light driven AOT
Ozone (O_3) Fenton(Fe^{+2} +H_2O_2) Electrolysis (electrodes + current) Sonolysis (Ultrasounds)	photolysis (UV +H_2O_2) photocatalysis (light +catalyst) photo-fenton (solar light +fenton)

These techniques (AOTs) abstract essential quantity of Chemical Oxygen Demand (COD) and Total Organic Carbon (TOC) from industrial effluents [9]. Only these oxidation techniques results in degradation of organics and more often turn in to H_2O and CO_2 [10,11].

The oxidation potential values of different oxidants are listed in Table (1-2) which shows that the $^{\bullet}OH$ radicals are extremely powerful oxidants [11].

Table (1-2): Standard electrochemical reduction potentials of common oxidants [11].

Oxidant	Half-cell reaction oxidation	Potential (V)
$^{\bullet}OH$ (hydroxyl radical)	$^{\bullet}OH + H^+ + e^- \rightarrow H_2O$	2.80
O_3 (ozone)	$O_3 (g) + H^+ + 2\ e^- \rightarrow O_2(g) + H_2O$	2.07
H_2O_2(hydrogen peroxide)	$H_2O_2 + 2H^+ + 2\ e^- \rightarrow 2H_2O$	1.77
HOCl (hypochlorous acid)	$2HOCl + 2H^+ + 2\ e^- \rightarrow Cl_2 + 2H_2O$	1.49
Cl_2 (chlorine)	$Cl_2 (g) + 2e- \rightarrow 2Cl$	-1.36

Hydroxyl radicals are non-selective in nature and they can react without any other additives with a broad field of contaminants whose rate constants are usually in the order of 10^6 to 10^9 $mol.L^{-1}.s^{-1}$ [8].

AOPs involve several steps schematized in Figure 1-1 below;

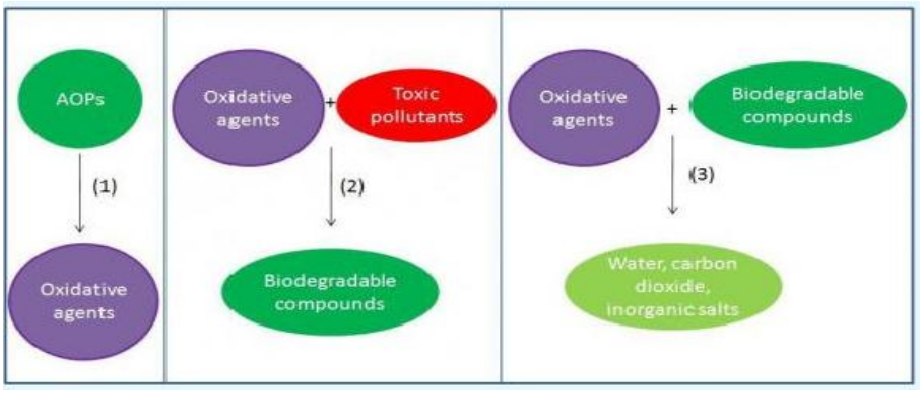

Figure (1-1): Main steps involved in AOPs treatment of water containing toxic organic compounds

- Excitation of TiO_2

$$\text{organic pollutants} + O_2 \xrightarrow[h\nu \geq E_{bg}]{TiO_2} CO_2 + H_2O + \text{mineral acid} \quad (1.1)$$

- Charge carrier generation:

$$TiO_2 + h\nu \longrightarrow h^+ + e^- \quad (1.2)$$

- Charge carrier trapping:

$$h^+ + Ti^{IV}OH \longrightarrow Ti^{IV}OH^{+\cdot} \quad (1.3)$$

$$e^- + Ti^{IV}OH \longrightarrow Ti^{III}OH \quad (1.4)$$

$$e^- + Ti^{IV} \longrightarrow Ti^{III} \quad (1.5)$$

- Charge carrier recombination:

$$e^- + Ti^{IV}OH+. \longrightarrow Ti^{IV}OH \quad (1.6)$$

$$h^+ + Ti^{III}OH \longrightarrow Ti^{IV}OH \quad (1.7)$$

- Interfacial charge transfer:

$$Ti^{IV}OH^{+\cdot} + \text{org. pol.} \longrightarrow Ti^{IV}OH + \text{oxidized Pollutants} \quad (1.8)$$

$$Ti^{III}OH + O_2 \longrightarrow Ti^{IV}OH + O_2^{-\cdot} \quad (1.9)$$

$$O_2^{-\cdot} \longrightarrow {}^{\cdot}OH, H_2O_2, HO_2^{\cdot}, HO_2^- + \text{Org. Pol.} \longrightarrow CO_2 + H_2O \quad (1.10)$$

1.2 Heterogeneous photocatalysis

The area of heterogeneous photocatalysis has extended quickly within the last four decades, having subjected to different developments mostly in connection to energy and the environment [12]. It can be clarified as the acceleration of photoreaction in the presence of a catalyst. The two most considerable enforcements of photocatalysis have been in solar water splitting and the purification of air and water containing low concentrations of pollutants. The multidisciplinary nature of the field has also increased safely and contains semiconductor physics, surface sciences, photo and physical chemistry, materials science and chemical engineering [13]. In heterogeneous photocatalysis, the reaction sketch suggests the prior formation of an interface between a solid photocatalyst (metal, semiconductor) and a fluid containing the reactants and products of the reaction. Procedures including illuminated adsorbate-metal interface are mostly categorized in the branch of photochemistry. Therefore, the term of "heterogeneous photocatalysis" is mainly used in cases where a light-absorbing semiconductor photocatalyst is used, which is in contact with either a liquid or a gas phase [14]. The heterogeneous photocatalysis reaction which is depicted in Figure (1-2) follows five steps which are [15];

(i) Diffusion of reactants to the surface, (ii) Adsorption of reactants onto the surface, (iii) Reaction on the surface, (iv) Desorption of products from the surface, and (v) Diffusion of products from the surface.

Figure (1-2): General mechanism of the photocatalysis on TiO_2 surface

The proposed general mechanism can be translated as follows;

There are two routes through which OH radicals can be formed. The reaction of the valence-band "holes" (h_{vb}^+) with either adsorbed H_2O or with the surface ^-OH groups on the TiO_2 particle [16], as shown in the following equation;

$$TiO_2\ (h_{vb}+) + H_2O_{ads} \longrightarrow TiO_2 + HO\bullet_{ads} + H^+ \qquad (1.11)$$

$$TiO_2\ (h_{vb}+) + HO^-_{ads} \longrightarrow TiO_2 + HO\bullet_{ads} \qquad (1.12)$$

In general, donor (D) molecules such as H_2O will adsorb and react with a hole in the valence-band and an acceptor (A) such as dioxygen will also be adsorbed and react with the electron in the conduction band (e_{cb}^-), according to the following equations;

$$TiO_2\ (h_{vb}+) + D_{ads} \longrightarrow TiO_2 + D+_{ads} \qquad (1.13)$$

$$TiO_2\ (e_{cb}-) + A_{ads} \longrightarrow TiO_2 + A-_{ads} \qquad (1.14)$$

Oxygen can trap conduction-band electrons to form superoxide ion ($O_2^{\bullet -}$), equation (1-15). These superoxide ions can react with hydrogen ions (formed due to water splitting), forming $HO_2^{\bullet}$;

$$TiO_2 (e_{cb}^-) + O_{2ads} + H^+ \longrightarrow TiO_2 + HO_2^{\bullet} \longrightarrow O_2^{\bullet -} + H^+ \quad (1.15)$$

H_2O_2 could be formed from $HO_2^{\bullet}$ via reaction (1-16)

$$TiO_2 (e_{cb}^-) + HO_2^{\bullet} + H^+ \longrightarrow H_2O_2 \quad (1.16)$$

Cleavage of H_2O_2 by one of the reactions (1-8, 1-9, and 1-10) may yield OH radical

$$H_2O_2 + h\nu \longrightarrow 2HO^{\bullet} \quad (1.17)$$
$$H_2O_2 + O_2^{\bullet -} \longrightarrow HO^{\bullet} + O_2 + HO^- \quad (1.18)$$
$$H_2O_2 + TiO_2 (e\text{-}_{cb})^- \rightarrow HO^{\bullet} + HO^- + TiO_2 \quad (1.19)$$

oxidation of the organic reactant by $^{\bullet}OH$ as follows;

$$R + {}^{\bullet}OH \rightarrow R^{\bullet} + H_2O \quad (1.20)$$

Then direct oxidation by reaction with holes

$$R + h^+ \rightarrow R^{+\bullet} \rightarrow \text{degradation products} \quad (1.21)$$

1.3 Cationic and anionic dyes

In 1856 William Henry Perkin found by accident the world's first successful synthetic dye in commerce. Dyes like that are known as colored bodies and when they applied to fibers they give them a permanent color which has the ability of resisting fading on vulnerability to sweat, light, water and other chemicals, which include

oxidants and microbial attack [17]. A first apparent transformation from past to present, where the things started to change, was discovering the synthetic dyes. Less cost to produce, brighter, colorful-fast and easy to use on cloth are some of the features of those new dyes. Scientists have contended to explicate beautiful new colors, and synthetic dyes had become outdated for many applications. Of course, this colorful material changed the world; yet, the chemicals that used to make dyes are often toxic, carcinogenic, or even detonative [18]. Among the different pollutants of aquatic ecosystem, dyes are a major group of chemicals [19]. Such substances with considerable coloring capacity are widely employed in the textile, pharmaceutical, food, cosmetics, plastics, photographic and paper industries use many synthetic dyes to color their products. Thus, effluents from these industries contain various kinds of synthetic dyestuffs [20]. In the chemical classification method, dyes are grouped according to certain common chemical structural features [21]. There are two types of dyes: cationic (basic) and anionic (acidic, reactive dyes) as shawn in Figure (1-3). Basic and reactive dyes are highly used in the material industry due to their good features of bright color, being easily water soluble, low cost and easier to use on fabric [22]. Dyes embrace a wide variety of structural types depending on the precise nature of electron donor (A) and electron acceptor (D) groups and can be subdivided into three main categories: cationic (z = + 1), anionic (z = - 1) and neutral (z = 0). Cationic dyes are positively charged and the most important group of this type of dye contains nitrogen atoms in both the D and A groups. On the other hand, a characteristic feature of anionic dyes is the presence of one or more sulfonate ($-SO^-_3$) groups, usually as sodium (Na^+) salts. These groups ensure that the dyes carry a negative charge [21]. Wastewaters that are produced from dye stuff industrial processes such as textile contain large amounts of dyes constituting an

important portion and having the least desirable consequences in points of surrounding ecosystems. As a result, they create an appreciable quantity of colorful wastewater. It is known that common perception of water quality is widely affected by the color. Color is the first material to be recognized in wastewater. The existence of tiny amounts of dyes in water (less than 1 ppm for some dyes) is very visible and unwanted [23,24]. Because of increasingly stringent restrictions on the organic content of industrial effluents, it is important to decrease dyes from wastewater before being discharged. Many of these dyes are also toxic, and even carcinogenic, and this comprises a dangerous hazard to aquatic living creatures [18].

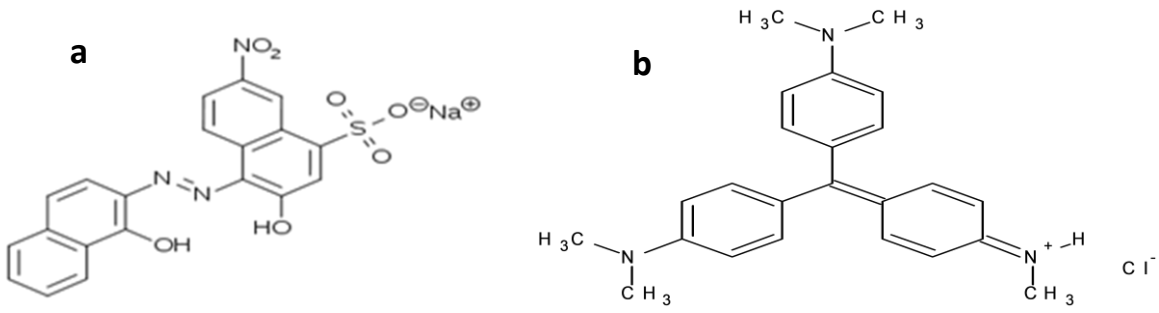

Figure (1-3) The molecular structures of a) anionic dye Eriochrom Black T (EBT), b) cationic dye Methyl Violet (MV)

1.4 Dye sensitization of TiO_2

Nano-crystalline TiO_2 has been comonly used to catalyze the photo-degradation of water impurities like chlorinated hydrocarbons, phenols, benzoic acid and others [25]. Most semiconductors like CdS, CdSe, GaP and Si undergo serious photo corrosion or even normal corrosion in the dark, thus a stable, wide band gap semiconductor, TiO_2, became the material of choice [26]. Inspite of many comon benefits of using TiO_2, it

suffers some shortcomings like large band gap (≈ 3.2 eV) which restricts its use to the UV region. Such radiations are not widely abundant in the solar radiations reaching the earth, which keeps the use of TiO_2 in solar energy utilization. For that reason, research has been directed to sensitize TiO_2 surfaces in order to officiate in the apparent region [25]. It is commonly known that a semiconductor that has a large band gap can be sensitized at a wavelength longer than the band gap wavelength by a photoexcited dye adsorbed on the surface of the semiconductor. This is called dye sensitization or spectral sensitization, whose principle is being applied to photography to increase the sensitization spectrum of silver halides into the longer wavelength region. Dye sensitization has been studied highly in the field of photoelectrochemistry [27]. Sensitization includes the incorporation of a substance (dye or metal complexes) that interacts with the surface of a wide band gap semiconductor, such as TiO_2, facilitating electron transfer between the incorporated molecules and the host semiconductor. The apparent light stimulates the sensitizer organic molecules adsorbed onto the TiO_2, thereby enabling electron injection into the semiconductor conduction band [27,28]. It can be said that the mechanism of the dye sensitized photo-degradation of pollutants is based on the absorption of apparent light for stimulating an electron from the highest occupied molecular orbital (HOMO) to the lowest unoccupied molecular orbital (LUMO) of a dye, and subsequently transferred into conduction band of the semiconducter. The advantage of sensitized photocatalysis is the fact that it extends the range of stimulation energy into visible range and thus gives full use of solar energy [29,30].

The scheme of dye-sensitization of TiO_2 is clarified in Figure (1-4), as follows;

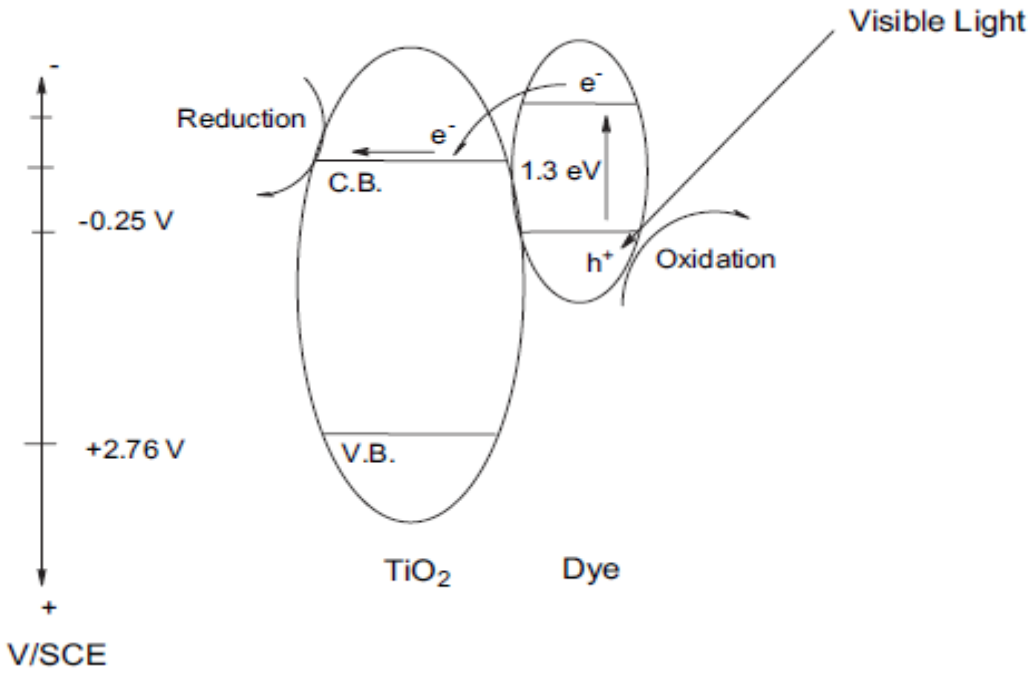

Figure (1-4): Schematic TiO_2 sensitization by visible light

The dye sensitization extends the range of stimulation energies of the semiconductor into apparent region, making a more complete use of solar energy and could accelerate the photodecay of contaminants and the activity of colored removal [31]. In systems with low concentrations of colored pollutants, it may increase the sensitivity of the photocatalytic process for removal of colored pollutants, which accordingly may make sensitized photocatalysis a more attractive large-scale process [32].

1.5 In situ dye sensitized nano TiO_2 for photocatalysis

Self sensitization (in situ sensitization) means that a system which is first insensitive to light of a certain wavelength becomes photoactive and sensitive to that light wavelength after certain in situ surface modifications. Galzaferri and Spahni [33] stated that in a control

experiment, which allowed us to keep parameters constant and to collect data for several days, we proved that self-sensitization really occurred. This process of self-sensitized oxidation is beneficial in degradation of colored pollutants with visible light. One of the important uses of the method of dye sensitization is in the field of treating textile wastewater [32]. Textile dyes are potentially toxic because of their low removal rate and if untreated would form aromatic amines which are potentially harmful to the living world [34]. After the photoinjection of an electron into the conduction band of TiO_2, the cation radical formed from dye can undergo rapid deprotonation to create the radical which can react with molecular oxygen, though the formation of several active oxygen species, hydrogen peroxide, perhydroxyl and the hydroxyl radicals in the photocatalytic process, had been proposed for the degradation of the dye [35]. A cardinal factor responsible for the increase in the efficiency of the process is the prevention of recombination of electrons in the conduction band of the TiO_2 with the radical cation of the dye. To enhance the forward reaction, it is imperative that the electron is taken up very easily by the oxygen molecule and recombination is prevented. It was found that the molecular oxygen supply onto the TiO_2 surface is the rate limiting step of the overall photooxidation process [32,35]. Reports on the degradation of other type of dyes like Methylene Blue (MB), Remazol Brill Blue R (RBBR) and Orange G (OG) had also been available in the literature [36]. It was seen that when these dyes were adsorbed onto the surface of the specially designed combustion synthesized nano-TiO_2 particles, their degradation rates were significantly higher as compared to that of adsorbed onto surface of the commercial Degussa P-25 TiO_2 catalyst. It had been reported that the dyes adsorbed strongly and irreversibly onto surface of the commercial P-25 Degussa TiO_2 semiconductor and blocked the active sites on the surface of the

commercial semiconductor leading to saturation and lower rates of degradation on the P-25 Degussa TiO_2 semiconductor catalyst [32,36].

1.6 Immobilization of TiO_2 photocatalyst

Two possible oxidation processes can happen during the photocatalytic reactions to remove toxic compounds [37]:

(i) Water can be oxidized to hydroxyl radicals by photogenerated positive holes and afterwards react with organic substrates to produce oxidized species.
(ii) The organic substrate can directly adsorb on the catalyst which may lead to oxidation of the substrate directly on the surface.
Kumar and Bansal [38] reported that the photodegradation process could be carried out using the suspension of nanocrystals of TiO_2 in watery solution. However, the use of watery suspension is not appropriate for business applications due to the clumsy and pricy separation of nano-particles of titanium dioxide for reuse. Moreover, suspension of fine particles limits the penetration of light leading to decrease efficiency of photodegradation. In order to solve these problems, immobilized photocatalysts have been employed [39]. These immobilization techniques reduce the cost of activity and also in some cases increase the efficiency of TiO_2 as photocatalyst, due to the synergistic effect of the substrate and TiO_2 [40]. Also, immobilized form of the catalyst is advantageous compared to the suspended powder form due to [41]:

1- Reduces losses of materials and requires less time to be separated from treated water at the end of the treatment.
2- Extremely efficient for photocatalysis, because TiO_2 good crystals are immobilized at high tightness at the surface of the particles.

3- Usually, the particular weight of the carrier bodies is very close to unity in order to be suspended very freely in water.

The most important features of a suitable support are to be chemically neutral, to give a very specific surface area and to be transparent to UV radiation [39]. One of the best familiar methods of photocatalyst immobilization is accumulation of TiO_2 powder on a glass surface by the dip coating technique. TiO_2 can firmly adhere to the glass surface due to the difference in the electrostatic charge [42]. Main advantage with glass substrate is the transparency of the system even after the immobilization. This can allow the penetration of light which can result in improved photocatalysis [43]. Various types for immobilizing TiO_2 nanoparticles such as glass, other materials, including quartz, sand, stainless steel, silica, activated carbon, alumina, and polymers, zeolites, clay [44]. These supports can be prepared in various forms and shapes, such as cylinders, tubes, sheets or plates, beads and mesh. Numerous techniques were reported for preparing supported titania, Both dip coating and sol-gel precipitation of TiO_2 on the support are considered the most common methods of photocatalyst immobilization [45]. Among the different supports, for many reasons stainless steel was considered an excellent substrate material [46]; first, it keeps its structural integrity under the high temperature required for calcination of the TiO_2 films whereas quartz glass, for example, softens and deforms. Second, quartz and ceramics cannot be used in the electrochemical process whereas stainless steel can be used because of their dielectric properties.

1.7 Adsorption

Is an operation that happens when a gas or liquid solute accumulates on the surface of a solid adsorbent or a liquid one , making a molecular or atomic film (the adsorbate) [47] . It differs from absorption, in which a body spreads into a liquid or solid to make a solution. The term sorption includes the two processes, while desorption is the reverse process. Adsorption is effective in most physical, biological, and chemical systems, and is commonly used in business applications such as activated charcoal, synthetic resins and water purification [48]. Isotherms for adsorption of instrumental solutes can be divided into four important classes Figure (1-5), depending on the nature of slope of the incipient portion of the curve, and thereafter into sub-groups. These four main classes are [49]: (i) ***S*** Curves, suggestive of vertical orientation of surface assimilation molecules at the surface. (ii) *L* Curves, the regular or " Langmuir " isotherms, usually suggestive of molecules adsorbed plane on the surface, or, sometimes, of perpendicularly oriented adsorbed ions with especially valid intermolecular attraction. (iii) *H* Curves ***(' I*** high affinity ") (starting at an actual value on the " concentration in solid " axis) , frequently given by solutes adsorbed as ionic micelles, and by high-affinity ions changing with low-affinity ions. (iv) C Curves (" constant partition "), narrow curves, granted by solutes which soak into the solid more quickly than does the solvent.

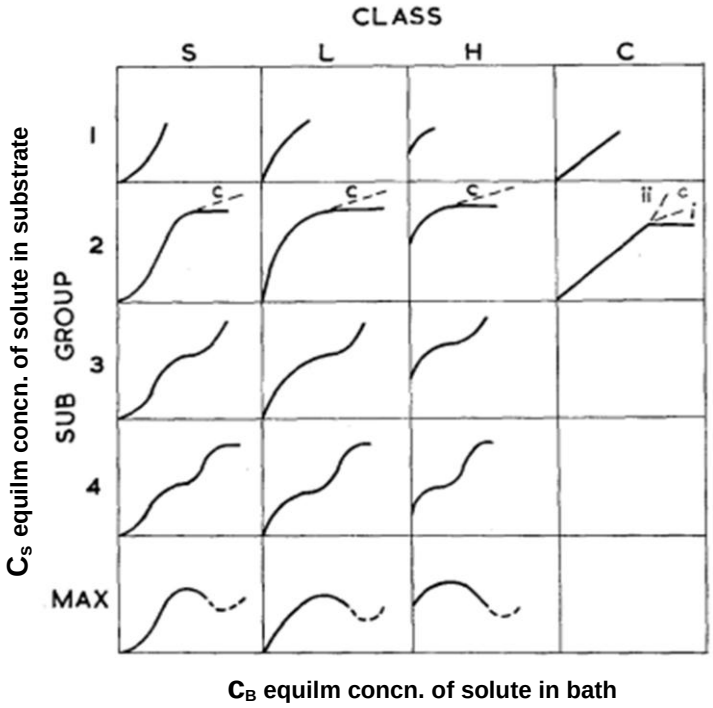

Figure (1-5): System of isotherm classification

The adsorption phenomenon is divided into [50];

a) **physisorption (physical adsorption):** long range and infirm Van der Waals attraction between adsorbate and substrate and hydrogen bonding, ($\Delta H_{physisorption} \sim 20$ kJ mol^{-1}) low enthalpy of adsorption, reversible, multi-molecular layers may be formed, this process is observed under conditions of low temperature.
b) **chemisorption:** short range and firm bonding between adsorbate and substrate. Valence forces of attraction are chemical bond forces, ($\Delta H_{chemisorption} \sim 200$ kJ mol^{-1}) high enthalpy of adsorption, often irreversible, generally, monomolecular layer is formed, this process takes place at high temperatures.

Chemisorption, is highly selective and occurs only between certain adsorptive and adsorbent species and only if the chemically active surface is cleaned of previously adsorbed molecules.

Both physical and chemical adsorption may occur on the surface at the same time; a layer of molecules may be physically adsorbed on top of an underlying chemisorbed layer. The same surface can show physisorption at one temperature and chemisorption at a higher temperature [51].

1.8 Removal of dyes by adsorption

Organic dyes are used widely in various industries [52,53]. The large use of organic dyes and their indiscriminate disposal lead to environmental dangers. Dyes delivered from industries principally cause water pollution and make threat to common hygiene, health, and environment [54,55] and make it unsuitable for aquatic life [56]. Furthermore, some of the dyes and their metabolites are toxic, carcinogenic and mutagenic. Therefore, the elimination of dyes from wastewater is of essential importance [54]. In order to treat contaminated wastewater via dye removal different techniques which include adsorption, photodegradation, chemical oxidation, coagulation, electrochemical oxidation have been employed [54,57]. The most generally used ways for dye removal are biological oxidation and chemical precipitation. Yet, these methods are effectual and economic just where pollutions majors are relatively high. At this time sorption methods is proved to be one of the effectual and attractive methods for the treatment of this dye-bearing wastewater [58]. Adsorption has been presented as an affordable strategy for the removal of various kinds of dyes. Adsorbents, such as active carbon [54], peat, wood chips, fly ash, coal [54,57] etc., have been searched and told in the literature. These adsorbents shown above suffer from some disadvantages usually such as high price, low adsorption ability, multi-step synthesis procedures, or inability to reproduce and recycle. Hence, it is important to develop new adsorption materials with low price, high adsorption ability, also reproductive and recyclable features [57]. Adsorption

methods supply an attractive treatment of wastewater which contains dyes over other stipulated wastewater treatment techniques because of economic consideration, it is available and easy to work as well as greater efficiency [53]. The important benefits of the adsorption are restoration of heavy metals, plainness of design and meeting of exact discharge designation. Adsorption has been presented as an effectual and plain separation way [59].

1.9 Literature survey

Advanced oxidation processes (AOPs) have been developed and employed to deal with the environmental problems emerged by a broad range of dye contaminated wastewater effluents [5, 7], that rely largely on the use of nano titanium dioxide as catalyst in a well known process called heterogeneous photocatalysis [14, 15]. Among the different pollutants of aquatic ecosystem, organic dyes are a major group of chemicals [19]. These dyes are subdivided into three main categories: cationic (z =+1), anionic (z =-1) and neutral (z =0) [21]. A characteristic feature of anionic dye (EBT) is the presence of one sulfonate ($-SO^-_3$) groups, usually as sodium (Na^+) salts. These groups ensure that the dyes carry a negative charge [21, 22]. Many researchers have worked to remove these pollutants via UV or VIS light illumination with pure or modified TiO_2 [72, 74, 85, 91, 110]. Rauf et al. [85] reported the influence of various parameters like amount of catalyst, concentration of dye, pH, temperature and light intensity. Sivaraj et al [74] noted a greater adsorption and hence increasing the degradation rate in the acidic media for Eriochrom black -T, and noted reverse image in the case of Methyl Violet [91]. Furthermore, as the dye initial concentration increases the rate of photocatalytic reaction becomes low [88,104]. Flores et al [72]

reported that the number of active sites on the photocatalyst surface increases by an increase in catalyst amount, Authors [71, 99, 100, 101] noted that the number of reached photons reduced when adding high catalyst amount that has negative effect on the degradation percent of dyes (EBT and MV). Suspension of fine particles limits the penetration of light leading to decrease efficiency of photodegradation [38] also, limited for industrial applications due to the high cost of the catalyst filtration process [138]. In order to solve these problems, immobilized photocatalysts have been employed [39]. These immobilization techniques reduce the cost of activity and also in some cases increase the efficiency of TiO_2 as photocatalyst [40]. Among the different supports, for many reasons stainless steel was considered an excellent substrate material due to, it keeps its structural integrity under the high temperature required for calcinations of the TiO_2 films [46].

1.10 Scope of the present work

A considerable attention has been paid over the last three decades on the synthesis, characterization and application of nanocrystalline materials, due to their ultrafine structures, fabulous chemical properties and wide applications in environmental remediation. Accordingly, in this study EBT and MV were chosen as model pollutants and photodetoxified onto nano anatase TiO_2 following the forthcoming experimental steps;

1. Preparation of the nano anatase TiO_2 on laboratory scale following sol-gel methodology. Afterwards, characterization of the synthesized nano anatase TiO_2 was implemented using XRD, EDXS, TEM, BET and SEM techniques.

2. Several operational parameters were investigated, based on in situ sensitization (self sensitization) concept for the nano photocatalyst under visible light illumination, namely initial pH, irradiation time, initial concentration of the model dyes (EBT and MV), TiO_2 photocatalyst loading, visible light source intensity and temperature on the photocatalytic degradation of anionic dye (EBT) and cationic dye (MV).

3. Many routes for the immobilization of nano TiO_2 onto stainless steel plates like swirling, rotating and dipping have been planned to be employed and optimized experimentally for best photodegradation of model pollutants.

4. The kinetic and thermodynamic studies for both EBT and MV dyes have been one of the objectives of this research work as well.

Eventually the escalation of the immobilization unit for the outdoor solar photocatalysis has also been conducted.

CHAPTER TWO

EXPERIMENT

2.1 Chemicals

Material	Purity	Source
Iron(II) Sulfate ($FeSO_4.7H_2O$)	99%	Riedel-Dehaen
Sodium Acetate (CH_3COONa)	98%	Riedel-Dehaen
1-10 Phenanthroline ($C_{12}H_8N_2$)	97%	BDH
Eriochrom Black T ($C_{20}H_{12}N_3O_7SNa$)	99%	Fisher Chemical
Titanium Dioxide (Nano TiO_2)	99.5%	Aldrich
Methyl Violet ($C_{24}H_{28}N_3Cl$)	99.8%	Fisher Chemical
Cetyl Tri Ethyl Ammonium Bromide ($C_{19}H_{42}BrN$)	96%	Aldrich
Sulfuric Acid (H_2SO_4)	98%	Himedih
Iso Propanol (C_3H_8O)	99.8%	Riedel-Dehaen
Nitric Acid (HNO_3)	69.5%	Medex
Iron(II) Ammonium Sulfate $Fe(NH_4)_2(SO_4)_2.6H_2O$	99%	Riedel-Dehaen
Titanium Iso Propoxide ($C_{12}H_{28}O_4Ti$)	97%	Aldrich
Ethanol (C_2H_6O)	97%	Merck
Aceton (C_3H_6O)	99%	Analyt
Piranha (H_2O_2+H_2SO_4)	3:1	
Hydrogen Peroxide (H_2O_2)	50% wt/wt	Scharlau

2.2 procedures

2.2.1 Preparation of actinometer K_3 [Fe $(C_2O_4)_3$]. $3H_2O$

1- Five gram of $Fe(NH_4)_2(SO_4)_2.6H_2O$ was weighed in a 125 milliliter Erlenmeyer flask and dissolved in 20 milliliter hot nano filterd de ionized water (NFDW) and then 1 milliliter of 3M H_2SO_4 was added.

2- 2.5g of oxalic acid ($H_2C_2O_4$) was dissolved in 25 milliliter of NFDW. This solution was added to the above solution in step 1, and then heated to boiling while stirring constantly to prevent bumping.

3- The Erlenmeyer flask was removed from the heat source and allowed the yellow precipitate of FeC_2O_4 to settle for 10 minutes.

4- The supernatant liquid was decanted and the precipitate was washed using 15 milliliter of hot NFDW. The mixture was swirled and filtered.

5- Ten milliliters of hot NFDW that contains 3.5g of $K_2C_2O_4$ was added to the precipitate, then was stirred and heated to 40°C. While the temperature was at 40°C, immediately, 8 milliliter of H_2O_2 was added dropwise and stirred continuously. Periodically the temperature of the solution was checked (40-50C^o) during the addition of H_2O_2. A precipitate of brown Fe $(OH)_3$ was observed.

6- The resulting solution was heated to boiling. 20 milliliter of $H_2C_2O_4$ was added (prepared by dissolving 1g in 30 milliliter of NFDW). It was stirred continuously and the last 10 milliliter of $H_2C_2O_4$ was added dropwise, while maintaining the temperature near boiling. The solution was turned clear green.

7-Twenty milliliters of ethanol was added to the solution of neglected precipitate (when crystals were formed, it was dissolved by heating in water bath).

8- The solution was kept in dark about 24 hrs.

9- The solution was filtered under vacuum and washed with 10 milliliter of 1:1 ethanol / NFDW solution.

10- Finally, the precipitate (potassium ferrioxalate) was washed using 10 milliliter of acetone.

2.2.2 Measurement of light intensity using actinometric method

The intensity measurement of the incident light was carried out with a potassium ferrioxalate actinometer as described by Hatchard and parker [60], and examind through a previous work in our laboratory [6,61]. This method is usually used to determine the number of quanta entering the reaction vessel and consequently, the apparent quantum yields for the photocatalytic reaction will be estimated. The actinometer solution (6×10^{-3} mol/L) was prepared by dissolving (2.947 g) of $K_3Fe(C_2O_4)_3.3H_2O$ in 800 milliliter of nano filtered deionized water (NFDW).

One hundred milliliter of 1N H_2SO_4 was added and the whole solution was diluted to one liter with NFDW.

The method used for the determination of light intensity involves irradiation of actinometer solution for known period time (1 hour).

Calibration curve

A calibration curve for Fe^{+2} was drawn using the following solutions :

1- 4×10^{-4} mol.L^{-1} of $FeSO_4$ in 0.1 N H_2SO_4.
2- 0.1% w\v phenanthroline monohydrate in water.
3- Buffer solution was prepared by mixing 600 milliliter of 1N sodium acetate and 360 milliliter of 1N H_2SO_4 then diluted to one liter.

Different concentrations of Fe^{+2} were prepared by further dilution of solution (1) in 25 milliliter volumetric flask. Then add to each flask;

a) Two milliliter phenanthroline solution.
b) Five milliliter of buffer solution.
c) Different volumes of 0.1N H_2SO_4 solution to make the acid equivalent to 10 milliliter 0.1 N H_2SO_4 and finally dilute the whole solution to 25 milliliter with NFDW.

The volumetric flask was covered with aluminum foil and kept in the dark for 30 minutes [60]. Then the absorbance at wavelength = 510 nm were measured. A blank solution was used as reference which contained all the solutions except the ferrous ion solution. Draw plot for optical density versus ferrous ion concentration, Figure (2-1). The slope of the straight line obtained which gives the extinction coefficient (absorptivity) of $FeSO_4$ solution.

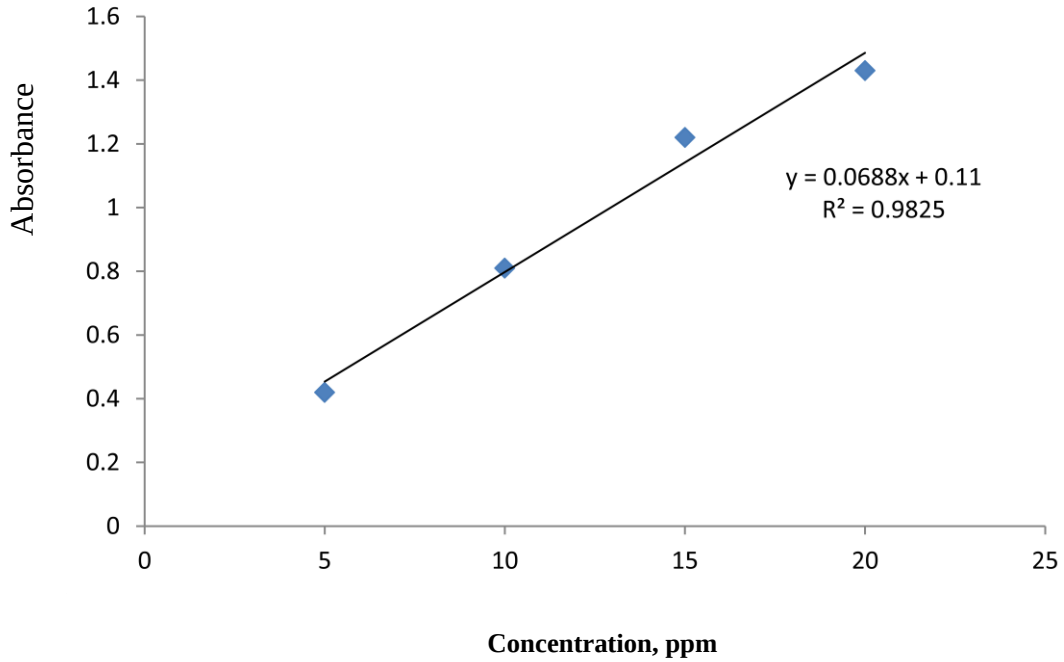

Figure 2-1: Calibration curve for Fe^{+2}

In order to determine the light intensity, 50 milliliter of actinometer solution was irradiated in the irradiation cell for 1 houre. Post illumination, one milliliter of the irradiated solution was transferred into 25 milliliter volumetric flask, two milliliter of phenanthroline solution and 0.5 milliliter of buffer solution were added to the flask, then it was diluted to 25 milliliter using NFDW.

Blank solution was prepared by mixing one milliliter of unirradiated potassium ferrioxalate solution with other components.

The mixture was kept in the dark for 30 minutes and then the optical density was measured.

The incident light intensity was calculated as follows:

$I_o = A \times V_1 \times 10^{-3} \times V_3 / Q_y \times € \times V_2 \times t$

Where:

I_o= photo flow (incident light intensity)

A= optical density (absorbance) at 510 nm

V_1=initial volume(50 milliliter) V_3=final volume(25 milliliter)

Q_y=quantum yield at 365 nm=1.21[60]

€=extinction coefficient=slope of calibration curve (1.912_x10^4)

V_2=volume taken from irradiated solution (1 milliliter).

t = irradiation time in seconds (sec)

then the apparent quantum yield is calculated using the following expression :

ϕ_{app} = rate of reaction / rate of absorbed photons (I_o)

2.2.3 Synthesis of TiO_2 nanoparticles on laboratory scale

Titanium dioxide nanosized catalyst was synthesized by the sol-gel method by means of a gradual addition of a solution of titanium isopropoxide (5milliliter isopropanol + 5 milliliter titanium isopropoxide) onto 200 milliliter of NFDW at pH=5 with a rate of addition of 2 milliliter /minutes. The mixture was kept, after completion of addition, under continuous vigorous mixing at room temperature until the completion of hydrolysis for 2 hours. The resulting transparent colloidal solution was left aging for 24 hours then filtered, dried at 90 C^o for two hours, and finally was calcined at 400 C^o for 4 hours. Grounding into fine powder, if needed, overcomes the agglomeration [62].

2.2.4 Preparation of dyes stock solution

2.2.4.1 Preparation of Eriochrom Black T (EBT) solution

1- A stock solution of EBT of 100 ppm was prepared by dissolution of 0.1 g of dye into 1000 milliliter NFDW.

2- The stock solution was diluted further to prepare a series of different concentrations of EBT (10, 20, 30, 40 and 50 ppm) for the preparation of the calibration curve.

3-The absorbance of each diluted solution was measured spectrophotometrically at 540 nm and subsequently the calibration curve, Figure (2-2), was drawn.

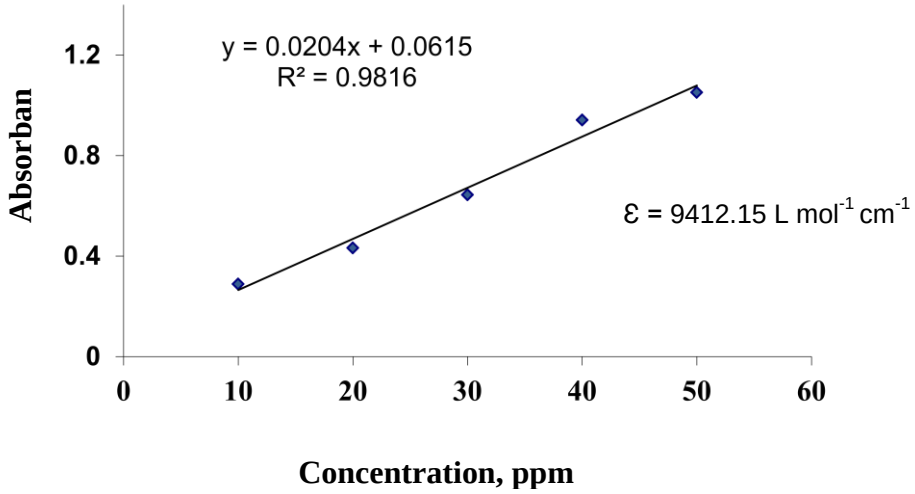

Figure (2-2): Calibration curve for Eriochrom Black T

2.2.4.2 Preparation of Methyl Violet solution

1- A stock solution of MV of 15 ppm was prepared by dissolving of 0.015g of dye into 1 liter NFDW.

2- Different concentrations (2, 4, 6, 8, 10 ppm) of MV were prepared from stock solution by a series of dilution in order to prepare the calibration curve.

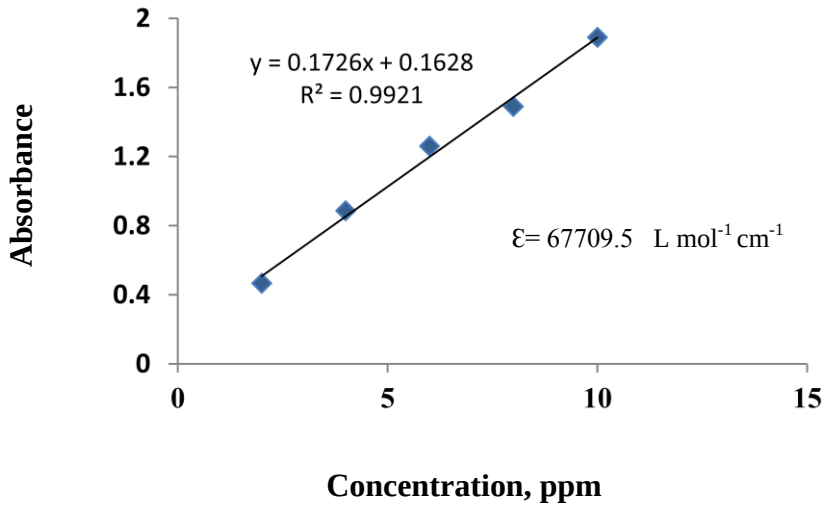

Figure (2-3): Calibration curve for Methyl Violet

2.2.5 Testing of degradation of dye in the dark

1- One hundred milliliters of dye (10 ppm) was added into a beaker.
2- A mass of 50 mg of nano powder (TiO_2) was added into 100 milliliter of dye aqueous solution.
3- The beaker of the solution was kept in the dark for 3 hours with continuous stirring.
4- About 4 milliliter was withdrawn after every 60 minutes of stirring time.
5- The catalyst (TiO_2) was separated from the suspension by centrifuge for 10 minutes using 3000 RPM, and filtered using cellulose membrane of 0.45 μm pore size.
6- The absorbance was measured for MV at 584nm and for EBT at 540 nm to compute the changes in concentration.

2.2.6 Testing of Degradation of dye in the absence of TiO_2 under UV-light

1- One hundred milliliters of dye (10 ppm) was added into the cell.
2- The sample was irradiated by Uv light (365 nm wavelength) using 24 cm cell-light source distance in the presence of lens for 3 hours.
3- About 4 milliliters was withdrawn after every 60 minutes of irradiation time.
4- The absorbance of dye was measured to estimate the degradation percent at 584, 540 nm for MV and EBT, respectively in order to calculate the changes in concentration**.**

2.2.7 Testing of Degradation of dye in the absence of TiO_2 under visible light

The effect of visible light on degradation of dye was studied as follows;

1- One hundred milliliter of EBT, MV dyes (10 mg/L) aqueous solution was irradiated using 500W halogen lamp at high intensity with stirring for 3 hrs.

2- The absorbance of dye was measured every 60 minutes at 584, 540 nm for MV and EBT, respectively in order to calculate the changes in concentration**.**

2.2.8 Testing of degradation of dye by visible Light in presence of TiO_2

1- One hundred milliliter of dye (10 mg/L) aqueous solution was irradiated using 500W halogen lamp (Philips) at high intensity (4.68×10^{-7} E/L.sec) with stirring for 3 hrs.

2- A mass of 50 mg of powder (TiO_2) was contacted with 100 milliliter of azo dyes aqueous solution.

3- The water suspension of dye and nanosized TiO_2 powder were stirred in the dark for 30 min to ensure the adsorption equilibrium was established prior to irradiation.

4- The sample was irradiated with a 500W halogen lamp at high intensity with stirring for 4 hrs.

5- About 4 milliliter was withdrawn after every 60 minute of irradiation time.

6- The catalyst (TiO_2) was separated from the suspension by centrifuge for 10 minutes using 3000 RPM and filtered using 0.45 μm cellulose membrane.

7- Absorbance of dye was measured to estimate the degradation percent.

2.2.9 Effect of initial pH on the degradation of dye under Visible light

1- One hundred milliliter of dye (10 ppm) was taken .
2- The pH of above solution was modified to 2, 3, 5, 7, 9 using either diluted HNO_3 (0.1M) or diluted NaOH (0.1M).
3- Fifty mg of powder (TiO_2) was added.
4- The solution was stirred with O_2 bubbling in the dark for 20 minutes.
5- The sample was irradiated with a 500W halogen lamp at high intensity with stirring for 3 hrs.

Note: O_2 used is standard with purity (97.5%) and the flow rate of O_2 is 50-55 ml\min to form superoxide anion that react with organic pollutants.

6- Five milliliter of solution was withdrawn every 15 minutes interval from illuminated solution.
7- The catalyst TiO_2 was separated from the suspension by centrifuge at 3000 RPM for 10 minutes and filtered using 0.45 μm cellulose membrane.
8- The absorbance of dye was measured to estimate the degradation percent.

2.2.10 Effect of initial dye concentration on the rate of reaction

1- One hundred milliliter of various initial concentrations of EBT dye (10, 20, 30, 40, 50, 60) ppm were taken and then adjust pH to 3, and (2, 4, 6, 8, 10) ppm for MV dye and then adjust pH to 7.
2- Eighty and thirty milligrams of TiO_2 powder were added to above solutions of EBT, MV respectively.
3- The solution was stirred with O_2 bubbling in the dark for 20 minutes to ensure the adsorption equilibrium was established prior to irradiation.
4- The sample was irradiated with a 500W halogen lamp at high intensity with stirring for 1hr.
5- About 4 milliliter of solution was withdrawn after every 10 minutes of irradiation time.
6- The catalyst (TiO_2) was separated from the suspension by centrifuge for 10 minutes using 3000 RPM and filtered using 0.45 μm cellulose membrane.
7- Absorbance of dye was measured to estimate the degradation percent.

2.2.11 Effect of TiO_2 loading on the degradation of dye

1- One hundred milliliter of (40ppm EBT and 5ppm MV) was taken and adjust to pH =3 and 7 using dilute HNO_3 (0.1M) for EBT, MV respectively.
2- Different amounts of TiO_2 (10mg, 20mg, 30mg, 40mg, 50mg, 80mg and 100mg) for EBT and (10, 20, 30, 40, 70mg) for MV were added to the cell.

3- The solution was stirred with O_2 bubbling in the dark for 20 minutes to ensure the adsorption equilibrium that was established prior to irradiation.

4- The sample was irradiated with a 500W halogen lamp at high intensity with stirring for 2 hr.

5- At every one hour interval, 5 milliliter from dye was taken, and the catalyst was separated from suspension by centrifuge for 10 minutes at 3000 RPM and filtered using 0.45 μm cellulose membrane.

6- The absorbance was measured at 584, 540 nm for MV and EBT, respectively.

2.2.12 Effect of visible light intensity on the degradation of dye

1- One hundred milliliter of EBT (40 mg/L), was adjusted to pH = 3.

2- Eighty mg of TiO_2 powder was added to above solution.

3- The solution was stirred with O_2 bubbling in the dark for 20 minutes to ensure the adsorption equilibrium which was established prior to irradiation.

4- The sample was irradiated with a 500W halogen lamp at high intensity (increasing light intensity can be achieved by increasing the potential shed on the visible lamp through the voltage change unit) with stirring for 1.5 hr.

5- 4 milliliter was withdrawn after every 15 minutes of irradiation time.

6- The catalyst (TiO_2) was separated from the suspension by centrifugation for 10 minutes using 3000 RPM and filtered using 0.45 μm cellulose membrane.

7- The absorbance of dye was measured to estimate the degradation percent.

2.2.13 Effect of temperature on the degradation of dye

1- Seventy five milliliter of (60ppm and 4ppm) were taken and adjusted to pH = 3 and 7 of EBT, MV respectively, using diluted HNO_3 (0.1M) or diluted NaOH (0.1M).

2- Eighty and thirty milligrams of TiO_2 were added onto the cell containing the above solutions for EBT, MV, respectivly.

3- The solution was equilibrated with O_2 for 20 minutes in the dark where water bath circulator was used to keep the temperature of solution at (20, 25, 30, 35, 40 and 45^o C).

4- The sample was irradiated with a 500W halogen lamp at high intensity (increasing light intensity can be achieved by increasing the potential shed on the visible lamp through the voltage change unit) with stirring for 1 hr

Note : the flow rate of O_2 is 50-55 ml\min.

5- At every 30 minte interval, 5 milliliter of irradiated dye was taken and the catalyst was separated by centrifuge for 10 minutes at 3000 RPM and filtered using 0.45 μm cellulose membrane.

6- The absorbance was measured at 584, 540 nm for MV and EBT, respectively.

2.2.14 Immobilization of TiO_2 photocatalyst

The stainless steel 316 L (st.st.) plates were cleaned according to following steps;

1- Slides were immersed inside a pyrex beaker containing about 120 ml of piranha solution and the whole content was ultrasonicated for 15-20 minutes.

2- The slides were washed with distilled water to remove the traces of piranha solution.
3- The process (steps 1 and 2) was repeated using aceton and then commercial ethanol solvents.
4- Finally the process was repeated using only distilled water.
5- Slides are ready to be used.
6- Two hundred and fifty milliliters of NFDW was taken and adjusted to pH = 3 using dilute HNO_3.
7- One gram anatase TiO_2 nanoparticle and 0.5g Cetyl Tri ethyl Ammonium Bromide (CTAB) were added to the cell containing the above solutions.
8- Only one side of the stainless steel slide was coated and then placed inside the above solution, which was used for three types of coating, as follows;

2.2.14.1 Swirling method

1- The cleaned st.st slide was settled into the coating solution (Figure 2-4) containing nano TiO_2 and CTAB. The solution was swirled for 24 hrs at room temperature. The slide was afterwards dried at $90C^o$ for one hr. This slide was coded S_1, which stands for single sided one swirling coating.
2- The slide S_1 was immersed in 75 ml of 60 ppm EBT solution and was illuminated with 500W halogen lamp for 3 hrs under vigorous stirring and O_2 gas bubbling.
3- About 4 milliliter of sample was withdrawn at every 60 minutes of irradiation time.
4- Absorbance of dye was measured at 540 nm to estimate the degradation percent.

5- Step 1 above was repeated for three and five times to prepare S_3 and S_5 swirling single sided coated slide.

Figure (2-4): Swirling coating

2.2.14.2 Dipping method

1- Similar coating solution mentioned above (2.2.14.1) was used for coating by dipping (Figure 2-5).
2- The dipping frequency was every 5-6 seconds for one hour period (600 dipping). The slide was afterwards dried at 90C^o for one hour. This slide was coded D_1, which stands for single sided one dipping coating.
3- The slide D_1 was immersed in 75 ml of 60 ppm EBT solution and was illuminated with 500W halogen lamp for 3 hrs under vigorous stirring and O_2 gas bubbling.

4- About 4 milliliter of sample was withdrawn at every 60 minutes of irradiation time.

5- Absorbance of dye was measured at 540 nm to estimate the degradation percent.

6- Step 1 above was repeated for three to five times to prepare D_3 and D_5 dipping single sided coated slide.

Figure (2-5): Dipping coating

2.2.14.3 Rotating method

1- The rotation assembly was used to prepare the slides which are coded R_1 (Figure 2-6). The cleaned slide was bound to the rotating shaft from upper edge and it (slide) was immersed in the similar coating solution mentined previously.

2- The slide was rotated steadily for (100 rotations/min.) 24 hrs at room temperature, then it was dried at $90C^o$ for one hr. This slide was coded R_1, which stands for single sided one rotating coating.

3- The slide $R_1$was immersed in 75 ml of 60 ppm EBT solution and was illuminated with 500W halogen lamp for 3 hrs under vigorous stirring and O_2 gas bubbling.
4- About 4 milliliter of sample was withdrawn at every 60 minutes of irradiation time.
5- Absorbance of dye was measured at 540 nm to estimate the degradation percent.
6- Step 1 above was repeated for three to five times to prepare R_3 and R_5 rotating single sided coated slide.

Figure (2-6): Rotating coating

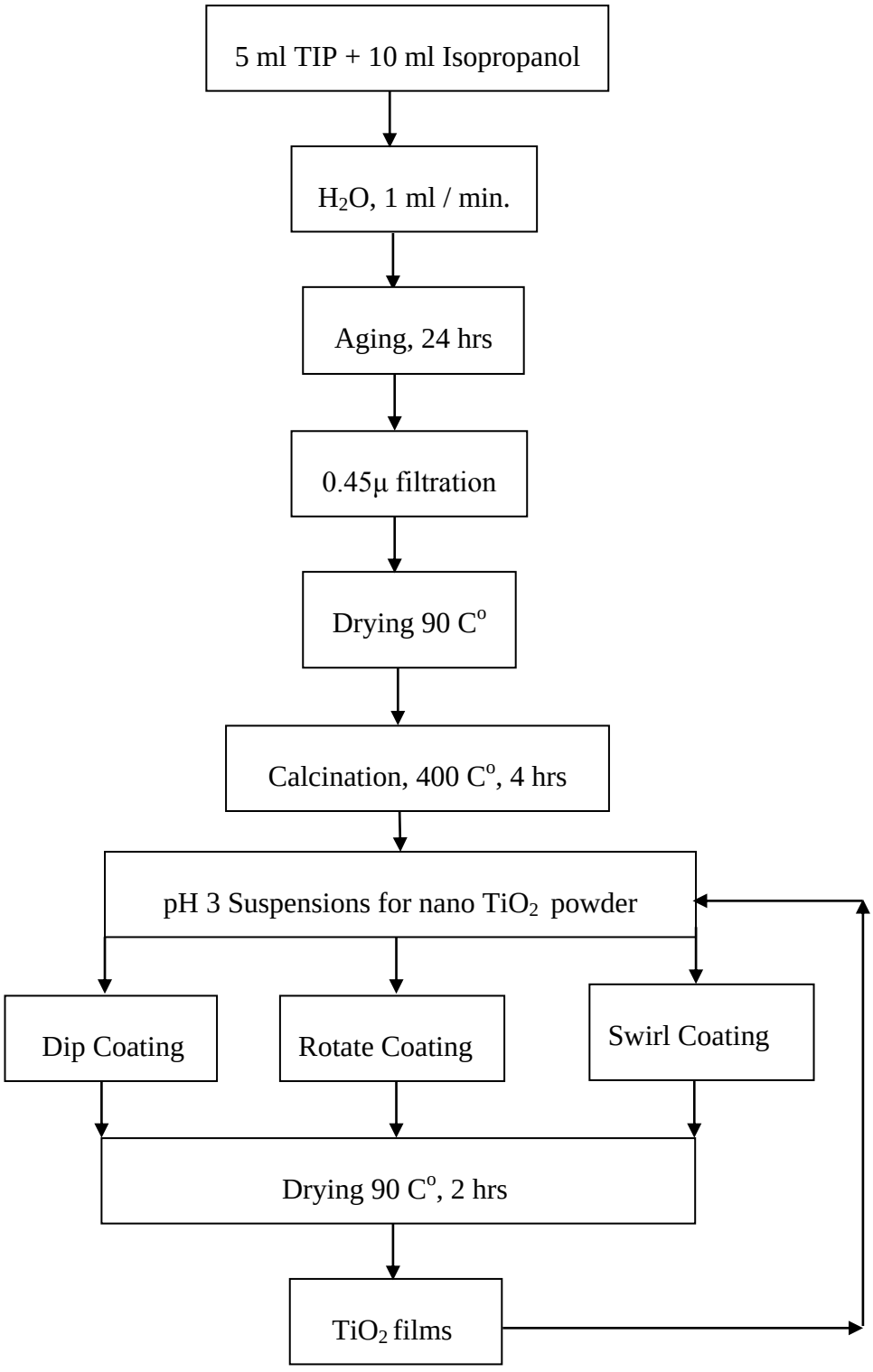

Figure (2-7): Preparation flow diagram of immobilized TiO_2 films on stainless steel slide via several coating methodologies

2.2.14.4 Prototype immobilization assembly

The homemade solar prototype assembly shown in Figure (2-8) has been exploited for the solar light induced catalytic degradation of EBT and MV dyes. The installation prototype is mainly composed of a stainless steel plate coated with TiO_2 located underneath the input contaminated reservoir, an immersion pump as a component of output part (discharge vessel) and O_2 gas cylinder to provide the solution with dissolved oxygen required for the experiment. The 316L stainless steel plate of 20x9 cm total dimensions was coated 5 times (15x8 cm coated dimensions) by means of TiO_2 + CTAB suspension at pH = 3 following rotation (100 rpm) approach (see Figure (2-9)). The edges of the plate were bended towards upside to keep smooth flowing of the contaminated water. The solar degradation experiments were conducted on the days of January 2016 under the following conditions; sunny to partly cloudy, relative humidity 75-80%, from 9 am till 1:30 pm, average temperature 10-12 C^o, flow rate of contaminated water one liter per minute and O_2 bubbling gas flow rate 50-55 ml per minute.

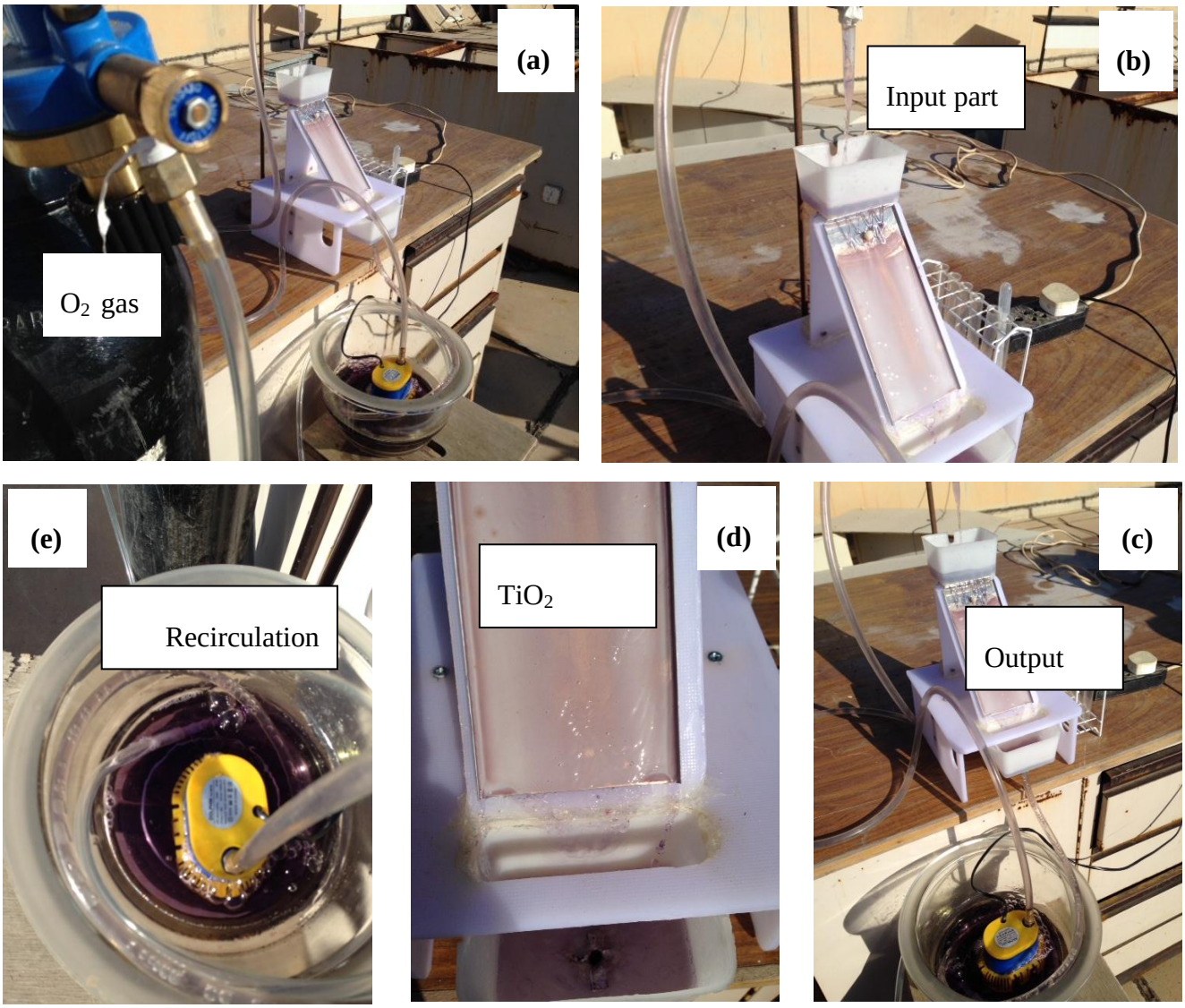

Figure (2-8): Prototype immobilization assembly; (a) General view; (b) Input part; (c) Output part; (d) TiO_2 coated film onto st.st plate ; (e) Recirculation discharge unit

Figure (2-9): TiO_2 coating onto st. st. plate for prototype unit following rotation technique.

2.2.15 Determination of pH of point zero charge (pH_{pzc})

1- 0.01M NaCl aqueous solution was prepared at pH (2, 4, 6, 8, 10).
2- The pH value of the solutions were adjusted with HNO_3 (0.1M)or NaOH (0.1M) solutions.
3- Ten milliliters from each solution kept in contact with 0.02g TiO_2 for 48hrs under vigorous stirring.
4- The supernatent was decanted and its pH was measured.
5- The pH_{pzc} value was determined using the plot of pH_i vs. pH_f.

2.2.16 The study of the adsorption of dye on TiO_2 surface

1- Five hundred ppm EBT stock solution was prepared, and then was diluted to 10, 20, 30, 40, 50, 60, 70, 80, 90 and 100 ppm in 100 ml flask.
2- The calibration curve was drawn by measuring absorbance at 540 nm for all prepared EBT solutions.
3- At natural pH (about 5), 90 ml of 50 ppm EBT was mixed with 10 mg catalyst at speed of 100 rpm.
4- Five ml sample was taken every 15 minutes (after settling), and the catalyst was separated from suspension by centrifuge.
5- The sample was fillterd, and absorbance was measured at optimum wavelength to calculate Qe (adsorption capacity) for each concentration. The optimum contact time was measured by drawing Qe vs. Time.
6- At 30 C^o, natural pH, 100rpm speed and optimum contact time, 50 ml of all the diluted solutions were mixed with 10 mg catalyst to calculate Qe and Ce (equilibrium concentration).
7- Step 6 was repeated again at 40 C^o and 50 C^o for the computation of thermodynamic parameters.

8- Step 6 was repeated again with pHs 3, 7 and 9 as well.

2.2.17 General procedure of photolysis for dyes

Photocatalytic degradation experiments for the synthesized nano anatase TiO_2 photocatalyst were conducted in the photolysis cell with 125 milliliter capacity under visible light with a 500 W halogen lamp which has been used as illumination source. The stock solution of dye (100 ppm) was prepared with NFDW water and diluted to different concentrations for photocatalytic reaction**.** The optimum conditions of photocatalytic decomposition of Eriochrom Black T dye were pH = 3, catalyst loading 80 mg. The pH of the dye solution was already adjusted using dilute aqueous solution of HNO_3. Oxygen gas was bubbled in the solution as induced electron scavenger and also to keep all the TiO_2 in the suspension**.** For methyl violet degradation the optimum conditions were pH =7, catalyst loading= 30 mg**.** The suspension was magnetically stirred for 15 minutes in the dark to ensure adsorption equilibrium**.** During irradiation, samples of 4-5 milliliter were collected at regular times, centrifuged at 3000rpm for 10 minutes and filtered using 0.45μm cellulose membrance. The discolouration was monitored using a single beam visible spectrophotometer by measuring the absorbance at λmax= 540 nm for Eriochrom Black T and 584 nm for Methyl Violet. In most of the experiments, the photocatalytic process was continued until complete mineralization of the compound was achieved.

2.3 Instruments

2.3.1 Refrigerated circulating bath. model (WCR-P12), wisecircu.

2.3.2 Nanofiltered-deionized water supply unit. model (Sm-11), Waterpia

2.3.3 Centrifuge (K centrifuge PLC series.)

2.3.4 Muffle furnace (SX-5-12).

2.3.5 Drying cabinet (K Hot Air Sterilizer).

2.3.6 Apel PD-303 single beam spectrophotometer has been used for visible light absorption measurements .

2.3.7 Double beam Shimadzu UV-VIS spectrophotometer. model (1650 PC) has also been used throughout this work.

2.3.8 Thermostat shaker water bath JEIOTECH (BS-11)

2.3.9 Photoreactor system

The Photoreactor configuration shown in Image (2-1), is local market made and consists of 500W halogen lamp (Philips) which is vertically fixed into stainless steel hollow cylinder of 10 cm in diameter and 27 cm in height. The heating effect stemmed from the lamp was minimized by circulating the water in the hollow cylinder through outlet and inlet slots in cylinder using circulating thermostate chilled water bath. The internal walls of the cylinder were covered with aluminium foil to avoid radiation losses and temperature rising. Lens is used for light collection and focusing. The solutions/suspensions of dye and photocatalyst were magnetically stirred. The flow rate of O_2 was kept at 50-55 mL /min with continuous stirring using a hot plate-stirrer. The concentration of dye was determined from its visible absorbance characteristic and calibration curve method at the wavelength of maximum absorption (540nm) for EBT and (584nm) for MV.

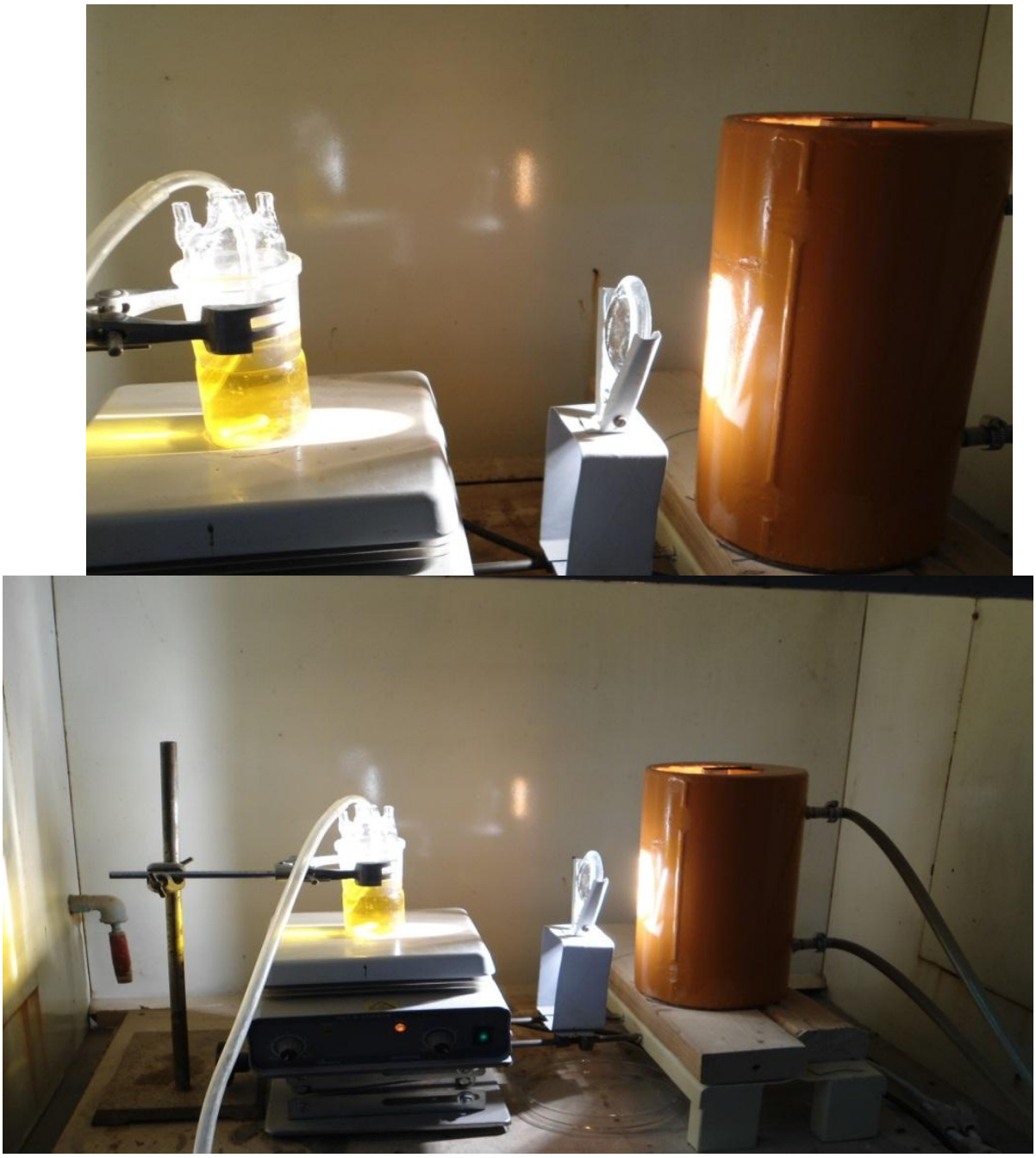

Image (2-1): Photolysis unit of visible light source

2.3.10 Photolysis unit of UV source

The photolysis unit which is shown in (Image 2-2), is laboratory-built (local market) system consisting of ultraviolet light source (125 W)

medium pressure mercury lamp (MPML) 365 nm wavelength fitted with a focusing lens to assure parallel beam of light.

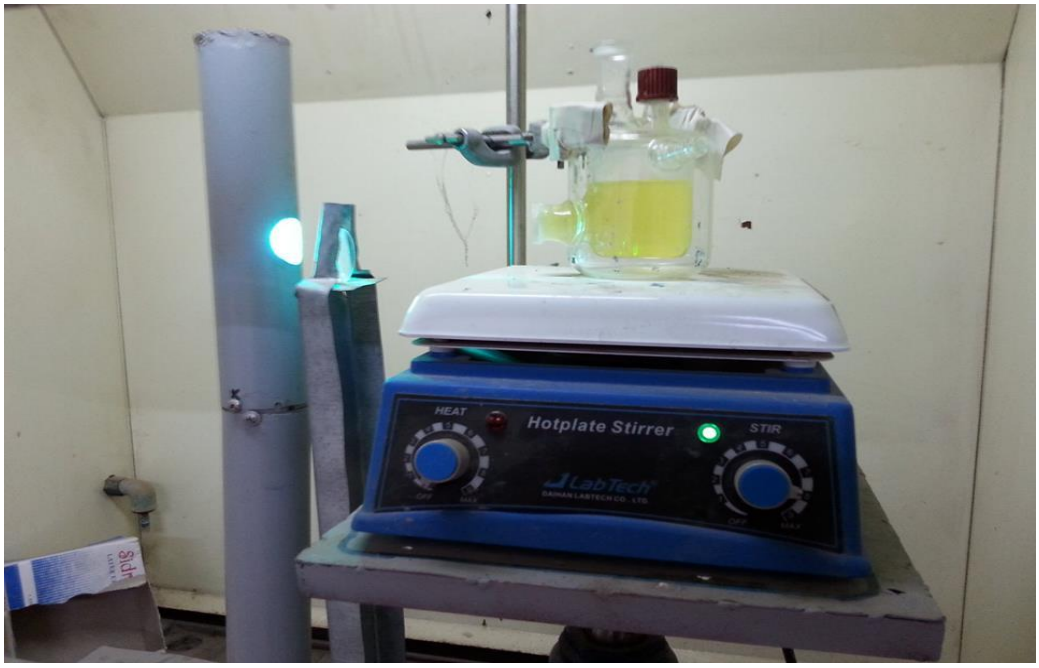

Image (2-2): photolysis unit of UV light source

2.3.11 X-ray Spectrometer

The X-ray diffraction (XRD) patterns were obtained on a Philips X-pert pro, panalytical XRD machine (image 2-3, KIT, Germany)using a Cu target Ka radiation (λ= 1.541A˚) to determine the crystalline size. The accelerating voltage and the applied current were 40 kV and 30 mA, respectively. The XRD patterns was at the scanning range 2θ from 5^{o} to 120^{o}.

2.3.12 Scanning Electron Microscopy (SEM) coupled with Energy dispersive X-ray spectroscopy (EDXS)

The LEO 982 SEM coupled with EDX was used to characterize the morphological and structural properties of the samples. Nearly 1 mg of a

sample was mounted on a SEM sample holder and was sputtered with gold prior to analysis for better conductivity and resolution of the sample. This SEM permits ultra high resolution imaging of semiconductor materials (Image 2-4, KIT, Germany).

2.3.13 Chemisorption Analyzer Brunauer, Emmett and Teller (BET)

Surface area and pore distribution of the samples were determined using nitrogen adsorption/desorption isotherm by means of micromeritics Autochem Chemisorption analyzer (Image 2-5, KIT, Germany).

2.3.14 Transmission Electron Microscopy (TEM)

High resolution Philips Tecnai TEM (Image 2-6, KIT, Germany) was used for the image observation for specimen and particle size analysis well. Images are supported by means of DF-STEM where Z-contrast imaging facilitates further structural analysis.

Image (2-3): Pananalytical Philips diffractometer (Karlruhe Institute of Technology, Germany)

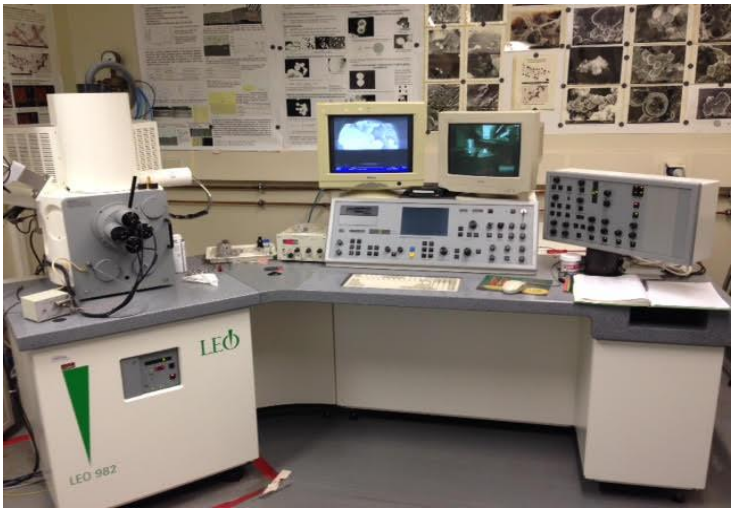

Image (2-4): LEO 982 SEM coupled with EDX (Karlsruhe Institute of Technology, Germany)

Image (2-5): Micromeritics AutoChem HP Chemisorption Analyzer (BET) (Karlsruhe Institute of Technology, Germany)

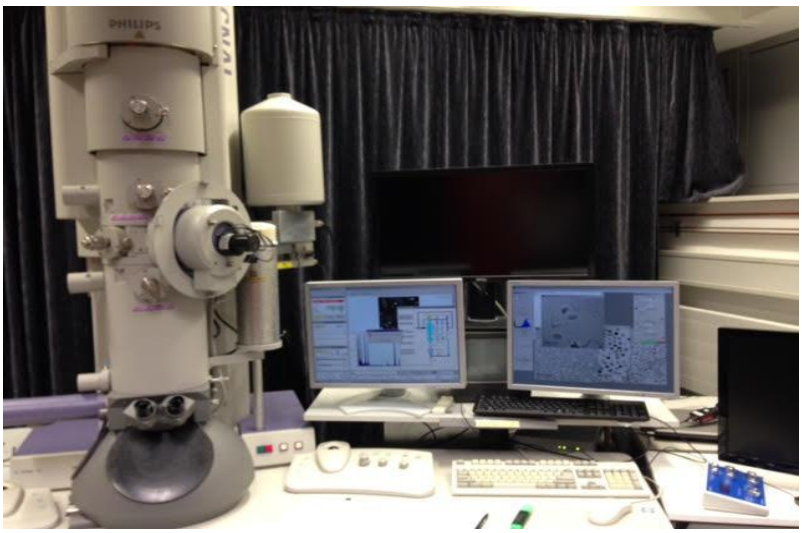

Image (2-6): Philips Technai TEM (Karlsruhe Institute of Technology, Germany)

CHAPTER THREE

DISCUSSION

3. Results and Discussion

3.1 UV-VIS Spectroscopic features of the anionic EBT and cationic MV dyes

Anionic dye Eriochrom Black T ($C_{20}H_{12}N_3O_7SNa$) (EBT), was chosen as a simple model of a series of common azo-dyes largely used in the industry. This compound, which is a well known metallochromic indicator widely used in complexometric titration, is blue in a buffer solution at pH 10 and it turns red when it forms a complex with calcium, magnesium or other matel ions. The chemical structure of EBT is shown in Figure (3-1). Figure (3-2) shows the UV-VIS spectrophotometric scan in the range of 250-800 nm. The molar extinction coefficient (absorptivity, ε) of 10 ppm of EBT in NFDW was measured at the maximum absorption wavelength, 540 nm, using Beer-lambert equation ($A= \varepsilon bc$), where A= absorbance, b = absorption light path, 1 cm and c = molar concentration of EBT. The absorptivity (ε) has been $7.1428 \times 10^{+4}$ L. mol^{-1}. cm^{-1}. The UV–Visible spectrum of EBT (Figure 3-2) showed two absorption maxima [63]. The first band observed at wavelength of 340 nm and the second band with higher intensity, at wavelength of 540 nm. The latter band was used to monitor the photocatalytic degradation of EBT.

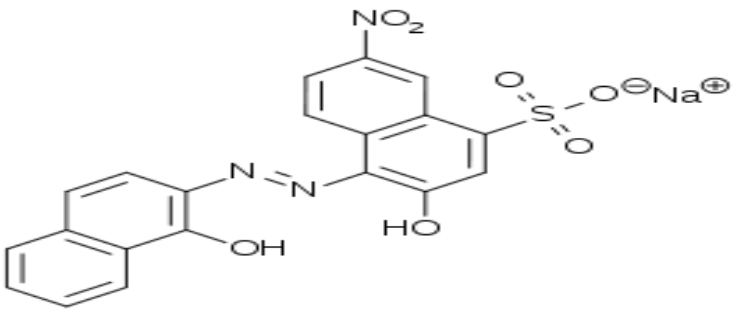

Figure (3-1): Chemical structure of Eriochrom Black T (EBT)

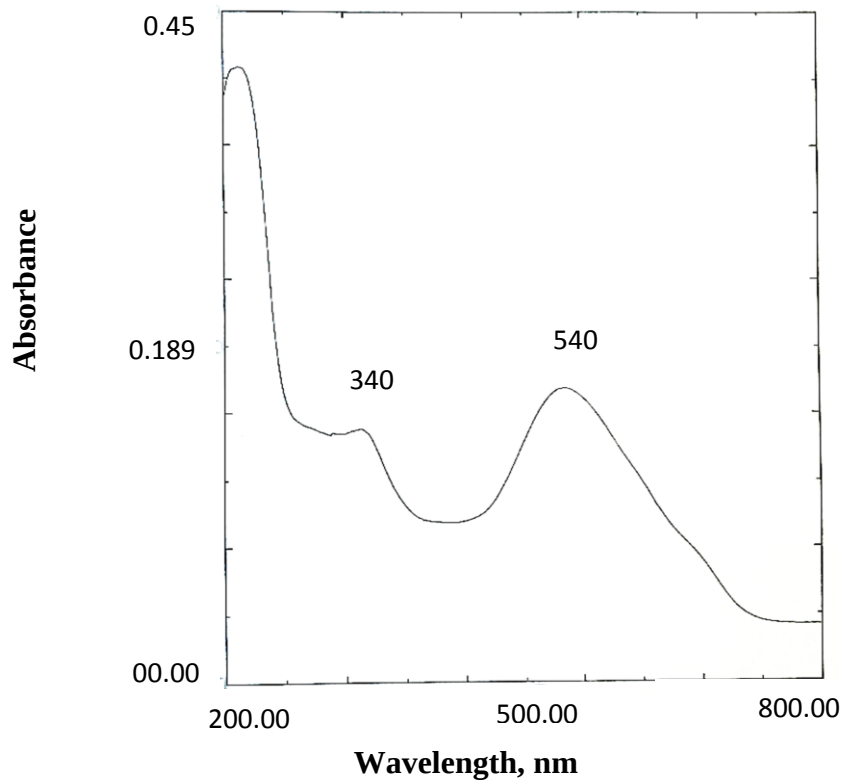

Figure (3-2): UV-VIS spectrum for Eriochrom Black T

Upon variation of solution pH towards lower and higher values a tautomeric equilibrium exists, Figure (3-3), between the ammonium form and azonium form. Consequently this phenomenon leads to increase in the absorbed wavelength due to the red shift [64], as explicitly exhibited in Figure (3-4).

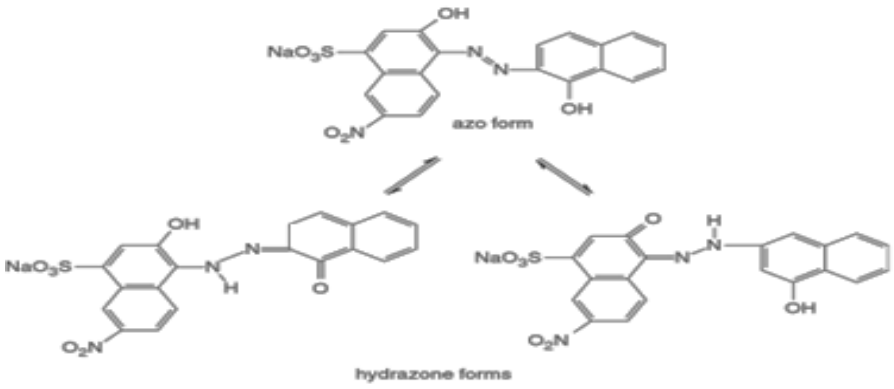

Figure (3-3): Protonation and tautomeric equilibrium of Eriochrom Black T molecule in acidic solution

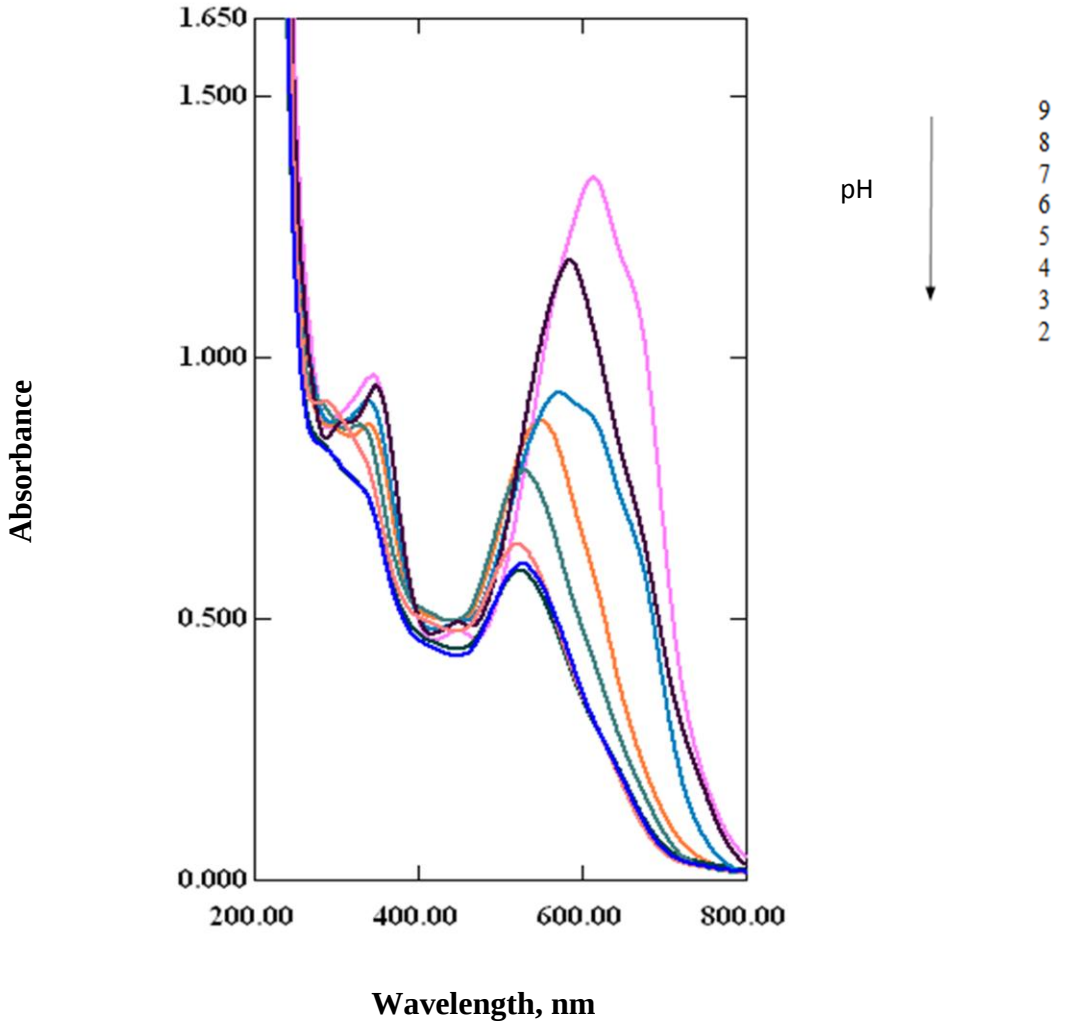

Figure (3-4): UV-VIS scan of Eriochrom Black T at different pH values at different concentration

Figure (3-5) presents the chemical structure of Methyl Violet (MV) dye [65]. This water-soluble dye has a molar extinction coefficient equals to 5.2x 10^{+5} L. mol^{-1}. cm^{-1} for molar concentration of 2.5 x 10^{-5}mole/L. The peak at ƛ= 584 nm has the highest intensity, Figure (3-6).

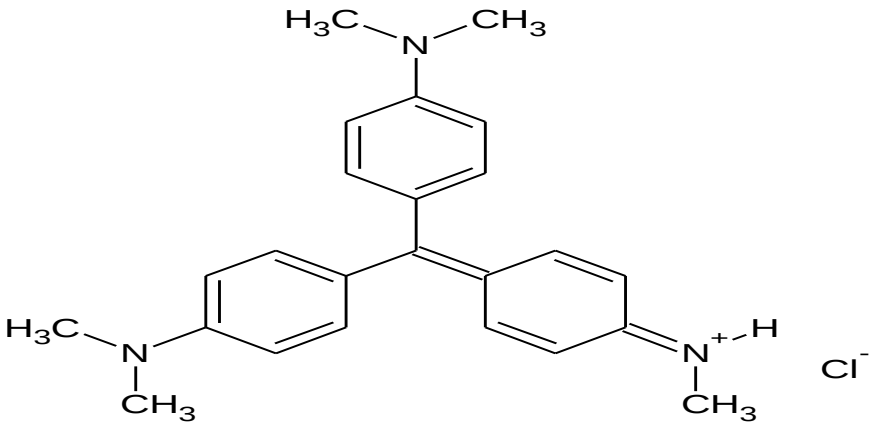

Figure (3-5): Chemical structure of Methyl Violet (MV)

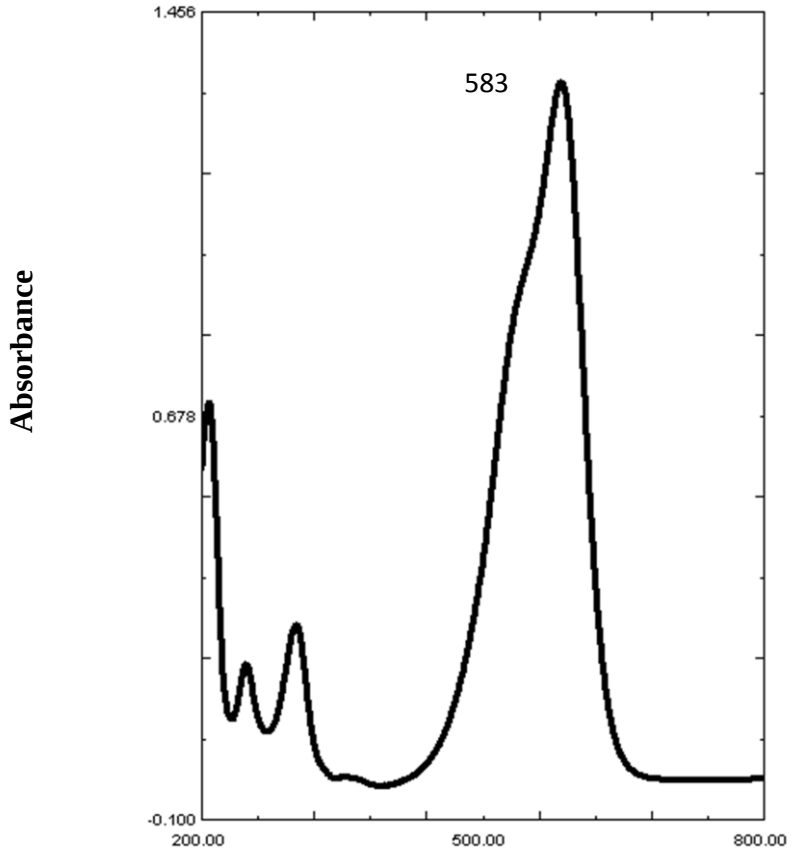

Figure (3-6): UV-VIS spectrum for Methyl Violet

MV^+ is the predominant form of Methyl Violet (also called Crystal Violet) in the solid state and in aqueous solution across a broad range of pH values from pH 2 to 9. The positive charge shown on the central carbon atom in Figure (3-7A) is delocalized via resonance to the three nitrogen atoms. See Figure (3-7B) for one of the three additional resonance forms with the positive charge on a nitrogen atom. Delocalization of the charge across the system of double bonds in the benzene rings stabilizes the carbocation and is responsible for the vibrant purple color of the dye [66].

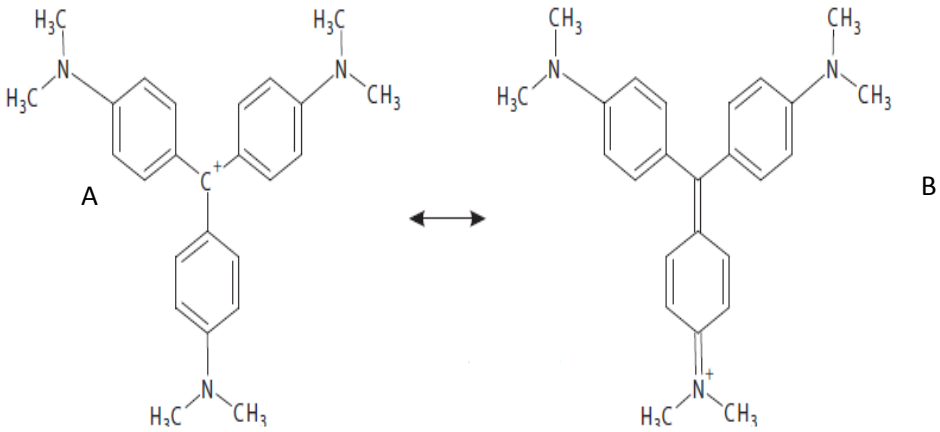

Figure (3-7): Structure of Methyl Violet

Figure (3-8) presents the UV-VIS scan of Methyl Violet at different pH values.

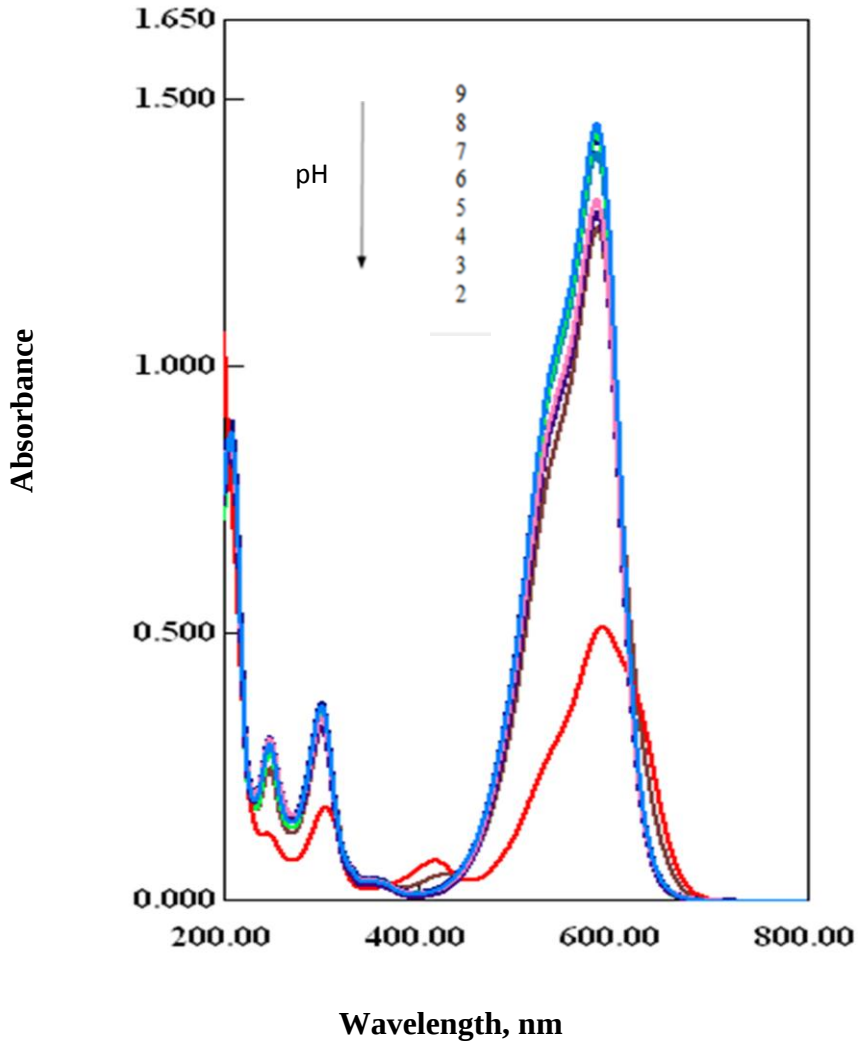

Figure (3-8): UV-VIS scan of Methyl Violet at different pH values

3.2 Characterization of the laboratory synthesized anatase TiO_2 nanoparticles

3.2.1 Morphology, Phase and composition aspects

The surface morphologies of neat reference anatase TiO_2 nanoparticles and the laboratory synthesized anatase TiO_2 nanoparticles are characterized by SEM, and shown in Figure (3-9). The SEM images reveal smooth, spherical and homogeneous surfaces formed by very fine separated and aggregated particles for both reference, synthesized nano TiO_2 powders. A closer look at the images peers to nanosized TiO_2 particles, and further, a lower size of the laboratory prepared TiO_2 (10-17 nm) in comparison to that of reference TiO_2 (19-37 nm). This verifies solely the efficiency of the nano material synthesis on laboratory scale following sol gel methodology.

The powder X-ray diffraction (XRD) technique was used to characterize the crystal structure of the reference and synthesized TiO_2 nanoparticles. The XRD patterns are presented in Figure (3-10) which merged upon using Cu Kα radiation (0.15425 nm) in the range of 2θ from 5 to 120 with scan rate of $2\theta = 0.10\ s^{1-}$. These patterns were used to determine the identity of any phase present. The TiO_2 mainly exists in anatase, rutile and brookite phases [67] among them, best photocatalytic activities have been found from anatase phase. The XRD peak at $2\theta = 25.4^o$ is often taken as the characteristic peak of anatase (101) crystal phase structure [62]. Accordingly, the diffraction signal which is assigned to the anatase (101) structure at 25.5^o (Figure 3-10 b ,in this work) is similar and clearly observed in reference TiO_2 (25.4^o), Figure (3-10a).

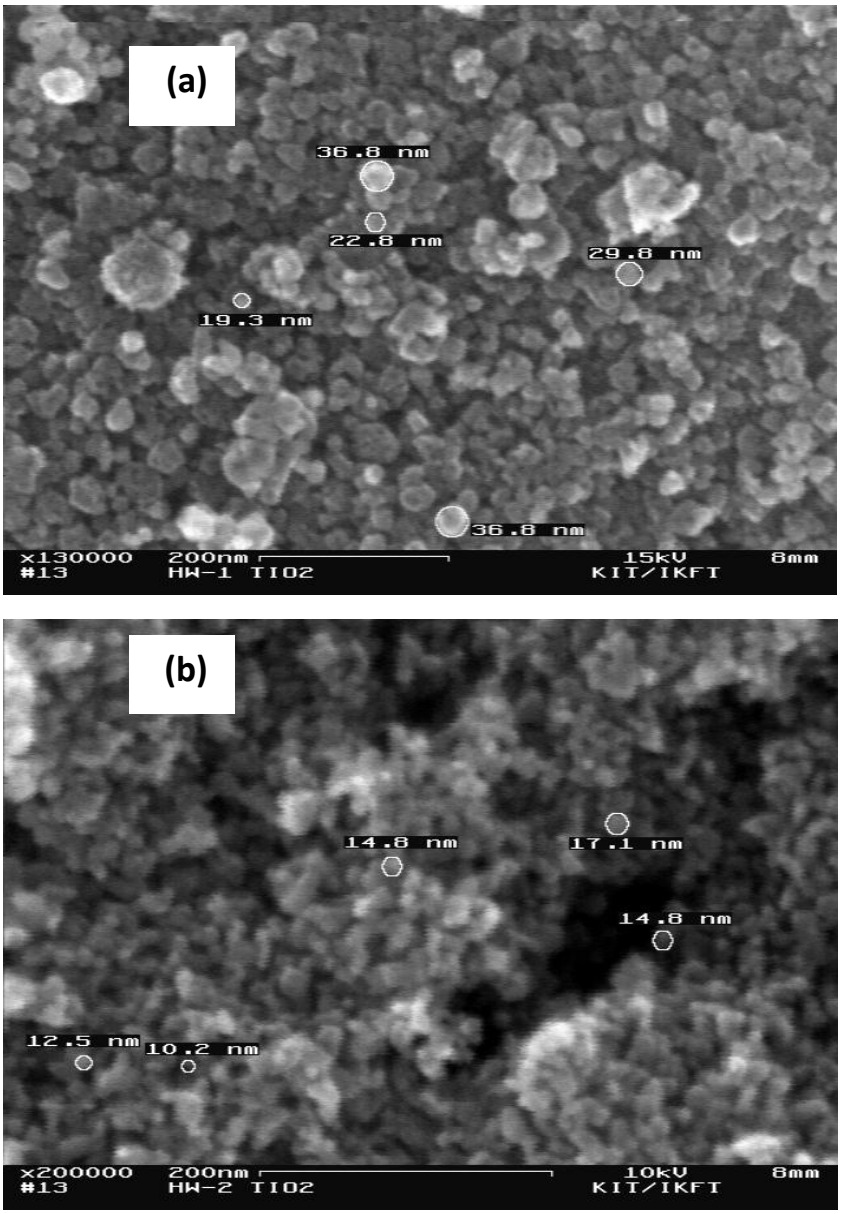

Figure (3-9): Scanning Electron Microscope (SEM) micrographs for; (a) Aldrich reference nano anatase TiO_2; (b) Synthesized nano anatase TiO_2

The average crystalline size of TiO_2 was calculated using the Scherrer equation on diffraction plane (101) according to the following expression [61].

Crystalline size = B x λ / F x cosθ (3-1)

where λ is the Cu K_α (0.1541 nm) radiation wavelength, F is the full width at half maximum (FWHM) of the (1 0 1) peak, θ is the half angle of the diffraction peak on the 2Theta scale and B is the shape factor of the particle whose value is computed as follows ;

$$B = 2\sqrt{\frac{\ln 2}{\Pi}} = 2\sqrt{\frac{0.693}{3.14}} = 0.94 \qquad (3\text{-}2)$$

The average crystallite size for reference and synthesized nano TiO_2 particles were 17.48 and 16.14 nm, respectively. The peak width inversely proportional with particle size in which by increasing the peak width the size of nano TiO_2 decreases. This is another self endorsement of lower particle size of the laboratory scale prepared nano TiO_2 in comparison to the reference nano TiO_2 particles.

Prior to the application of the synthesized anatase nano TiO_2 powder on the photo degradation of EBT anionic dye and MV cationic dye, the atomic composition of the synthesized nano anatase TiO_2 was verified using Energy Dispersive X-ray Spectrometer (EDXS). The spectra shown in Figure (3-11b) for the prepared nano anatase TiO_2 is to an excellent extent similar to that of reference specimen which is shown in Figure (3-11 a).

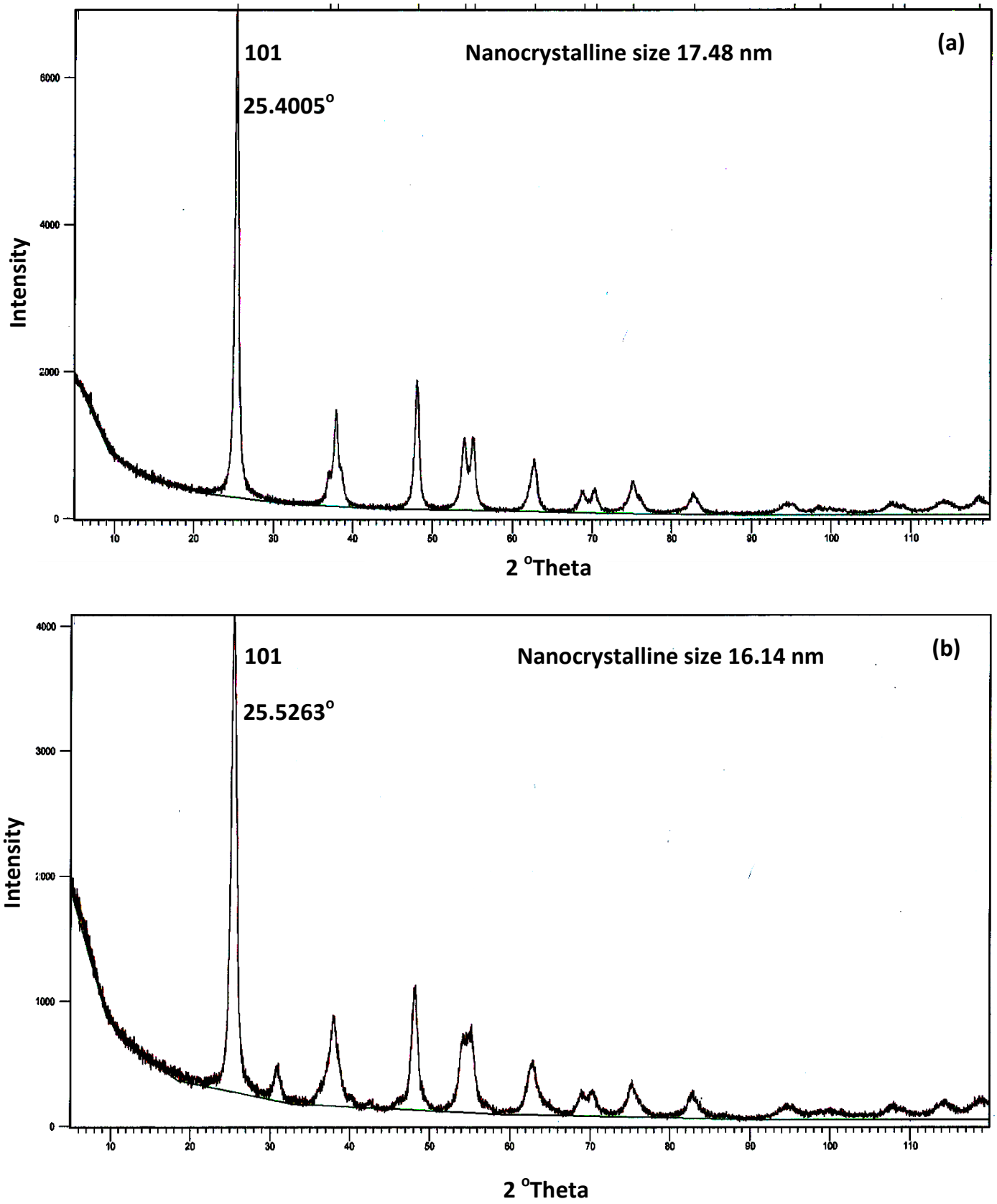

Figure (3-10): X-Ray Diffraction (XRD) pattern for;(a) Aldrich reference nano anatase TiO_2;(b)Synthesized nano anatase TiO_2

Element	Mass%	Atom%
O	38.17	64.89
Ti	61.83	35.11
total	100.00	

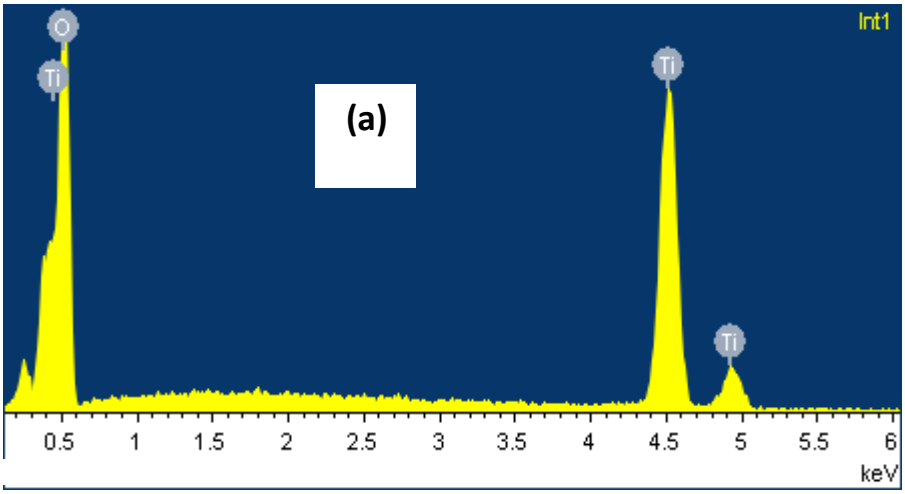

Element	Mass%	Atom%
O	39.87	66.44
Ti	59.90	33.34
total	100.00	

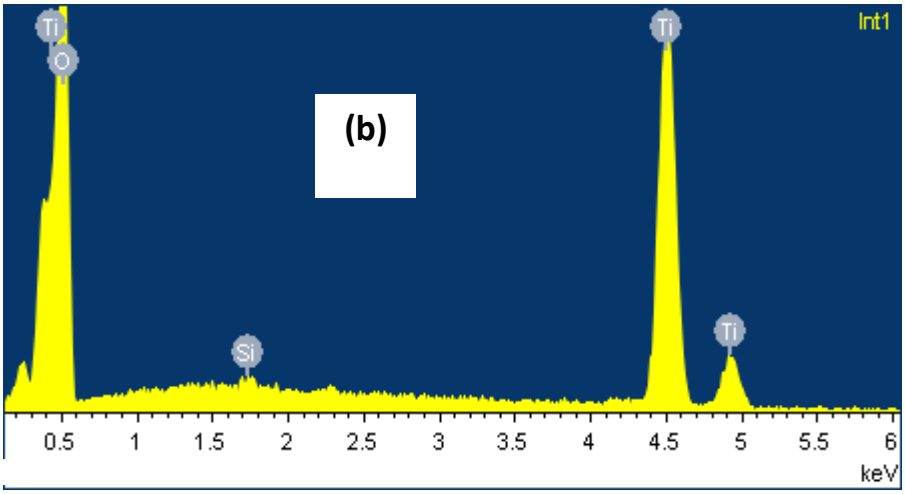

Figure (3-11): EDX spectra and composition of ;(a) Aldrich reference TiO_2 nano powder; (b) Synthesized nano TiO_2 powder.

3.2.2 Porosity, surface area and particle size analysis

The porosity and surface area of the reference and synthesized anatase TiO_2 nanoparticles are measured employing Brunauer, Emmett and Teller (BET) methodology, which based on nitrogen adsorbtion-desorption isotherms. The inset in Figure (3-12a) depicts the adsorption-desorption isotherm plot, for the reference specimen, which results in porosity and surface area of 7.845 nm and 109.4 m^2/g, respectively. Whereas, the inset in Figure (3-12b) which illustrates the adsorption-desorption isotherm plot for the synthesized specimen, results in porosity and surface area of 6.804 nm and 130.14 m^2/g, respectively. On one hand, one could conclude that both powders are mesoporous since their porosity is within the range from 2 to 50 nm [68]. On the other hand, the synthesized nano TiO_2 particles posses lower pore size and higher surface area than that of the reference nano TiO_2 particles. In other words, the speed of the photocatalytic reaction is enhanced further in the case of prepared nano TiO_2 particles. Hence, this is again a stand alone confirmation for the high quality synthesis of nano TiO_2 material on laboratory scale.

Other than the measurement of particle size using SEM and crystalline size employing XRD, Transmission Electron Microscope (TEM) was also exploited to explore the particle size of the reference and synthesized nano anatase TiO_2 particles as illustrated in Figures (3-13a) and (3-13b), respectively. A small amount of dry powder was dispersed in ethanol by ultrasonic agitation. Two droplets of the suspension were placed on a carbon-coated copper grid, dried in air and analyzed with TEM. A close

look at Figure (3-13) may verify the lower particle size of the synthesized nano TiO_2 particles than that of the reference sample. Based on the above results, the particle size values of the reference and laboratory prepared

nano TiO_2 powders determined by XRD and SEM techniques are in an excellent agreement with the average particle size derived from TEM analysis.

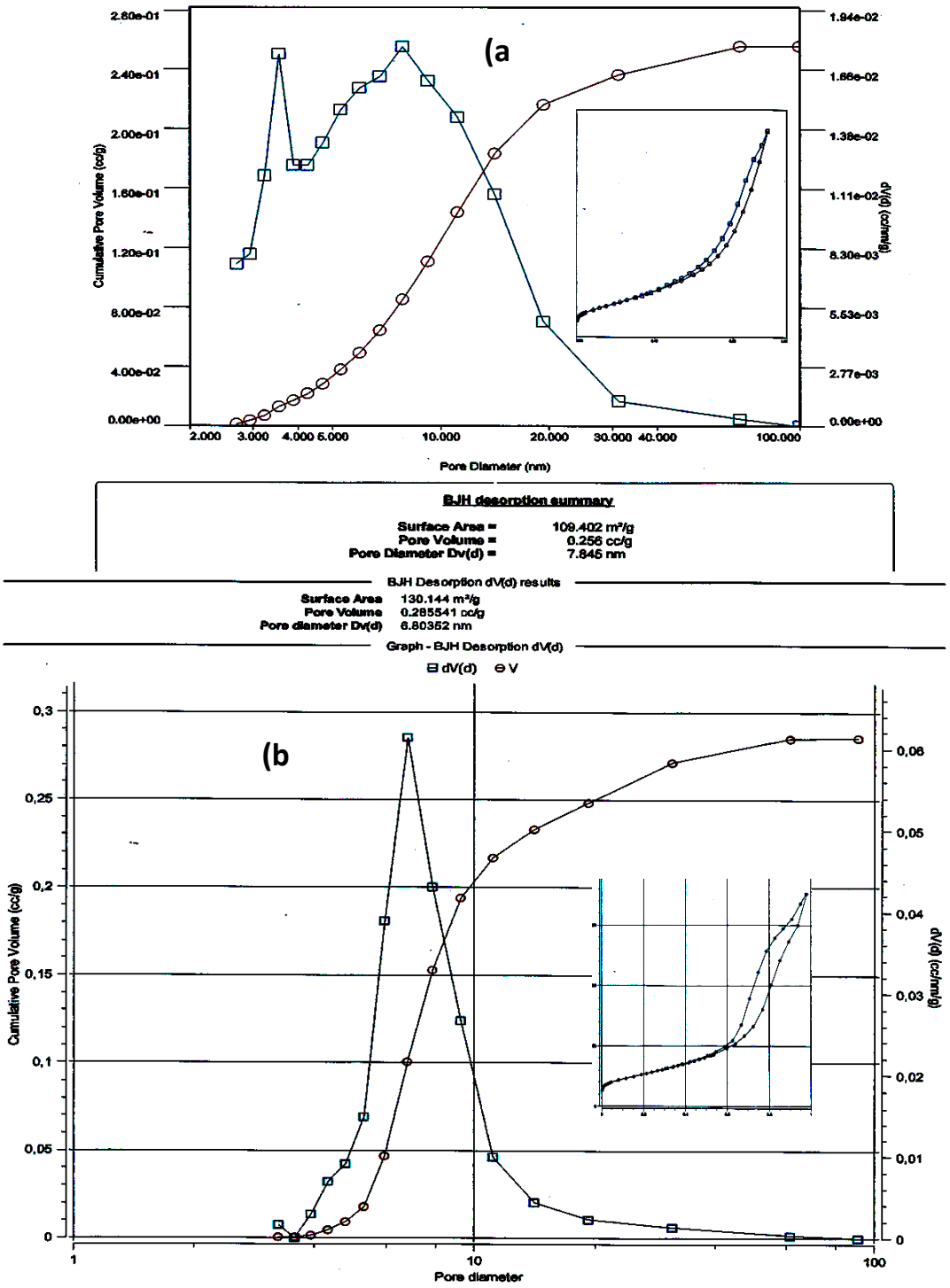

Figure (3-12): Pore size measurements for ;(a) Aldrich standard nano anatase TiO_2; (b) Synthesized nano anatase TiO_2; insets represent adsorption-desorption isotherms

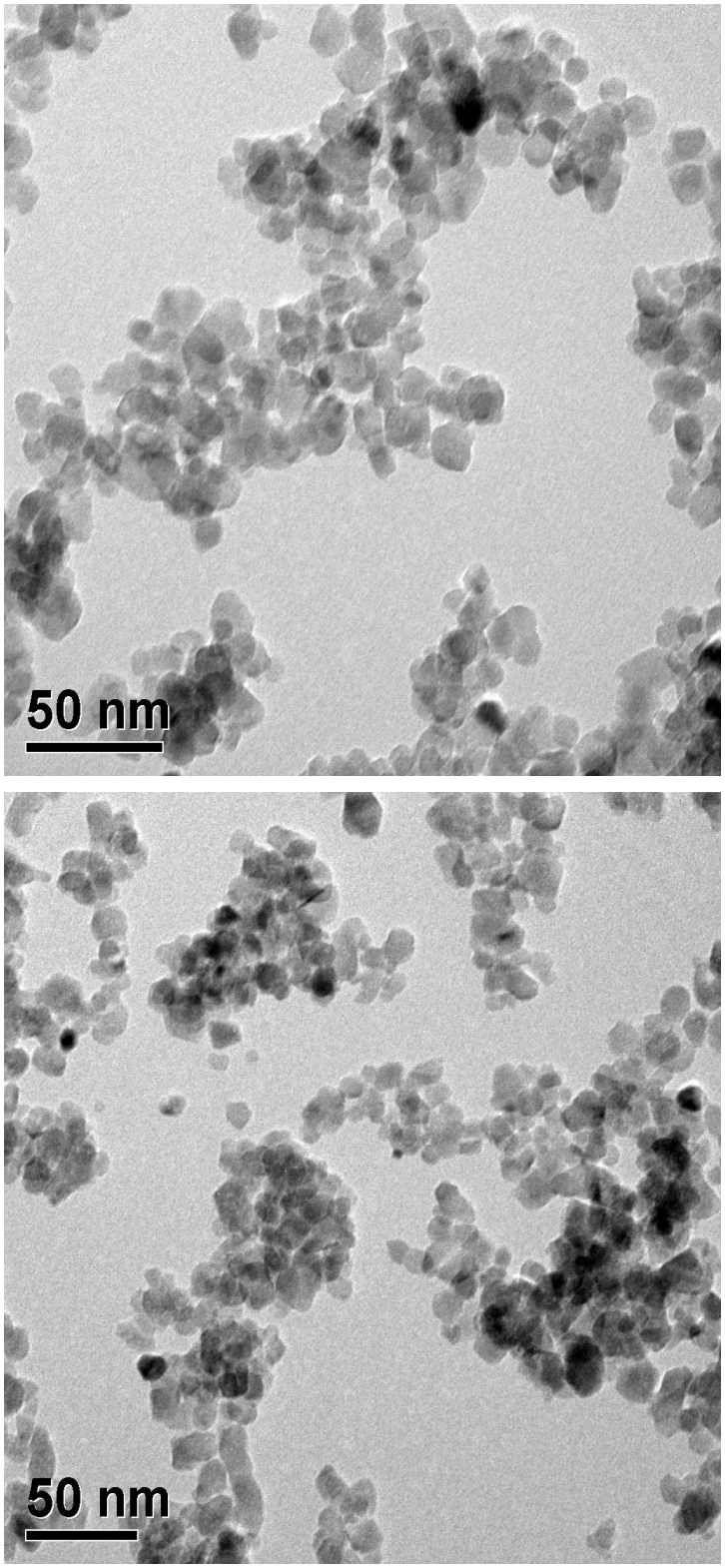

Figure (3-13): Transmission Electron Microscope (TEM) micrograph for; (a) Aldrich standard anano anatase TiO_2 particles; (b) Synthesized nano anatase TiO_2 particles

3.3 Control experiments

A series of control experiments were carried out to assure that the decolorizing process of dyes is pure heterogeneous photocatalytic reaction rather than homogeneous or/and adsorption phenomenon. The photolysis experiments, in the absence of TiO_2, at room temperature for duration of 180 minutes and the pH of dye solution about 5, showed that the degradation of EBT was almost negligible under visible illumination (Figure 3-14 a) , (Figure 3-15a) and also under UV irradiation (Figure 3-14b), (Figure 3-15b) for EBT and MV respectivily, and this verifies that the optical homogeneous photolysis did not happen under the ongoing experimental conditions. On the other hand and to ascertain that the reaction is not only adsorption but both adsorption and photocatalysis reactions, the synthesized nano TiO_2 powder was stirred together with the dye in the dark for 180 minutes. Table (3-1), Figure (3-14c) and Figure (3-15b) depict that only ≈ 20% of dye adsorption onto TiO_2 nano particles took place. While the percent increased when dye was mixed with catalyst under visible and irradiation and acidic pH = 3, Figurs (3-14d) and (3-15c) for EBT and MV, respectively. This verifies the self sensitization phenomenon which leads to in situ photodegradation in which the color removal of EBT pollutant was almost complete in 40 min under halogen lamp illumination and at optimum conditions pH = 3, 80 mg TiO_2, Figure (3-16). The last experiment in dark where there was a slight degradation in the dye solution with the presence of the catalyst, was due to the adsorption of Eriochrome Black T on the surface of the TiO_2 [69]. Nevertheless, the extent of adsorption is necessary to some extent in the evolution of the photochemical process [70]. Figure (3-14) and Table (3-1) display the control tests of photodegradation experiments listed below;

a) EBT (10ppm) + visible light + during 3h

b) EBT (10ppm) + UV light + during 3h

c) EBT (10ppm) + TiO_2 (0.05g) + dark + during 3h

d) EBT (10ppm) + TiO_2 (0.05 g) + visible light + during 3h

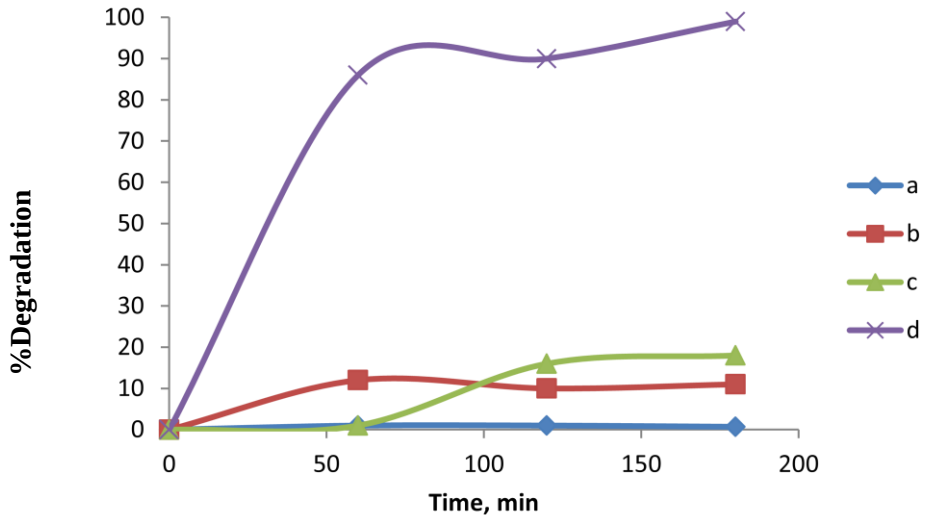

Figure (3-14): Degradation percent of Eriochrom Black T for control experiments

Table (3-1): Degradation percent of Eriochrom Black T for each control

Time,min	a	b	c	d
0	0	0	0	0
60	1	12	1	86
120	1	10	16	90
180	0.7	11	18	99

Figure (3-15) displays the control tests results for photodegradation of MV dye solution. The first set was implemented by exposing MV to Vis. light source with absence of TiO_2 photocatalyst Figure (3-15a). The second set was performed with MV solution exposed to TiO_2 without Vis. light irradiation (in dark), Figure (3-15b). The last set was accomplished in the presence of Vis. light and TiO_2 semiconductor, which represents the photocatalysis circumstances. A very small change in the concentration of MV and no significant degradation was observed when only TiO_2 is used in dark or when only Vis. light is present. Hence, MV could be degraded efficiently via by Vis. light illuminated in presence of TiO_2. Accordingly, these experiments demonstrated that both Vis. irradiation and the TiO_2 photocatalyst are needed for the effective photolysis of MV dye also. This clearly indicates that this phenomenon is photocatalytic in nature [71], and confirms explicitly the self or in situ sensitization phenomenon.

Time,min	Deg.% a	Deg.% b	Deg.% c
0	0	0	0
60	10	50	25
120	18	25	69
180	20	22	87

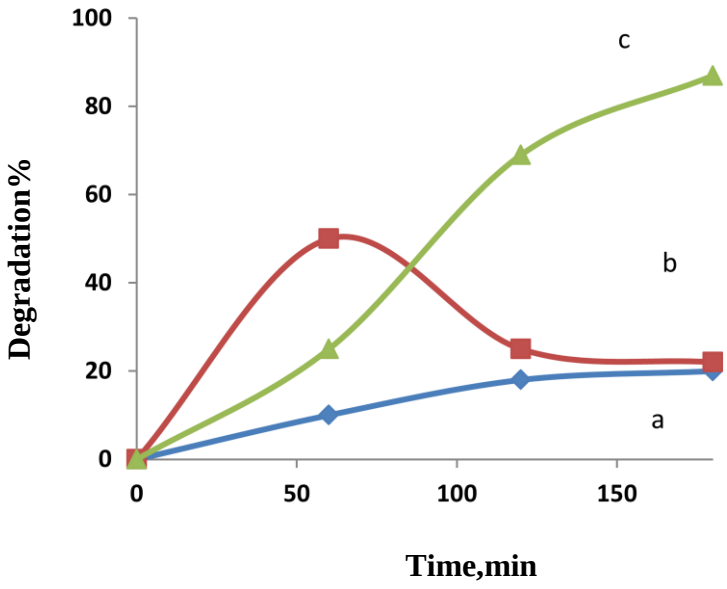

Figure (3-15): Degradation percent of Methyl Violet as a function of irradiation time: (a) Vis. irradiation in absence of TiO_2; (b) TiO_2 in dark (c) Vis. illumination in presence of TiO_2

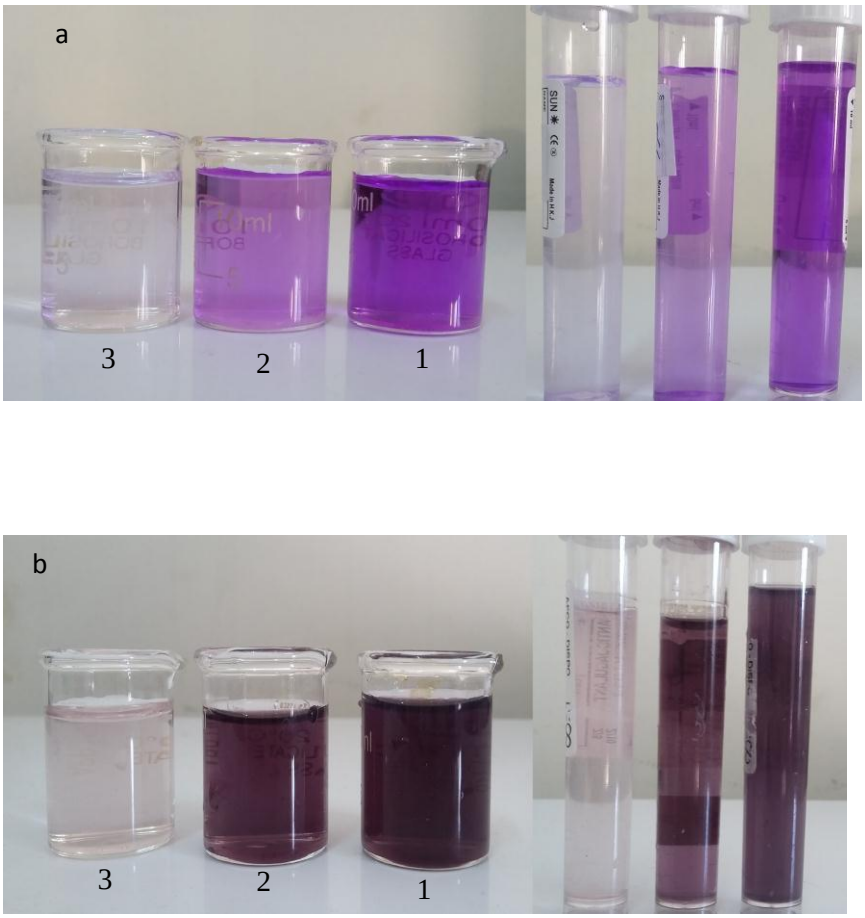

Figure (3-16): Self sensitization (in situ sensitization) phenomenon; (1) Initial solution; (2) After adsorption; (3) After visible illumination for a) MV; b) EBT dye.

3.4 Adsorption of EBT onto TiO_2 nanoparticles

3.4.1 Effect of contact time

The effect of contact time on the adsorbed amount of EBT dye per unit of adsorbent was investigated at room temperature with constant pH and dye concentration. Figure (3-17) and Table (3-2) show the variation of Qe and Ce of 50 ppm EBT at 298K and pH =5.

The dye adsorption increased significantly as the shaking time increased upto 15 minutes with a quick uptake of the dye. The adsorption rate

however decreased to a stable value with increase in contact time due to probably a shortage of available adsorption sites for binding [72]. However, a maximum value of adsorption is attained after 30 minutes of shaking time. Therefore, the time of 30 minutes may be treated as the optimum contact time and accordingly was used for the following adsorption experiments.

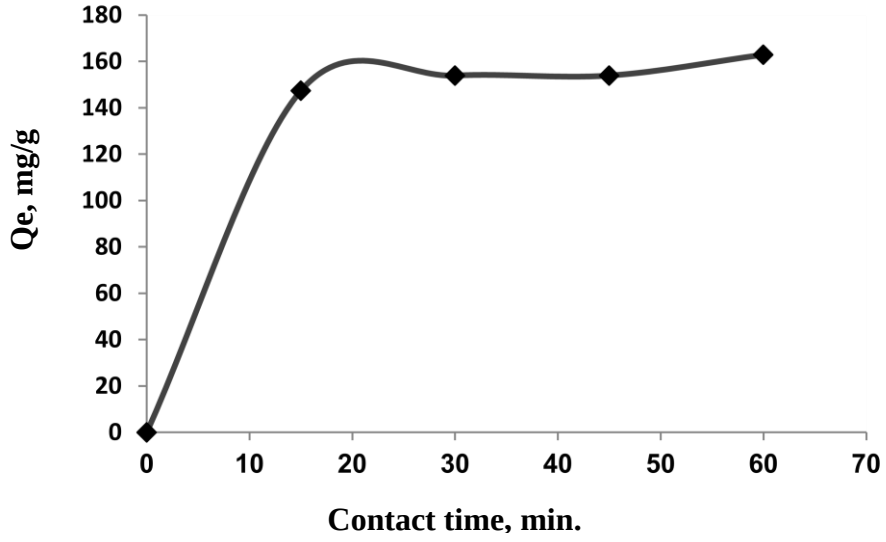

Figure (3-17): The variation of Qe with contact time of 50 mg EBT L^{-1} solution at 298K temperature and pH=5

Table (3-2): The values of Q_e and C_e at different time of adsorption for 50ppm of EBT solution at 298K temperature

Time ,min	C_e,mg/l	Q_e,mg/g
15	41.5	147.3
30	40.8	153.9
45	40.8	153.9
60	39.8	162.9

3.4.2 The Effect of pH

The pH of dye solution has been identified as one of the significant parameter because it plays an important role in the whole adsorption process and particularly on the adsorption capacity [58]. The activity of adsorption depends on the solution pH, since variation in pH leads to the variation in the degree of ionization of the adsorptive molecule and the surface properties of adsorbent [73]. From Figure (3-18) we observe that the sorption of EBT dye attained the maximum at the initial pH = 3 and decreased with increasing the pH within the investigation range of 5– 9. At alkaline pH, two governing factors play a significant role, first, lower adsorption of anionic dye, EBT, due to the presence of excess of ^{-}OH ions which competing with the dye anions for the adsorption sites [74], and on the other hand, TiO_2 is negatively charged at higher pH, which also contributes in the electrostatic repulsion between the negatively charged dye molecule and the negatively charged adsorbent [53]. Whereas, as the pH of the system decreases, the number of positively charged surface sites on the adsorbent increases and consequently favors the adsorption of the anions due to Columbic electrostatic attraction [74]. One could also report that at high pH the sulphonic acid group is completely deprotonated which make the dye molecule more soluble in water, so the adsorption decreased with increasing pH.

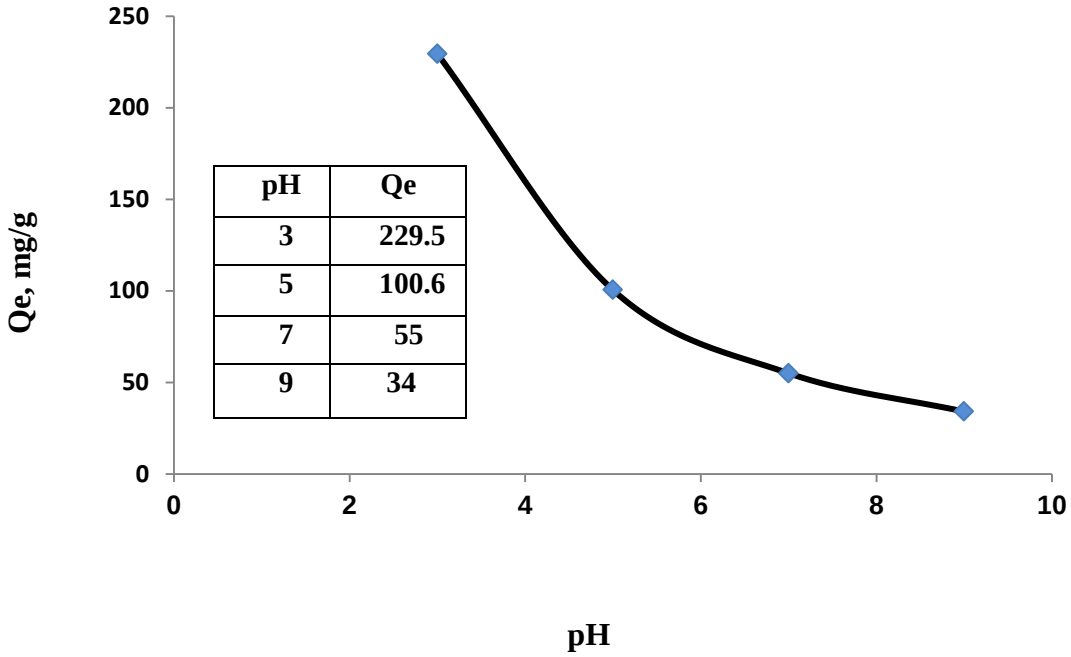

Figure (3-18): Effect of initial pH on the sorption of EBT on TiO_2

3.4.3 Effect of adsorbent loading

The adsorbent loading determines the capacity of the adsorbent for a given initial dye concentration. Figure (3-19) illustrates the impact of adsorbent loading on the removal of 50 mg L^{-1} EBT dye. The dye removal percentage extends as the adsorbent dose increases from 0.1 to 0.4 g. At a low loading of 0.1 g TiO_2, there is firm competition between the EBT molecules due to the limited number of available binding sites; hence a low sorption was achieved. An increase in adsorbent dose to 0.4 g certainly causes a corresponding increase in removal yield due to higher active adsorption sites [75].

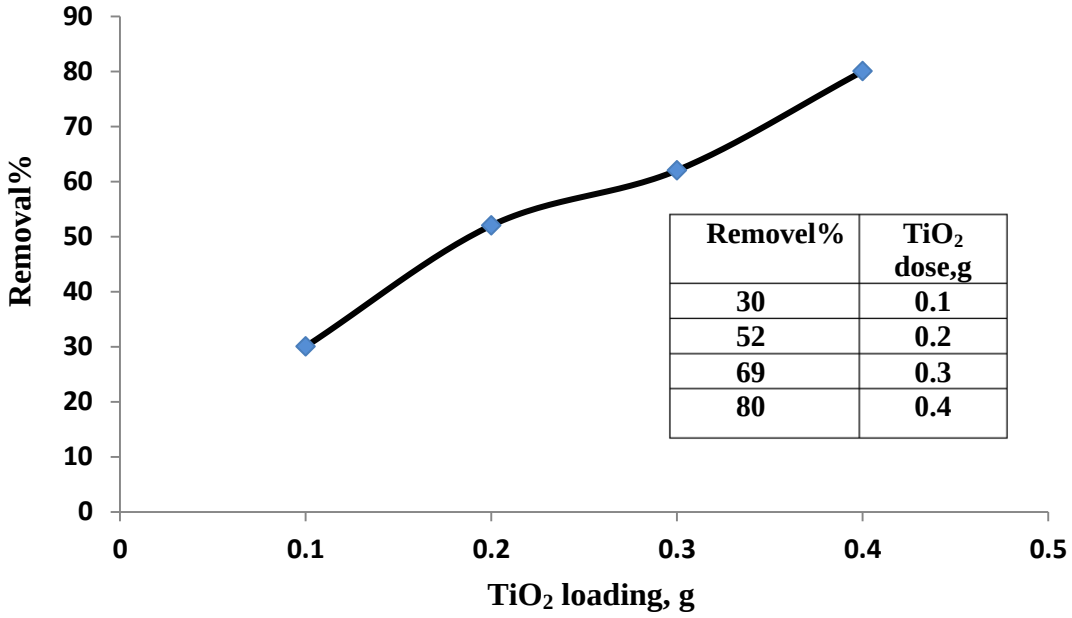

Figure (3-19): Effect of adsorbent loading on EBT removal

3.4.4 Effect of initial dye concentration

The effect of initial dye concentration depends on the immediate relation between the concentration of the dye and the available sites on an adsorbent surface [52]. From Fig. (3-20) we observe that the adsorption capacity Q_e increases with increasing the initial dye concentration until attains the maximum at Q_e = 143 mg/g, and then starts decreasing. This is due to saturation of adsorption sites of the adsorbent material [75].

Hence, the amount of adsorbed EBT is highly dependent on the initial dye concentration**.**

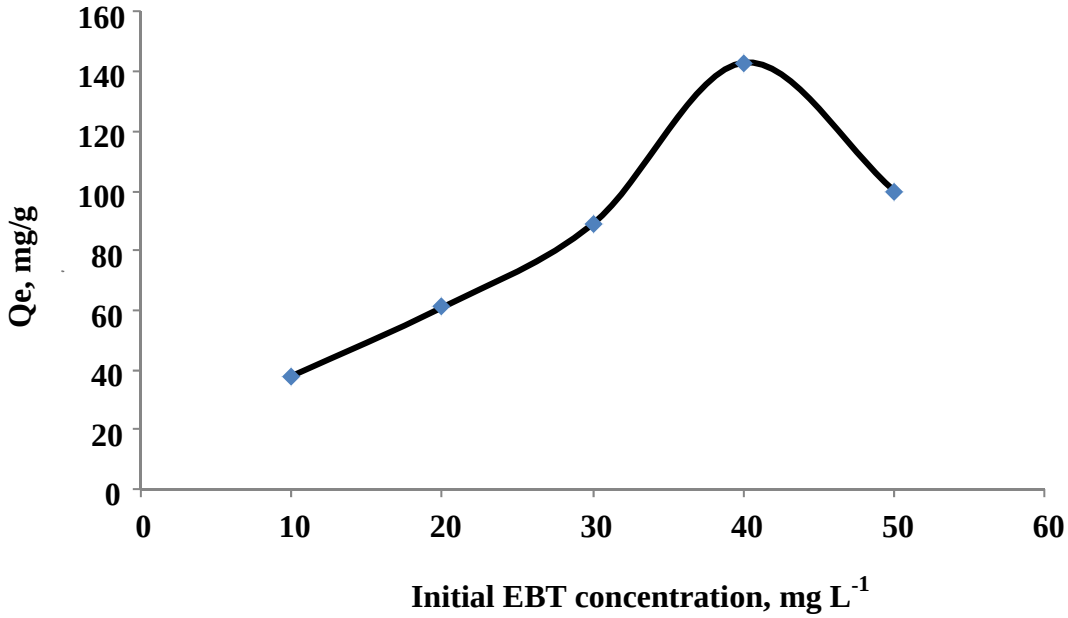

Figure (3-20): Impact of initial dye concentration on the adsorption of EBT onto TiO_2

3.4.5 Effect of Temperature

The adsorption process temperature is another important physico-chemical operational parameter, because it contributes massively in variation of adsorption ability of the adsorbent [52]. The adsorption experiments of EBT onto nanosized TiO_2 were carried out at three different temperatures namely; 30, 40 and 50°C with an accuracy of ±0.5 ºC. It is known that the process of adsorption is often an exothermic in nature, thus a decrease in temperature of the system would result in an increase of adsorption and vice verse [76]. Figure (3-21) corroborates the effect of the process temperature on the adsorption efficiency at TiO_2 dosage of 10 mg, agitation time of 30 min and 40 mg L^{-1} EBT concentrations. In chemisorption, the quantity adsorbed may increase or

decrease with the rising temperature depending on the type of interaction and bonding between the adsorbate molecules and the adsorbent surface,

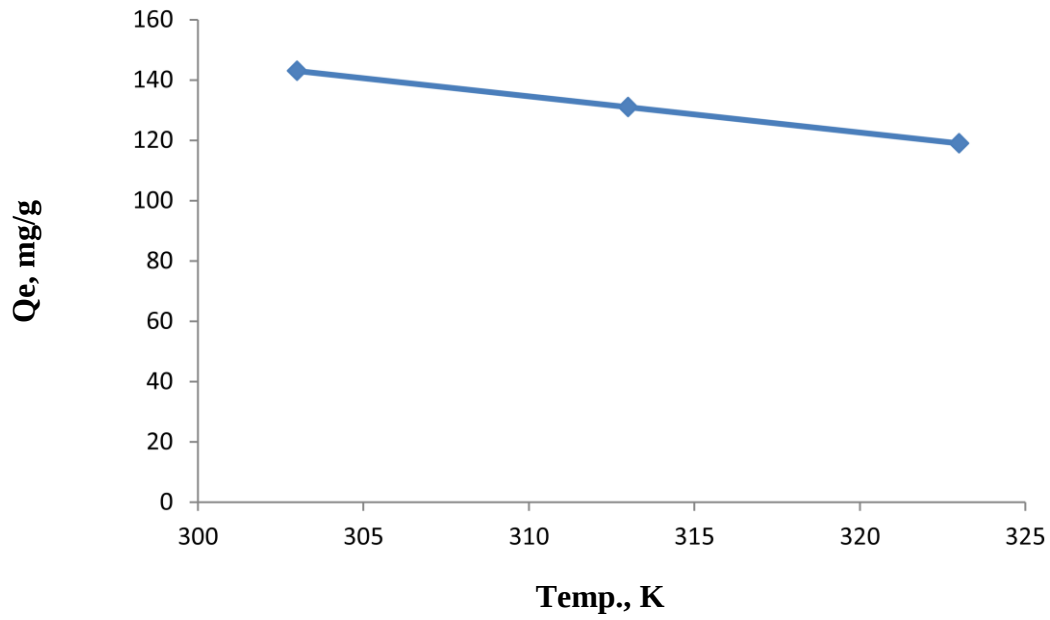

Figure (3-21): Effect of temperature on the adsorption of 40 mg L^{-1} EBT onto TiO_2

while in physisorption a decrease in temperature enhances the extent of adsorption [77] Also from Fig. (3-21), a decrease of adsorption ability with increasing temperature verifies the exothermic feature of the adsorption process. Because higher temperature induces higher mobility of the adsorbate causing desorption [78].

3.4.6 Thermodynamic parameters

In order to evaluate the present adsorption process, certain thermodynamic factors were computed, because the thermodynamic functions contribute essentially in understanding the nature of adsorption. The thermodynamic parameters which are related generally to the adsorption of dyes, such as, enthalpy change ΔH^o (kJ/mol), entropy

change ΔS^o (J/ mol. K) and Gibbs free energy change ΔG^o (kJ/mol) have been calculated according to the following expressions:

$$K_p = Q_e / C_e \quad (3.3)$$

$$\Delta G = -R\,T \ln K_p \quad (3.4)$$

$$\ln K_p = -\Delta H^o / RT + \Delta S^o / R \quad (3.5)$$

Where K_p is the thermodynamic equilibrium constant, i.e., the ratio of the equilibrium concentration of EBT on TiO_2 (Q_e) to that in solution (C_e). T is the absolute temperature in Kelvin, and R is the universal gas constant (8.314 J/mol. K). ΔH^o has been calculated according to Van't Hoff equation (eq. 3-4) via plotting logarithmic value of the thermodynamic equilibrium constant (K_p) against the reciprocal of absolute temperature as (1/T). The Plotting of $\ln K_p$ against 1/T gives a straight line with slope and intercept equal to $-\Delta H^o/R$ and $\Delta S^o/R$, respectively (Fig. (3-22)). A linear fit with an equation of $\ln K_p = -1900.3/T - 5.4716$ was obtained in this experiment and the values of ΔH^o and ΔS^o calculated from Fig. (3-22) were -15.79 kJ/mol and -45.49 J / mol. K, respectively.

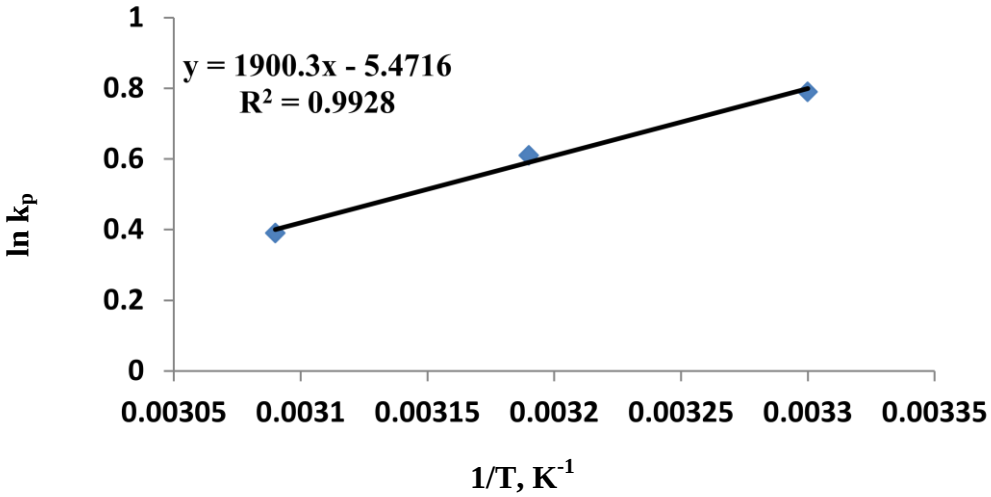

Figure (3-22): Van't Hoff plot for adsorption of EBT on TiO_2

The values of thermodynamic parameters are presented in Table (3-3). The ΔH˚ negative value indicates that the adsorption of EBT dye onto nanosized TiO_2 has been an exothermic process, which was supported by the increase of adsorption of the dye with decrease of temperature (Fig. (3-20)). The ΔS˚ negative value indicates that the degrees of randomness (freedom) decreased at the solid – liquid interface during adsorption of EBT [73]. Also from Table (3-3), we report here that the negative ΔG^o values indicate the feasibility of the EBT adsorption process onto solid TiO_2 surface in addition to the spontaneous nature at all the studied temperatures. This conclusion is well concerted with other authors [79, 56]. Hence, we conclude that the adsorption of EBT onto nanosized TiO_2 is spontaneous and thermodynamically favourable. On the other hand, some authors [76-79] found that the ΔG˚ value for physisorption process is between 0 and -20 kJ/mol, whereas it could attain a value of -400 for chemisorption process.

Table (3-3) Thermodynamic functions of the adsorption process

Temp., K	ΔG, kJ/mol	ΔH, kJ/mol	ΔS, $JK^{-1}mol^{-1}$
303	**-2.006**	**-15.79**	**-45.49**
313	**-1.55**		
323	**-1.09**		

3.4.7 Adsorption kinetics

In this work, pseudo-first-order and pseudo-second-order kinetics model were applied to examine the controlling mechanism of EBT adsorption onto nanosized TiO_2 from aqueous solutions. The rate of adsorption of

EBT has been studied as a function of time as it is depicted in Fig. (3-17). The adsorption equilibrium was reached in approximately 30 minutes. Both the first and the second-order rate equations were used to determine the most suitable rate expression for adsorption of the investigated dye on TiO_2. The optimal model was considered based on correlation coefficient (R^2).The correlation coefficient was frequently used to decide whether the model represents correctly the experimental data.

3.4.7.1 The first-order kinetics model

The rate constant of adsorption is determined from the first-order rate expression given by the famous linearized form of Lagergren rate equation [80] as follows:

$$\ln (q_e - q_t) = \ln q_e - k_1 t \qquad (3.6)$$

where q_t and q_e (mg. g^{-1}) are the amount of material adsorbed (adsorption capacity) at time t and at equilibrium, respectively. k_1 (min^{-1}) represents the rate constant of the first-order model.

3.4.7.2 The pseudo-second-order kinetics model

The pseudo-second-order equation was defined as follows [81]:

$$t/q_t = 1/(k_2 q_e^2) + t/q_e \qquad (3.7)$$

where k_2 (g. mg^{-1} min^{-1}) is the rate constant of the second-order model.
The kinetics parameters for adsorption of EBT under different conditions were calculated from equations 6 and 7 and are given in Table (3-4). The

correlation regression coefficient (R^2), for the first-order kinetic model is 0.75 while the correlation regression coefficient (R^2), for the pseudo-second-order kinetic model is 0.995 (figures were not shown). Calculated correlation regression coefficient (R^2) is closer to unity for second-order kinetics model; therefore the adsorption kinetics could well be approximated more favorably by second order kinetics model for EBT adsorption. Azizian [82] explored the kinetics of adsorption from a solution onto an adsorbent theoretically, and found that the adsorption process obeyed first-order kinetics at high initial concentration of solution while it obeyed pseudo-second-order kinetics at lower initial concentration of solution.

Table (3-4): Comparison of the first and second-order adsorption rate constants for 50 mg L^{-1} EBT adsorption onto TiO_2

	Fisrt order kinetics model					**Second order kinetics model**		
Time	**R^2**	**k_1**	**q_e**	**q_t**	**lnq_e-q_t**	**R^2**	**K_2**	**t/q_t**
15	**0.75**	**0.0180**	**162.9**	**147.3**	**2.747**	**0.99**	**0.0058**	**0.108**
30				**153.9**	**2.197**			**0.19**
45				**153.9**	**2.197**			**0.29**
60				**162.9**				**0.36**

3.4.8 Adsorption isotherm models

They adsorption isotherms play an important role in elucidating the interaction between the adsorbent and the adsorbate , and further deepen the understanding of the mechanism of adsorption phenomenon. Several isotherm models are presented in the literature [83]. Langmuir and

Freundlich models are the most widely used to describe the adsorption isotherm. The Langmuir model assumes that adsorption takes place at uniform energy sites on the surface of the adsorbent. The linearized Langmuir isotherm equation can be expressed as follows:

$$\mathbf{C_e/Q_e = C_e/Q_{max} + 1/K_L Q_{max}} \qquad \mathbf{(3.8)}$$

where C_e is the equilibrium concentration of EBT in solution (mg/L), Q_e is the amount of dye adsorbed on adsorbent (mg/g) at equilibrium, Q_{max} is the maximum adsorption capacity (mg/g), and K_L is the Langmuir binding constant, which is related to the energy of adsorption (L/mg). The slope and intercept of C_e / Q_e vs. C_e plot were utilized to calculate $1/Q_{max}$ and $1/(K_L Q_{max})$ respectively, as exhibited in Fig. (3-23).

The Freundlich isotherm, Fig. (3-24), is an empirical equation based on adsorption on a heterogeneous surface. The equation is commonly represented by:

$$\mathbf{\log Q_e = \log K_f + \log C_e/n} \qquad \mathbf{(3.9)}$$

Where K_f and n are the Freundlich constants as characteristics of the system, indicating the adsorption capacity and the adsorption intensity, respectively. When the value of 1/n is lower than 1 (n > 1), it indicates a normal Freundlich isotherm, otherwise, it is indicative of cooperative adsorption.

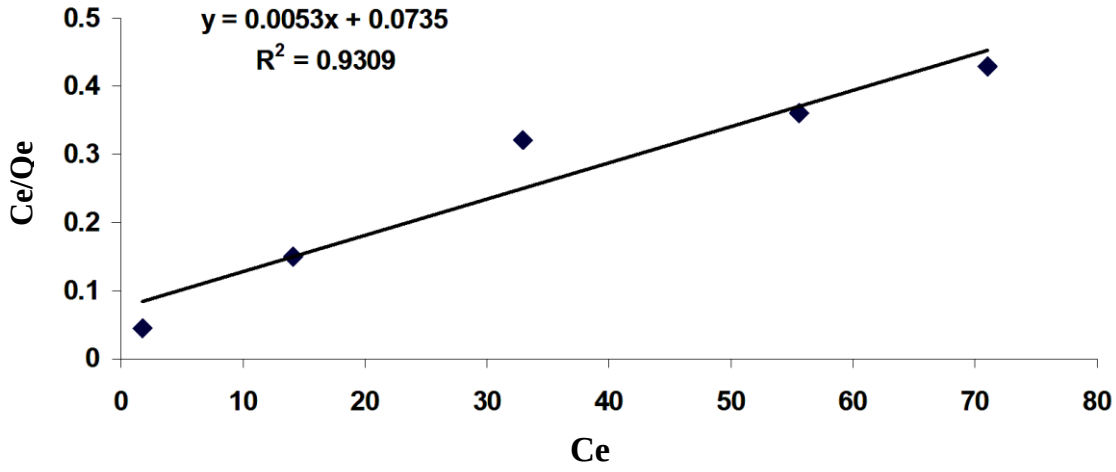

Figure (3-23): The linear plot of Langmuir isotherm for adsorption of EBT onto TiO_2

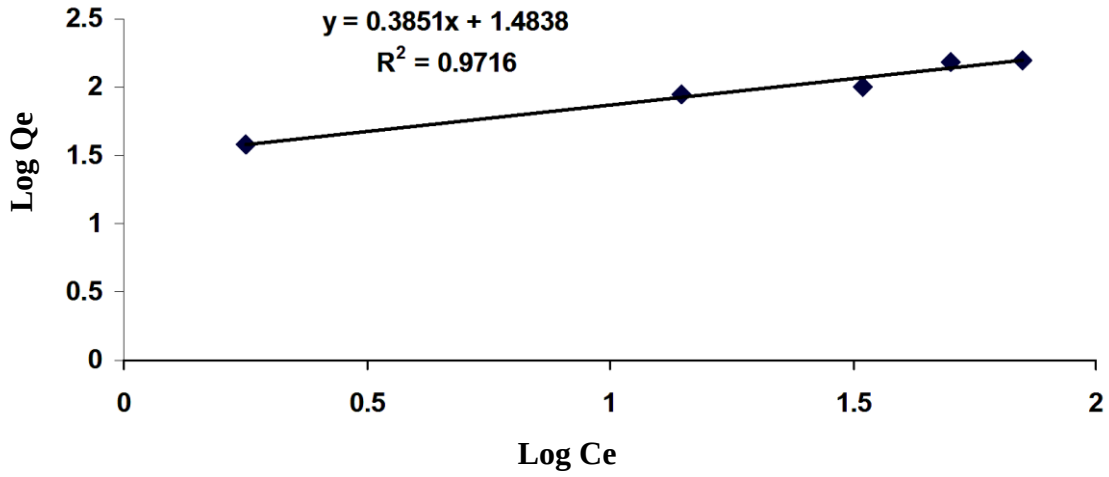

Figure (3-24): The linear plot of Freundlich isotherm for adsorption of EBT onto TiO_2

The calculated parameters of both Langmuir and Freundlich models which resulted upon the correlation of adsorption data for different initial EBT concentrations are presented in Table (3-5). The comparison of correlation coefficients (R^2) for Figs. (3-23) and (3-24) refers to higher R^2 value possessed by Freundlich model. This suggests that this model yields a better fit in describing the experimental equilibrium adsorption of EBT onto TiO_2. Hence, The Freundlich isotherm is an empirical equation that assumes heterogeneous adsorbent surface with its adsorption sites at varying energy levels [84]. Moreover, the maximum adsorption capacity, Q_{max}, of the process of this work is compared in Table (3-6) with the data reported by other authors for EBT adsorption.

Table (3-5): Adsorption isotherms parameters for EBT adsorption onto TiO_2

Freundlich isotherm			**Langmuir isotherm**		
1/n	**K_f**	**R^2**	**Q_{max}**	**K_L**	**R^2**
0.38	**1.48**	**0.971**	**188.6**	**0.072**	**0.931**

Table (3-6): Maximum adsorption capacities of EBT from aqueous media onto various adsorbents

Adsorbent	**Max. Capacity, Q_{max}, mg/g**	**Reference**
Nano TiO_2 (this work)	**188.6**	**-**
Activated carbon	**160.4**	**75**
Eucalyptus bark	**52.4**	**56**
$NiFe_2O_4$ nanoparticles	**47**	**76**

3.5 Operational factors influencing the photocatalytic degradation

The oxidation rates and efficiency of the photocatalytic system are highly dependent on a number of operational parameters that govern the photodegradation of the organic molecule [85]. This section will briefly discuss the significance of each operational parameter

3.5.1 Influence of initial pH on the degradation

Wastewater containing organic dyes may have different pHs; therefore it is important to study the role of pH on removal of colored dye. To study the effect of pH on the decolorization efficiency, experiments were performed at various pH values, ranging from acidic to basic media for constant concentration of dye. Under highly acidic conditions the TiO_2 particles tend to agglomerate and the surface area available for dye adsorption and photon absorption would be reduced [86-87]. Hence, pH plays an important role both in the characteristics of textile waters and in the reaction mechanisms that can contribute to dye degradation. Also its influence on catalyst surface charge namely, hydroxyl radical attack, direct oxidation by the positive hole and direct reduction by the electron in the conducting band [88]. At different pH conditions the surface charge of photocatalyst is variable. The following acid–base equilibrium reaction may occur on the surface of TiO_2 at different pH values [30].

$$TiOH + H^+ \rightarrow TiOH^{+2} \quad (3.10)$$

$$TiOH + {}^-OH \rightarrow TiO^- + H_2O \quad (3.11)$$

Thus, the TiO_2 surface is positively charged in acidic media (pH < 6.9), whereas it is negatively charged under alkaline conditions (pH > 6.9). Figure(3-25) present point of zero charge for anatase TiO_2 surface,

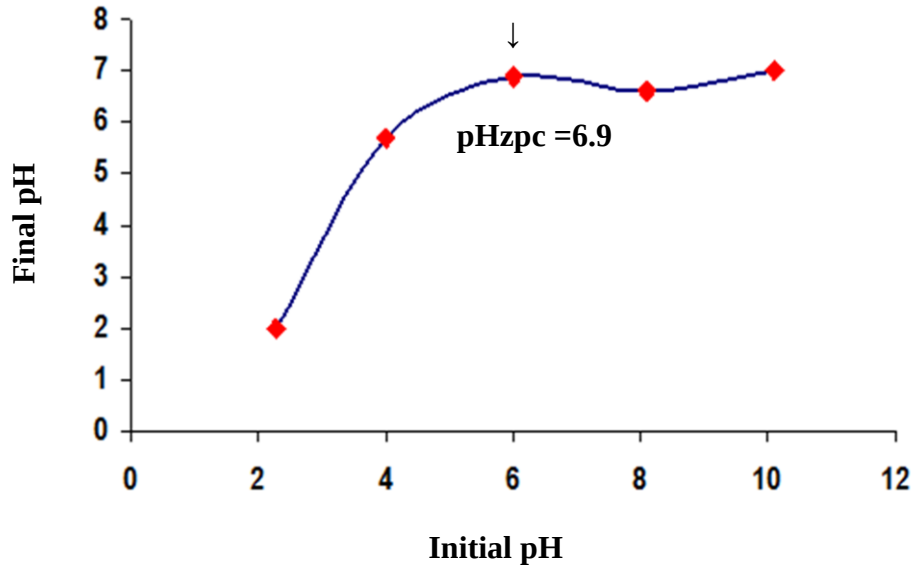

Figure (3-25): Determination of point of zero charge (pHpzc) for anatase TiO_2

While point of zero charge for TiO_2 surface is widely reported at 6.25–6.90 [86,88,30]. The color of EBT changes from blue (alkaline color) to red (acidic color) while from red to blue for MV by protonation of dye .

Results obtained experimentally by varying initial pH of polluted solution from 2 to 9 with keeping all other parameters unchanged. It could be noticed from Figure (3-26 a) that the final degradation obtained in acidic solution at pH equal 3 was 99.22%. This could be explained from the surface charge of TiO_2 point of view. In acidic pH, the surface of TiO_2 gains a positive charge there by attracting the anionic EBT dye, leading to a greater adsorption and hence increasing the degradation rate in the acidic media. However, the reverse image is observed in the basic medium where the TiO_2 surface was negatively charged which repels the dye molecules away from the surface of the catalyst thereby decreasing the degradation rate [89]. However, As it is shown in the Figure (3-27), in the case of MV dye (cationic) the maximum decolorization efficiency was obtained in pH=7. Since the photooxidation of dyes is accompanied

by the release of protons, its efficiency may then change because of the reversible protonation of the Ti surface [90]. At lower pH, below pH_{pzc}= 6.9, the H^+ ions compete effectively with cationic dye, causing a decrease in removal efficiency of color dye.

Furthermore, a low pH associated with a positively charged surface, cannot provide hydroxyl groups which are needed for hydroxyl radical formation, the rate of photo bleaching of MV decreases due to columbic repulsion between the surface of photocatalyst that have positivly charged and H^+ ions [91]. At higher pH, above (pH_{pzc}), the surface of catalyst gets negatively charged, which enhances the positively charged dye cations.

Meanwhile, the higher pH value can provide the higher concentration of hydroxyl ions to react with holes to form hydroxyl radicals. However, the decolorization of dye molecules is inhibited when the pH value is so high (pH > 7), because the hydroxyl ions compete with dye molecules in the adsorption on the surface of photocatalysts [92]. The rate of EBT photodecolorization increased with decreasing initial pH, exhibiting maximum efficiency (k = 0.024 min^{-1}) at pH 3, while it is (k = 0.015 min^{-1}) at pH 7 for MV as shown in Figures (3-26b) and (3-28), respectively. Furthermore, Figures (3-26a) and (3-27) with Tables (3-7) and (3-8) illustrated degradation percent with varying of pH of EBT and MV solutions, respectively. Wang et al. [93] have reported that the state of the chemical species presented in water is not affected only by pH, but also closely related to the dissociation constant (pK_a) of the species. When pH < pK_a of the species, it primarily presents in molecular state, whereas, at pH > pK_a it exists as ionic state. The pH_{zpc} of TiO_2 used in this study is about 6.9 and the pK_a's EBT, MV are 6.2 [56], 0.8 [94] respectively.

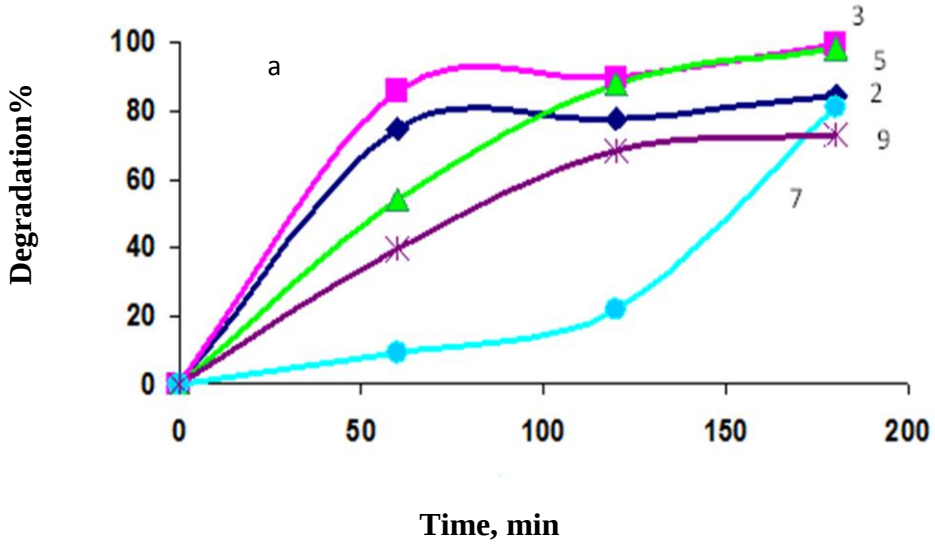

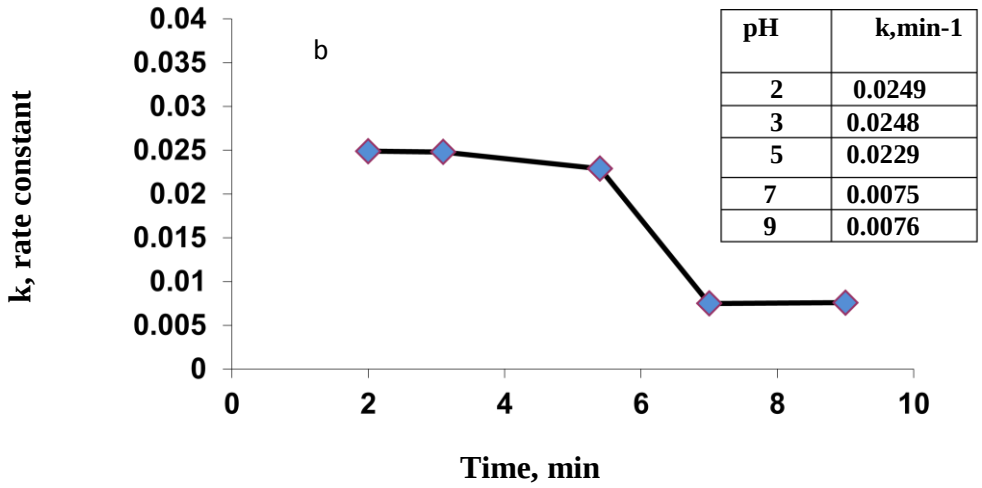

Figure (3-26): a) Influence of initial pH on degradation percent of EBT; numbers on curves refer to pH values; b) Influence of initial pH on photobleaching rate of EBT

Table (3-7): Degradation percent of EBT at different pHs

Time,min.	Degradation% at pH= 2.	Degradation% at pH= 3	Degradation% at pH= 5	Degradation% at pH= 7	Degradation% at pH= 9
0	0	0	0	0	0
60	82.8	85.6	54.3	9.4	39.9
120	84.1	89.5	87.7	21.7	68.4
180	84.1	99.2	98.4	80.7	72.8

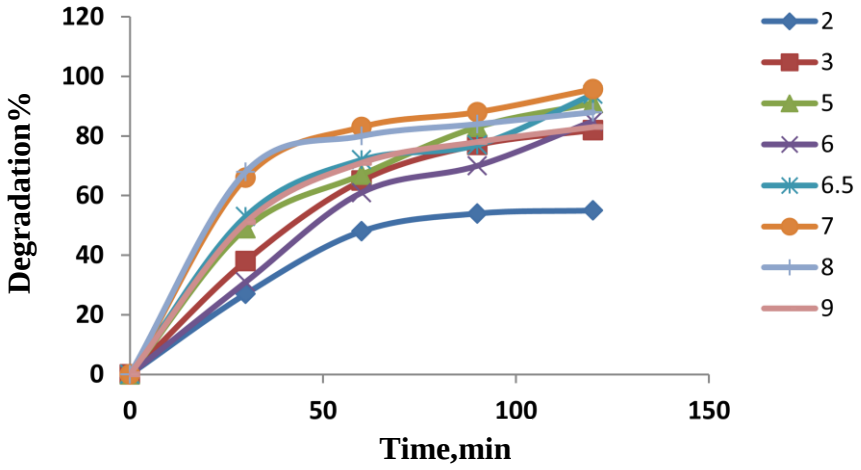

Figure (3-27): Influence of initial pH on degradation percent of MV; numbers on curves refer to pH values.

pH	k, min^{-1}
2	0.0065
3	0.014
5	0.0199
6.5	0.021
7	0.025
9	0.014

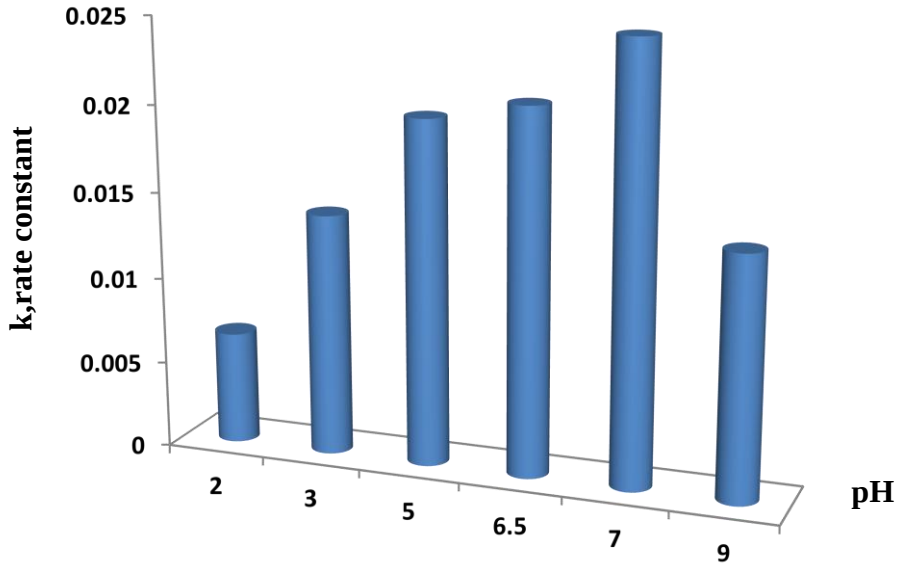

Figure (3-28): Influence of initial pH on photobleaching rate of MV

Table (3-8): Degradation percent of MV at different pHs

Time	Degradation% at pH= 2	Degradation% at pH= 3	Degradation% at pH= 5	Degradation% at pH= 6	Degradation% at pH= 6.5	Degradation% at pH= 7	Degradation % at pH= 8	Degradation % at pH= 9
0	0	0	0	0	0	0	0	0
30	27	38	49	31	53	66	68	51
60	48	65	67	61	72	83	80	71
90	54	77	83	70	77	88	84	78
120	55	82	91	85	94	95.7	88	83

3.5.2 Variation of pH and conductivity during photocatalysis process

The TiO_2 catalyst photodegradation of MV has also been monitored by in situ measurements of the pH and of the conductivity of the suspension with time of irradiation. The change in pH was studied as a function of the irradiation time. However, after 60 min of irradiation no significant changes in pH were observed that is indicated the organic pollutants were continuously decomposed forming inorganic ions (K^+, Na^+, Cl^-, Mg^{+2}), which is in accordance with the photocatalytic decomposion in the presence of TiO_2 catalyst [95]. The amount of dissolved ions in solution estimates by the conductivity (electrical current). This current depends on the temperature of the solution, ion mobility and concentration or numbers of ion present [96]. Figure (3-29) shows the time variation of conductivity of the dye. One could observe an increase in the conductivity of the dye with increasing reaction time, and the change trend is consistent with the removal efficiency of color dye, which means that ions in the solution augment with increasing reaction time and the dye molecules have been decomposed to ions and other substances [97,98].

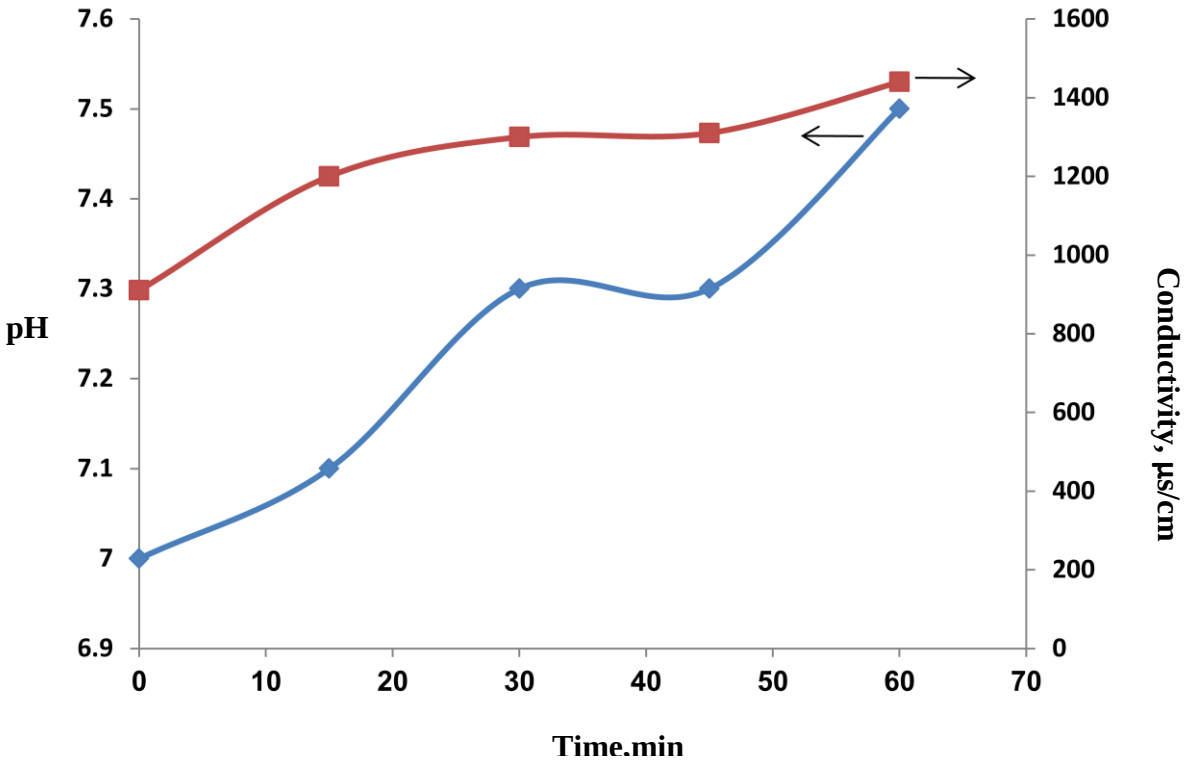

Figure (3-29): Changes of pH and conductivity during the photocatalysis process for MV dye

Table (3-9): Variation of pH and conductivity during the photocatalysis process

Time,min	pH	Conductivity,µs cm^{-1}
0	7	910
15	7.1	1200
30	7.3	1300
45	7.3	1310
60	7.5	1440

3.5.3 Effect of catalyst loading

Dye degradation is also influenced by the amount of the photocatalyst and aggregation of catalyst particles in high amounts of catalyst. The dye degradation increases with increasing catalyst dose, which is characteristic of heterogeneous photocatalysis [85]. Increases in the number of active sites on the photocatalyst surface by an increase in catalyst amount thus causing an increase in the number of •OH radicals

which can take part in actual discoloration of dye solution. Beyond a certain limit of catalyst amount, the solution becomes turbid and thus blocks radiation for the reaction to proceed and therefore percentage degradation starts decreasing [99,100,101]. All these behaviors are due to (screening effect) caused by the suspended TiO_2 layers located closer to the radiation source, which reduces the site density for surface holes and electrons Hence, an optimum amount of catalyst has to be added in order to avoid unnecessary excess,unfavorable light scattering and also ensure total absorption of light photons for efficient photomineralisation [71].The effect of catalyst concentration on decolorization rate was studied by varying catalyst dose from 10 mg to 100 mg. The results are illustrated in Figures (3-30) and (3-31) for EBT and MV, respectively. It is found that the decolorization degradation of both dyes solutions increased significantly with increase concentration of catalyst and then decreased with further increase of the catalyst concentration due to light scattering and screening effect. Some authors [101] stated that there is fluctuation of degradation percent with further increases of concentration of catalyst. With ascending added amount of catalyst lead to gradual increase in the degradation percent due to the increase of the surface area and then high adsorbability of dye and also increase the density of particales in the area of illumination [102]. The observed optimum concentration of the catalyst has been about 80 mg for a given concentration of 40 ppm of EBT solution and 30 mg for 4 ppm of MV.

TiO_2 loading (mg)	Degradatio %n
10	52
20	80.6
30	86
50	89.8
80	98.5
100	95

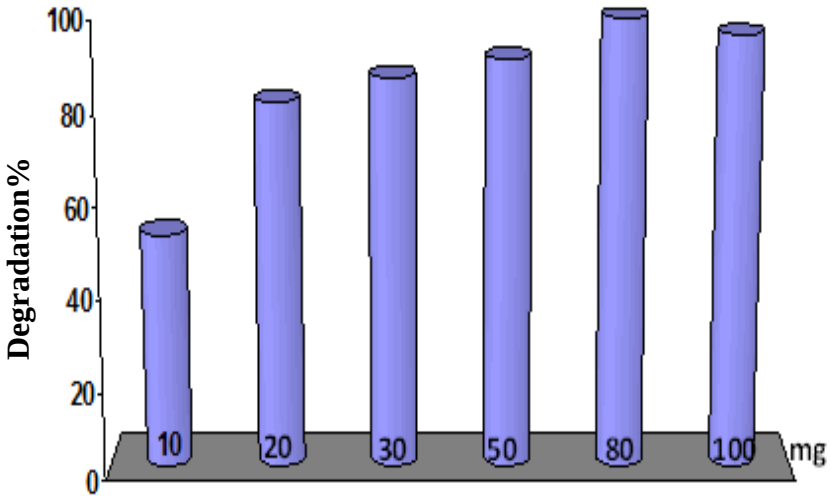

Figure (3-30): Variation of EBT photobleachingwith catalyst loading

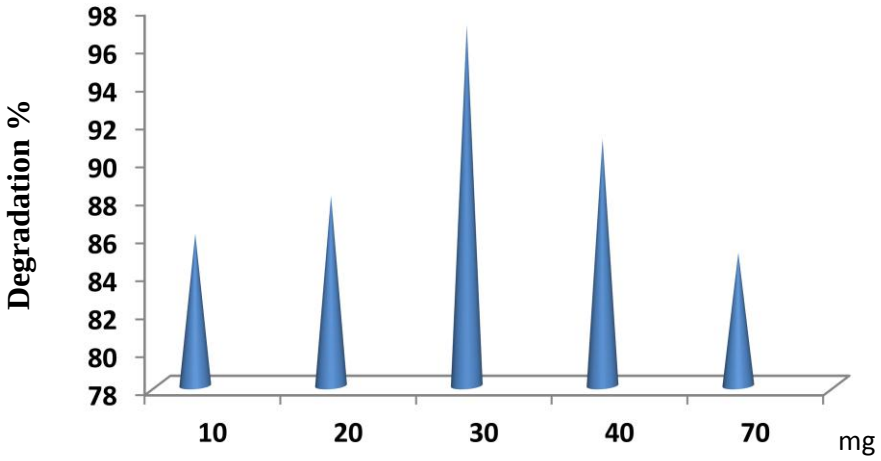

%deg	TiO_2loading mg
86	10
88	20
97	30
91	40
85	70

Figure (3-31): Effect of TiO_2 loading on the removal of MV

3.5.4 Effect of initial dye concentration on the degradation

The effect of initial dye concentration on dye degradation efficiency has been investigated by varying the EBT dye concentrations (10, 20, 30, 40,

50, 60 mg/L). For the concentration of 30 mg/L, complete discolouration of EBT solution was observed (96%) after 60 min. of illumination. For concentrations of EBT above 30 mg/L, the degradation ratios become almost fixed due to that at high substrate concentrations all catalytic sites of the semiconductor surface are occupied. Therefore, a further increase in substrate concentration does not affect the efficiency of the photo-oxidation. At low concentrations, the number of catalytic sites is not the limiting factor of the rate degradation which is now proportional to the concentration of substrate in accordance with apparent first-order kinetics [103]. The photocatalytic decomposition of the MV was also studied by varying the initial concentration from 2-10 mg. L^{-1}. For the concentration of 4 mg/L a complete discolouration of the solution was observed (97%) after 40 min of illumination. For concentrations of MV below 4 mg/L, practically the total dye disappeared with 91 % and the solution becomes completely transparent. Beyond 4 mg/L, degradation of MV becomes very slow. Figures (3-32) and (3-33) show the relations of dye concentration and degradation for EBT and MV, respectively. However, better results can be obtained by extension of reaction time. The rate of degradation relates to the probability formation of $^{\bullet}OH$ radicals on the catalyst surface and to the probability of $^{\bullet}OH$ radicals reacting with dye molecules [88]. According to Beer–Lambert law, a decrease of penetration of photons into the solution occurs by increasing the molecules of the dye, which consequently causes lower photonic adsorption on the nano photocatalyst and reduction in the efficiency of (e^-_{CB}/h^+_{VB}) pair formation [104]. Once the dye concentration is increased; firstly, the adsorption amounts of catalyst attain the saturation for superfluous dye. Secondly, the mutual screens among dye molecules also increase along with the concentration rising of dye. Thus, once the concentration of dye is increased, it also causes light screening by dye

molecules and the photons never reach to the surface of photocatalyst and therefore less ·OH are formed, thus resulting in less degradation percentage [105].

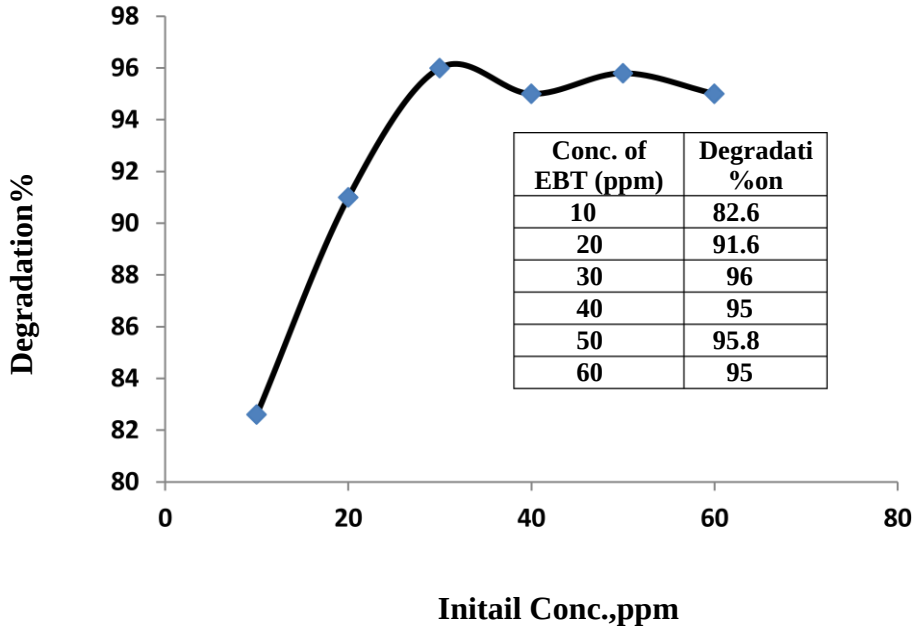

Conc. of EBT (ppm)	Degradati %on
10	82.6
20	91.6
30	96
40	95
50	95.8
60	95

Figure (3-32): Plot of percent degradation vs. initial concentrations of EBT; (Catalyst loading = 0.08 g/l; pH = 3.0; time= 60 min)

Conc. of MV (ppm)	Degradation %
2	91
4	97
6	71
8	65
10	60

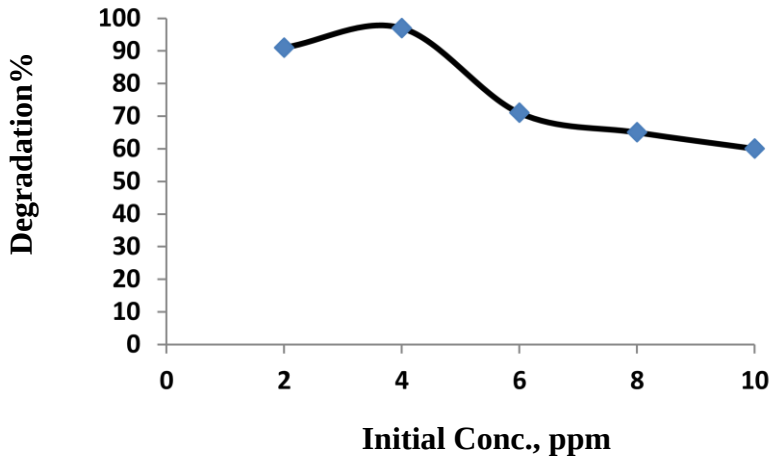

Figure (3-33): Plot of percent degradation vs. initial concentrations of MV; (Catalyst loading = 0.03 g/l; pH = 7.0; time= 45 min)

3.5.5 Effect of radiation dose on the degredation of dyes

Radiation absorption of the photocatalyst affect the photocatalytic reaction rate [106]. Some authors [86] have shown that at low light intensities (0–20 mW/cm^2), the rate would increase linearly with increasing light intensity (first order), whereas at intermediate light intensities (25 mW/cm^2) the rate would depend on the square root of the light intensity. While at high light intensities the rate is independent of light intensity. The authors [85] also stated that at low light intensity reactions involving electron–hole formation are predominant and electron–hole recombination is negligible. On the other hand, when light intensity was increased, the electron–hole pair separation competes with recombination, thereby causing lower effect on the reaction rate [107].

At a high radiation dose, increasing of the number of photons occurs to reach the active site of catalyst and also number of excited catalyst molecules increases, which consequently increase the number of hydroxyl radicals and the rate of degradation of dye molecules [98,108]. Figure (3-34) shows variations of the; initial rate and degradation yield of EBT as a function of visible light source intensity. The degradation rate was appreciably higher under higher intensity of halogen lamp (4.65 x 10^{-8} mol l^{-1} sec^{-1}) than of an medium and low intensities of visible light (3.98 x 10^{-8} mol l^{-1} sec^{-1}) and (2.5 x 10^{-8} mol $l^{-1}sec^{-1}$), respectively. The kinetic rate constant, k, for EBT degradation is directly proportional to the light intensity, I_o, due to the increase in visible light power. The high light intensity would also increase the photo generating rate of electron-hole pair at the surface of TiO_2 which consequently enhance the oxidizing ability of the system [109]. The calculated quantum yield of EBT degradation under high, medium, and low intensity of halogen lamp is 0.0995, 0.159 and 0.627, respectively. For validating the theoretical reasoning above, the calculated first-order rate constant, k, of EBT

degradation under high intensity of a halogen-lamp (0.032 min^{-1}) is significantly higher than that under the medium and low intensities of the visible lamp 0.027min^{-1} and 0.0176 min^{-1}, respectively. For better evaluation the efficiency of the photocatalytic and photobleaching processes, we estimated the quantum yield Φ,

Φ = rate of reaction/ rate of absorption of radiation

Table (3-10) was reported the values of Φ. On the basis of above data, it is evident that the percentage of decolorization and photodegradation increases with increase in irradiation time. The reaction rate decreases with irradiation time since it follows apparent first-order kinetics, however, it increases with increasing the light intensity (Figure 3-34) and additionally a competition for degradation between the reactant and the intermediate products should also be taken into consideration.

Table (3-10): Quantum yields of photodegradation of EBT obtained at different intensities

Intensity (E/L.sec) x10^{-7}	**Rate (mol/L.sec) x10^{-8}**	**Quantum yield Φ%**
4.68	**4.65**	**0.0995**
2.5	**3.98**	**0.1596**
0.4	**2.5**	**0.627**

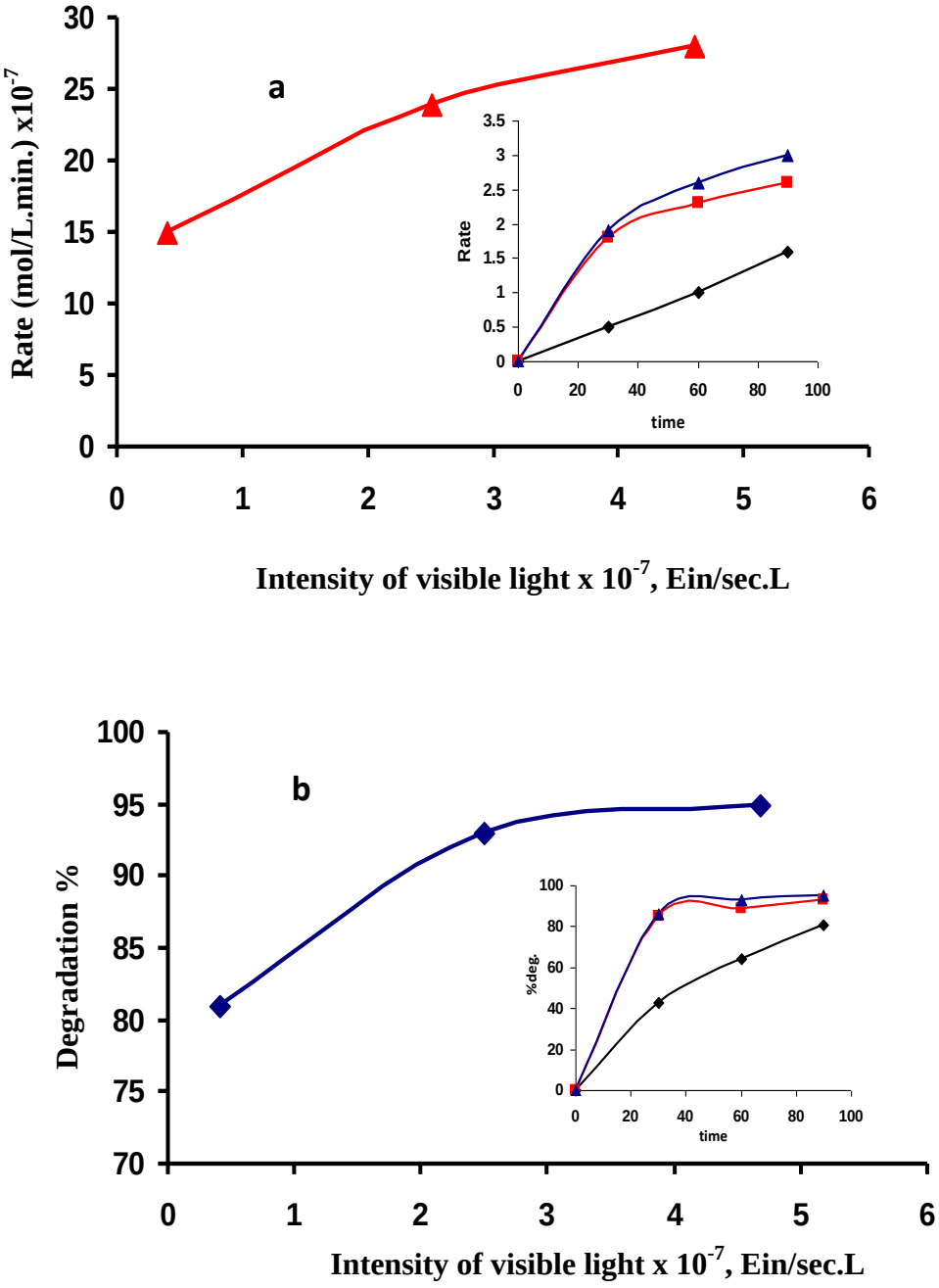

Figure (3-34): Variations of the a) initial rate and b) degradation% of EBT as a function of visible light source intensity. Insets reveal the relations of rate and degradation % with time.

3.6 Kinetic study

3.6.1 Influence of irradiation time on the reaction kinetics

The slow kinetics of dye degradation after certain time limit is mainly attributed to the difficulty in the reaction of short chain aliphatics with •OH radicals, and the short lifetime of photocatalyst because of active sites deactivation by strong by-products deposition [110]. Figures (3-35) and (3-36) and Tables (3-11) and (3-12) depict the effect of light irradiation time on the decline of dyes concentration (96%) of the EBT and (98%) of MV were degraded, after an irradiation time of 60 and 45 minutes for EBT and MV, respectevily. The photocatalytic decolourisation of the dye occurs on the surface of TiO_2. When the concentration of dye and intensity of light are constant, the number of $^{\bullet}OH$ and $^{\bullet-}O_2$ radicals increase with an increase in the irradiation period. These radicals are trapped by the holes of the reactive species, as oxygen and water are essential for photocatalytic decolourisation. Furthermore, the $^{\bullet}OH$ radicals are strong enough to break the bonds of the dye molecules absorbed on the surface of TiO_2 [111,112].

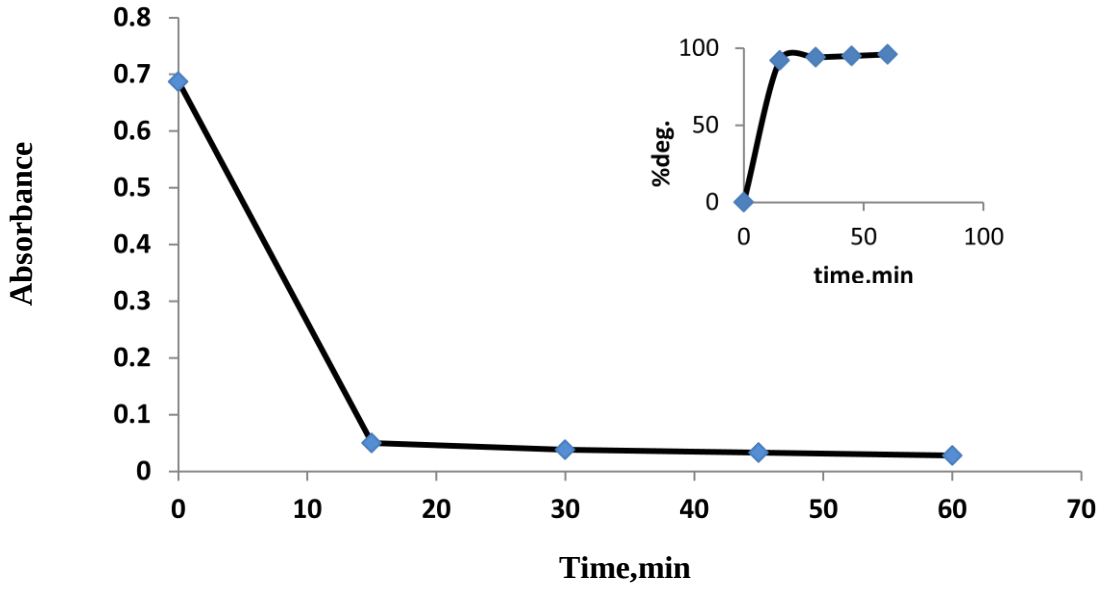

Figure (3-35): Correlation of EBT concentration with irradiation time

Table (3-11): Variation of concentration and degradation percent of EBT

Time	At	Degradation%
0	0.687	0
15	0.05	92
30	0.038	94
45	0.033	95
60	0.028	96

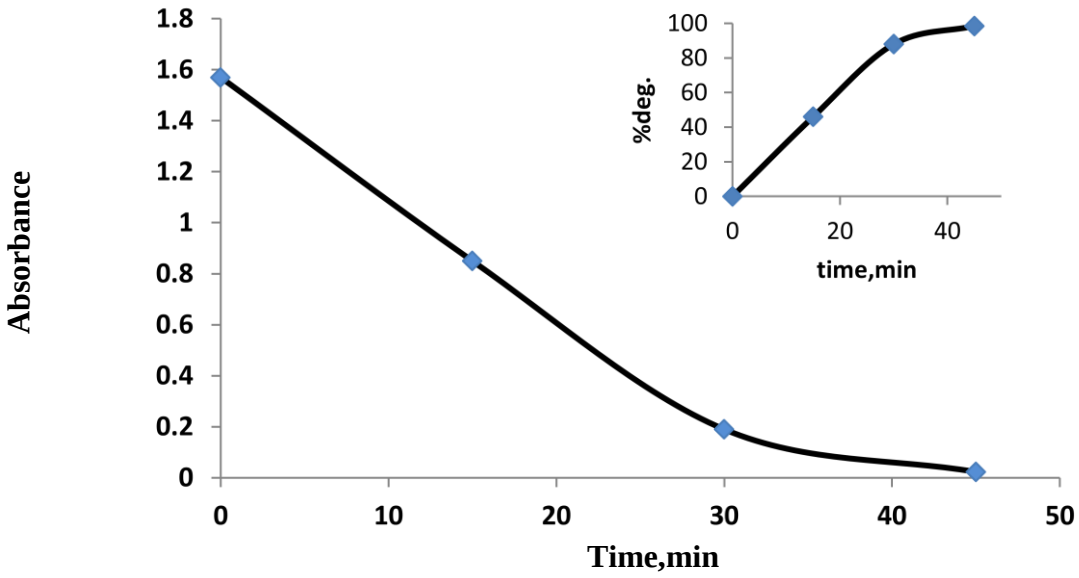

Figure (3-36): Correlation of methyl violet concentration with irradiation time

Table (3-12): Variation of concentration and degradation percent of MV

Time	At	Degradation%
0	1.57	0
15	0.85	46
30	0.19	88
45	0.023	98.5

3.6.2 Kinetic model

It is necessary to determine the kinetic order and apparent rate constant for the degradation of the dyes and further to investigate the overall order of reaction with respect to the initial dye concentration. According to some researchers [113,114], the photocatalytic degradation of organic pollutants is described by pseudo-first order kinetics.

$$-dC/dt = k_{app}C \qquad (3.12)$$

Integrating the eq. (3-11) with the boundary conditions that at the start of irradiation (t = 0), the concentration is the initial one, results in the following expression:

$$-\ln (C_t/ C_o) = k_{app}t \qquad (3.13)$$

Where k_{app} is the apparent first order rate constant (min^{-1} or sec^{-1}) and Co and C_t are the concentration of the dyes at t=0 and a given irradiation time, t (min), respectively. Kinetic studies were monitored by the change in azo dye concentration at certain interval of time (C_t). A linear correlation was observed by plotting ln C_o/C_t versus time, Figures (3-37) and (3-38), which may indicate that the photodegradation is pseudo-first-order kinetics [114]. The slope equals to the first-order rate constant k_{app} . The half life of the reaction accordingly computed from the expression $t_{1/2} = 0.693/ k_{app}$, which has been equal to 7 min. for EBT and 9 min. for MV.

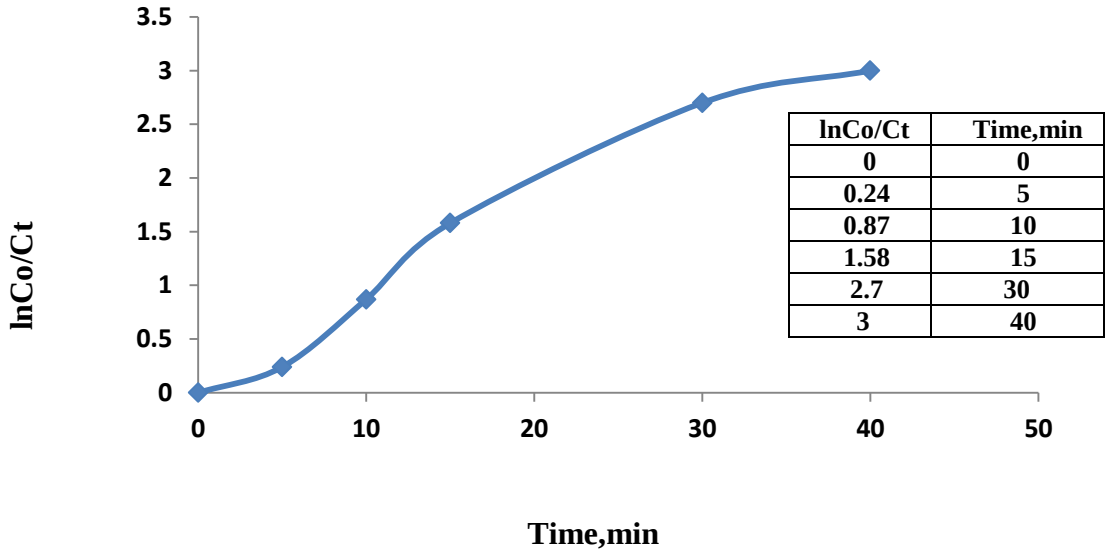

Figure (3-37): Degradation rate of Eriochrom Black T at optimum conditions

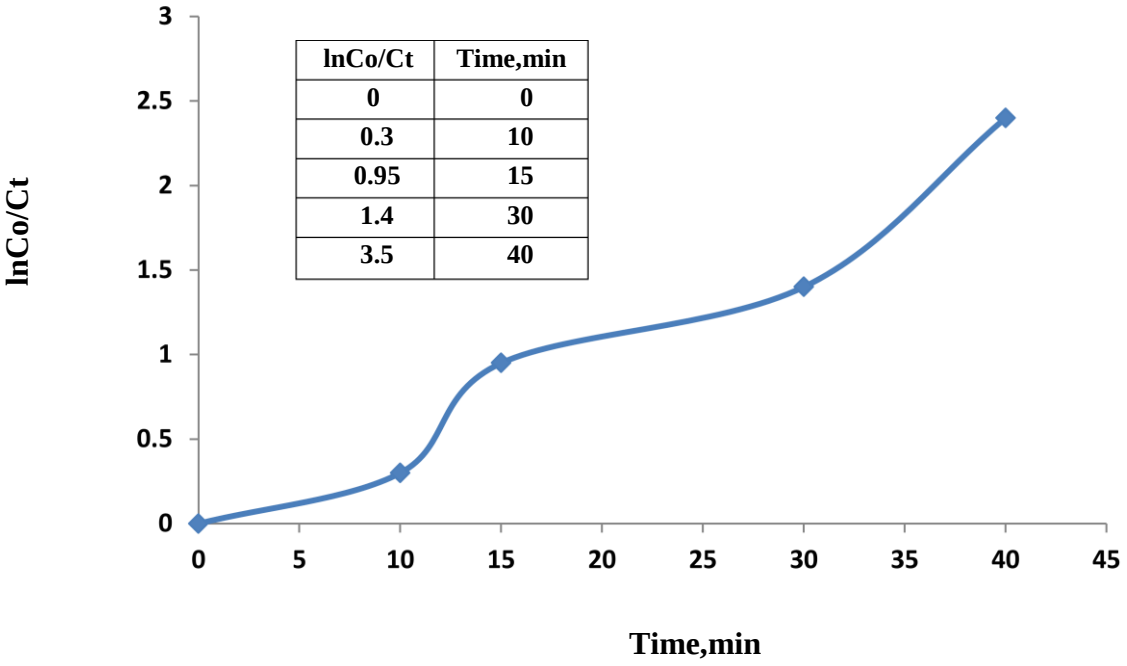

Figure (3-38): Degradation rate of Methyl Violet at optimum conditions

3.6.3 Langmuir-Hinshelwood kinetic model for the Photocatalysis of EBT and MV dyes

The Langmuir–Hinshelwood model is usually used to describe the kinetics of photocatalytic reactions of aquatic organics [115]. Furthermore, the Langmuir-Hinshelwood rate used successfully for heterogeneous photocatalytic degradation [116]. It relates the rate of photodegradation (r) and the concentration of organic compound (C), which is expressed as follows:

$$r = dC / dt = k_r k_{ad} C / 1 + kC \qquad (3.14)$$

where kr is the reaction rate constant (M/min), k_{ad} is the adsorption equilibrium constant of dye on catalyst particle (M^{-1}), and t is the irradiation time (min). When the concentration of the dye is low, the equation can be simplified to an apparent first-order equation [117,118].

$$Ct = C_o\, e^{-kapp.t} \qquad (3.15)$$

If the pseudo first-order kinetics is applicable, the plot of $-\ln(C/C_o)$ against t should yield a straight line as indicated in Eq. (3-14) from which k_{app} is obtained from the slope of the plot. Most authors [119,120,88] agree that when the following assumptions were established, heterogeneous photocatalysis could be analyzed using the Langmuir-Hinshelwood model:

(i) at equilibrium, fixed number of catalyst surface adsorption sites,

(ii) the surface of catalyst can be covered to the maximum by one layer; only one substrate may bind at each surface site.

(iii) the adsorption reaction is reversible, (iv) the catalyst surface is homogeneous and (v) there is no interaction between adjacent adsorbed molecules.

To determine rate constants, k, of adsorbed dyes and the adsorption constants k_{ads}, the Figures (3-39) and (3-40) are used for EBT and MV, respectively. These values are reported in Table (3-15).

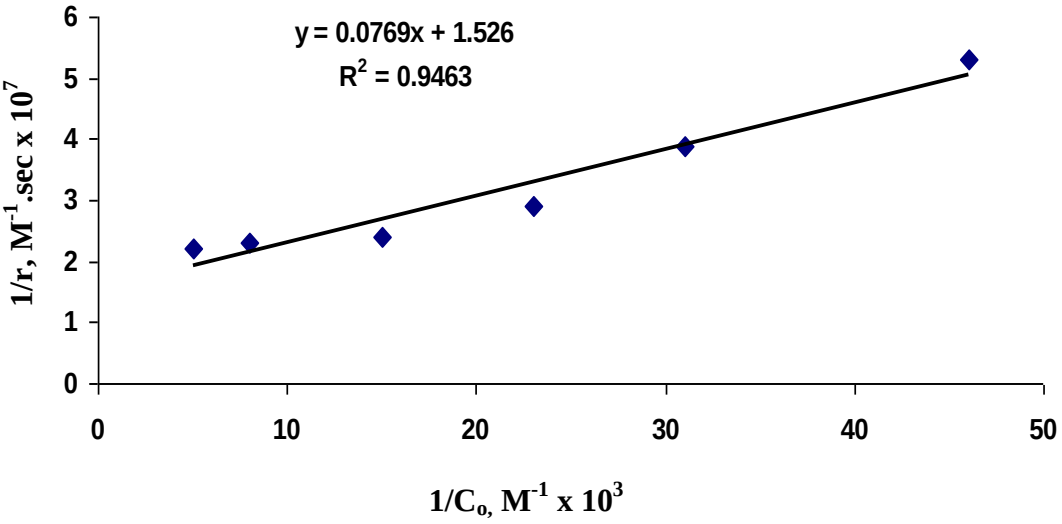

Figure (3-39): Langmuir-Hinshelwood model outcomes for the disappearance of EBT at different initial concentrations; TiO_2 loading = 0.08 g/l; pH = 3.0

Tables (3-13) and (3-14) demonstrate the detailed calculation and comparision between computed and observed rate constants, k, for EBT and MV dyes, respectively.

Table (3-13): The observed and calculated initial rates of EBT photobleaching

Co ppm	Co, M	k, sec^{-1}	1/r M^{-1}. sec	1/Co M^{-1}	Observed rate ($\mu M.sec^{-1}$)	Calculated rate ($\mu M.sec^{-1}$)
10	$0.216*10^{-4}$	$8.90*10^{-4}$	$5.3*10^{7}$	$46*10^{3}$	$1.92*10^{-2}$	$1.97*10^{-2}$
15	$0.325*10^{-4}$	$8.10*10^{-4}$	$3.9*10^{7}$	$31*10^{3}$	$2.63*10^{-2}$	$2.56*10^{-2}$
20	$0.433*10^{-4}$	$7.90*10^{-4}$	$2.9*10^{7}$	$23*10^{3}$	$3.42*10^{-2}$	$3.02*10^{-2}$
30	$0.649*10^{-4}$	$6.30*10^{-4}$	$2.4*10^{7}$	$15*10^{3}$	$4.09*10^{-2}$	$3.67*10^{-2}$
60	$1.300*10^{-4}$	$3.36*10^{-4}$	$2.3*10^{7}$	$8*10^{3}$	$4.37*10^{-2}$	$4.69*10^{-2}$
90	$1.950*10^{-4}$	$2.38*10^{-4}$	$2.2*10^{7}$	$5*10^{3}$	$4.64*10^{-2}$	$5.17*10^{-2}$

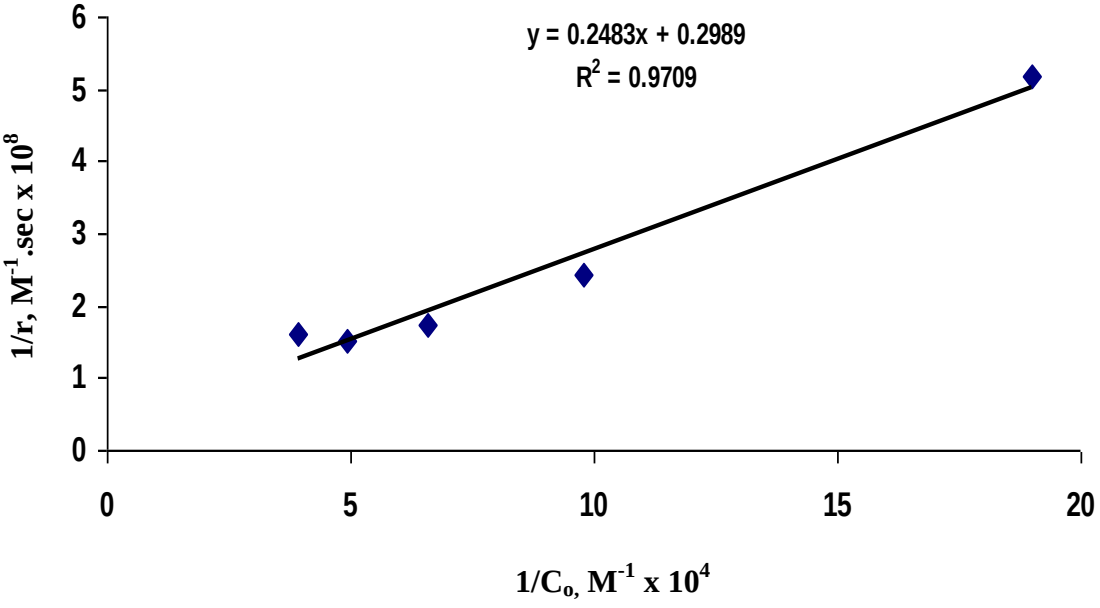

Figure (3- 40): Langmuir-Hinshelwood model outcomes for the disappearance of MV at different initial concentrations; TiO_2 loading = 0.03g/l; pH = 7.0

Table (3-14): The observed and calculated initial rates of MV photobleaching

Co ppm	Co, M	k, sec^{-1}	1/r M^{-1}. sec	1/Co M^{-1}	Observed rate ($\mu M.sec^{-1}$)	Calculated rate ($\mu M.sec^{-1}$)
2	$5.08*10^{-6}$	$8.4*10^{-4}$	$5.17*10^{8}$	$1.9*10^{5}$	$2.010*10^{-3}$	$1.965*10^{-3}$
4	$1.016*10^{-5}$	$1.2*10^{-3}$	$2.428*10^{8}$	$9.8*10^{4}$	$4.084*10^{-3}$	$3.63*10^{-3}$
6	$1.524*10^{-5}$	$9.3*10^{-4}$	$1.74*10^{8}$	$6.56*10^{4}$	$6.126*10^{-3}$	$5.08*10^{-3}$
8	$2.03*10^{-5}$	$5.1*10^{-4}$	$1.517*10^{8}$	$4.92*10^{4}$	$8.160*10^{-3}$	$6.35*10^{-3}$
10	$2.54*10^{-5}$	$3.3*10^{-4}$	$1.621*10^{8}$	$3.92*10^{4}$	$9.809*10^{-3}$	$7.416*10^{-3}$

Table (3-15): Rate constants and adsorption coefficients of

Dye	K_{ads} (μM^{-1})	k ($\mu M. sec^{-1}$)
Eriochrom black T	0.0199	0.0655
Methyl violet	0.0120	0.0335

From Tables (3-13) and (3-14), we notice that the observed degradation rates in case of EBT are higher concerted with the L-H calculated rates than in case of the MV (the triaryl methane dye). Furthermore, Table (3-15) presents higher adsorption coefficient value (K_{ads}) for EBT in comparison to that of MV, i.e. stronger adsorption of EBT moiety onto the electrophilic (Ti^{+4}) sites at TiO_2 surface. This is likely attributed to the possible EBT adsorption geometries which stem from various adsorption sites, like anionic sulphonate site [6], chair adsorption via NO_2 group [121] and via coordinative azo group [61]. Correspondingly, EBT exhibited better decomposition rate (Table 3-14) than that of MV, despite of the higher initial concentrations for the former dye.

3.7 Influence of some experimental variables on apparent quantum yield

The quantum yield, Φ, of a photochemical process is defined as the rate of radiation-induced primary events divided by the rate of photon absorption, and is generally used as a measure of the efficiency of a photochemical process [106].

Φ = rate of reaction/ rate of absorption of radiation

Figures (3-41a) and (3-42a) show quantum yield variation in suspension with different TiO_2 loadings for EBT and MV, respectively**.** Incrasing the loading of suspension, the flux of absorbed photons increases resulting in an increase in quantum yield. But the excess concentration of catalyst leads to unfavorable light scattering and reduction of light penetration into the solution as we indicated previously. Figures (3-41b) and (3-42b) rationalize the initial pH and Φ of EBT and MV photo-decomposition, respectively. It could be concluded that the pH variation could result in enhancement of the efficiency of photo removal of organic pollutants in presence TiO_2 [122]. The initial dye concentration is another important variable in the evaluation of photocatalytic efficiency. The results which are shown in Figure (3-41c) elucidates the relation between EBT initial concentration and the process quantum yield**.** The quantum yield increased with increasing the initial concentration of EBT from 10 ppm to 60 ppm for EBT dye. With the visible light irradiation period and catalyst dose are kept constant, the increase in initial concentration of dye, more dye molecules are adsorbed onto the surface of catalyst and hence the amount of decomposed dye is increased [6]. In contrary an increase in the concentration of MV above 4ppm a decrease in the quantum yield is observed in 60 min irradiation of visible light because at

high-substrate concentration, the photonic efficiency diminishes and consequently quantum yield is lowered [123], Figure (3-42c).

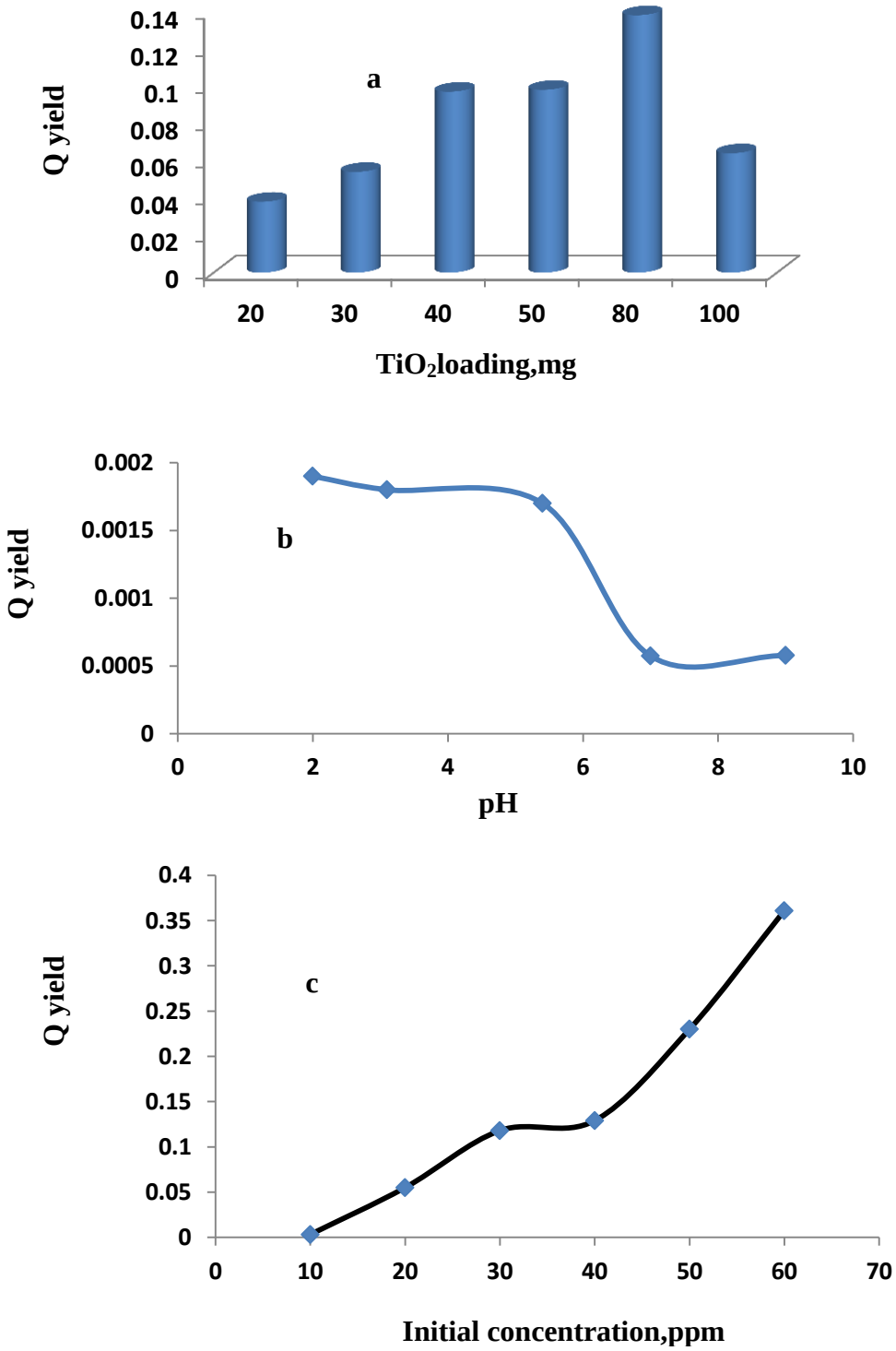

Figure (3-41): Effect of (a) TiO_2 loading (b) pH and (c) EBT initial concentration on the quantum yield of photocatalytic degradation of EBT at optimum conditions

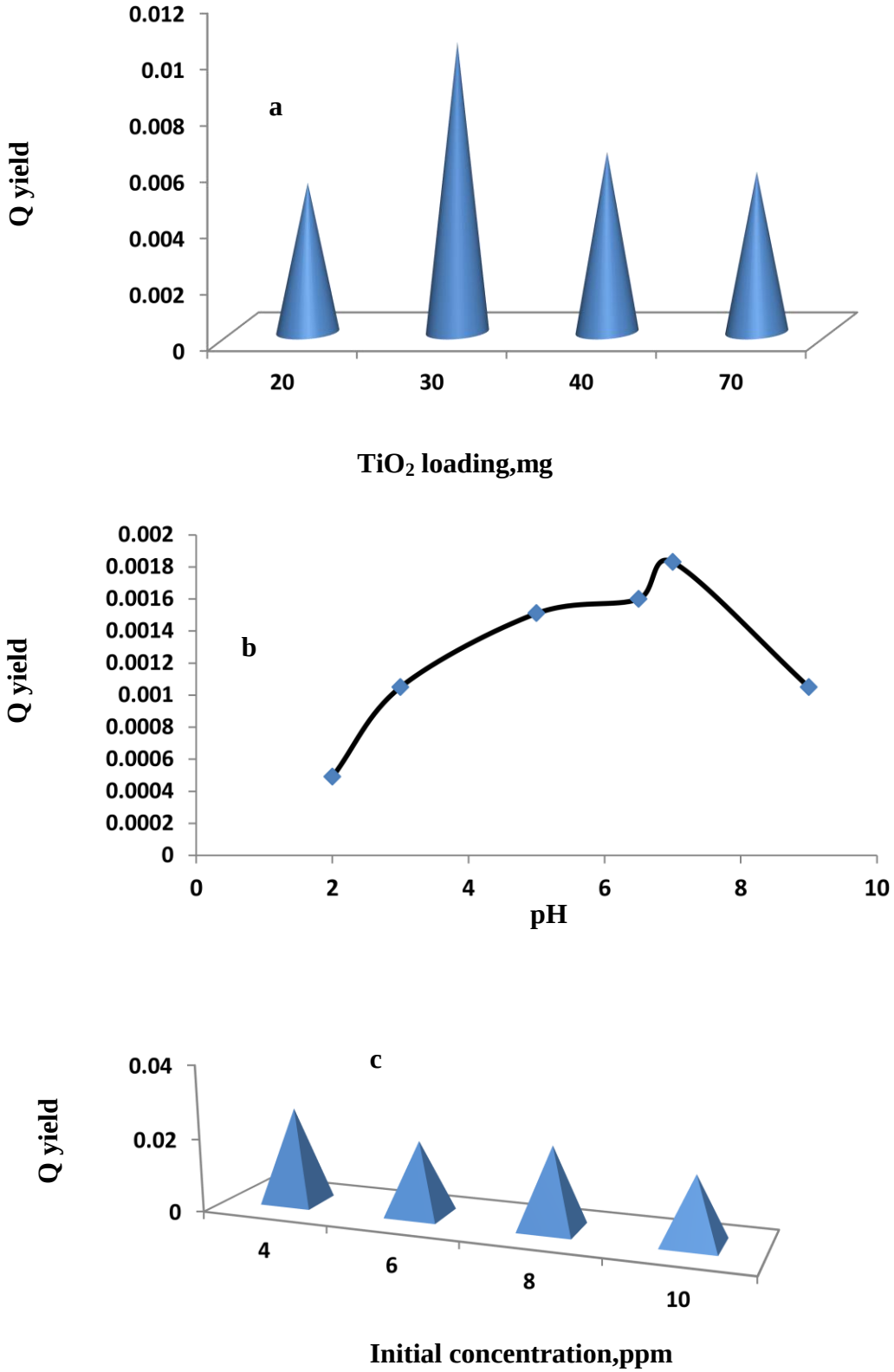

Figure (3-42): Effect of (a) TiO_2 loading (b) pH and (c) MV initial concentration on the quantum yield of photocatalytic degradation of MV at optimum conditions

3.8 Effect of temperature and the thermodynamic parameter s

Various operational parameters including temperature and corresponding thermodynamic functions impact on the photocatalytic degradation rate of organic compounds [124]. Figure (3-43) shows the effect of aqueous solution temperature on the degradation of EBT in the range of 20 C^o -45 C^o. The degradation rate of the dye increases with the temperature increase in the presence of nano TiO_2 powder. The degradation percent increases from73% to 99.6% when the temperature rises from 20 C^o to 45C^o. The apparent rate constant and activation energy can be determined via Arrhenius relation as follows [125,126];

$$k_{app} = Ae^{-Ea/RT} \qquad (3.16)$$

where k_{app} is the apparent rate constant, A is the frequency factor or pre-exponential factor, E_a is the activation energy of the reaction, R is general gas constant (8.314 J mol^{-1} K^{-1}) and T is the absolute temperature. Translation of Eq. (3-16) resulted in the following equation

$$\ln k_{app} = \ln A - E_a /RT \qquad (3.17)$$

The activation energy (E_a) was obtained from a plot of ln k_{app} versus 1/T as shown in Figures (3-43) and (3-44) for EBT and MV, Respectively. The other thermodynamic parameters, free energy, enthalpy and entropy of activation were calculated as presented in (Table 3.16) and (3.17) for EBT and MV, respectively. The value of $\Delta G^{\#}$ (the free energy of activation) may be determined from following equations [127]:

$$k_{app} = k_B T/h \text{ exponential } (-\Delta G^{\#}/RT) \qquad (3.18)$$

$$\Delta G^{\#} = RT \text{ x } [\ln (k_B T/h) - \ln k_{app}] \qquad (3.19)$$

where k_B is Bolzmann constant ($1.3805x\ 10^{-23}$ J K^{-1}), h is Planck constant ($6.6256X\ 10^{-34}$ J s). Which after introduction of the constant values, leads to:

$$\Delta G^{\#} = RT\ x\ (23.76 + \ln T - \ln k_{app}) \quad (3.20)$$

The enthalpy ($\Delta H^{\#}$) and entropy ($\Delta S^{\#}$) of activation are derived from equations (3.17) and (3.18), leading to the final relations

$$\ln k_{app} = \ln A - E_a / RT \quad (3.21)$$

$$d(\ln k_{app}) / dT = E_a / RT^2 \quad (3.22)$$

equation (3.18) is rewritten as:

$$\ln k_{app} = \ln (kBT/h) - \Delta H^{\#} / RT + \Delta S^{\#} / R \quad (3.23)$$

$$d(\ln k_{app}) / dT = 1 / T + \Delta H^{\#} / RT^2 = (\Delta H^{\#} + RT) / RT^2 \quad (3.24)$$

Solving equations (3.22) and (3.24) for the activation enthalpy gives

$$\Delta H^{\#} = Ea - RT \quad (3.25)$$

finally giving access to the entropy of activation

$$\Delta S^{\#} = (\Delta H^{\#} - \Delta G^{\#}) / T \quad (3.26)$$

From Tables (3-16) and (3-17), one could observe that the degradation rate increase at higher temperatures. This fact indicates that with the temperature increase the mobility of dye molecules increases. Also an increase in collision frequency of molecules in solution due to molecules possessing more kinetic energy and moving faster. Additionally, also increased the number of molecules possessing enough energy to overcome the activation energy [128]. In a photocatalytic process the existence of an activation energy barrier has so far been mainly linked

with an increase of the desorption of adsorbed products with increasing temperature and enhances recombination of charge carriers [122,129]. On the other hand, the exothermic adsorption of reactants becomes disfavored and tends to become the rate limiting step, when temperature increases above 80 C^{o} and approaching to the boiling point of water [130]. The positive values of $\Delta G^{\#}$ gives an indication of non-spontaneous process as one expected. The process was endothermic due to positive values of $\Delta H^{\#}$ i.e., that higher temperatures are favored for enhanced removal of organic pollutant. The negative values of $\Delta S^{\#}$ suggest the decreased randomness at the solid/ solution interface during the adsorption of dye on catalyst and further ratification for the non spontaneous process.

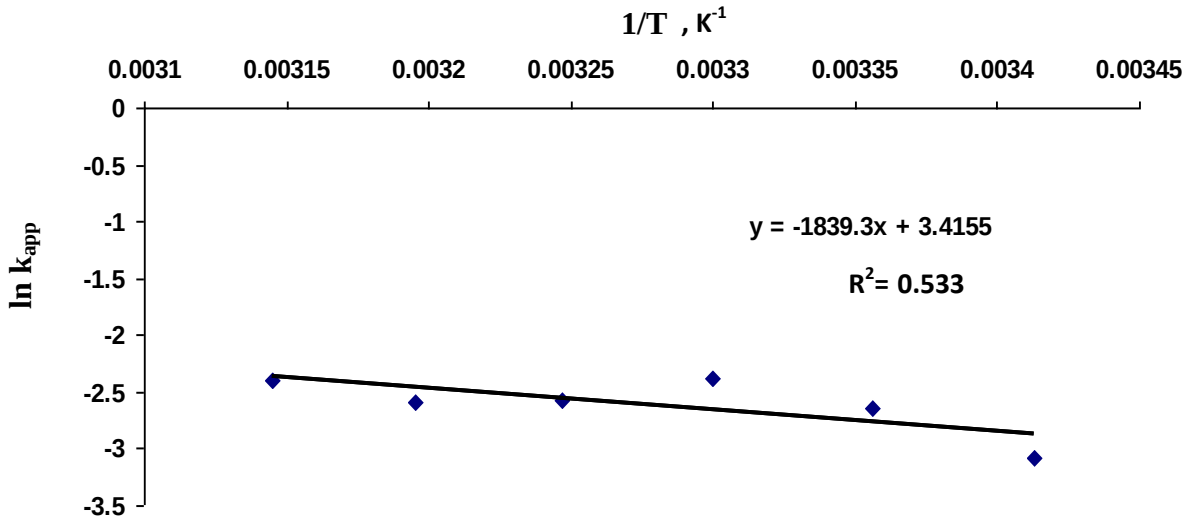

Figure (3-43): Arrhenius plot of rate constant versus reciprocal of reaction temperature for degradation of EBT

Table (3-16): Thermodynamic parameters for the photocatalytic degradation of EBT

T (K)	E_a (kJ mol^{-1})	$\Delta G^{\#}$ (kJ mol^{-1})	$\Delta H^{\#}$ (kJ mol^{-1})	$\Delta S^{\#}$ (JK^{-1} mol^{-1})
293	15.3	64.22	12.86	-175.29
298		66.44	12.82	-179.93
303		68.25	12.78	-183.07
308		68.96	12.73	-182.56
313		70.05	12.70	-183.23
318		71.72	12.66	-185.72

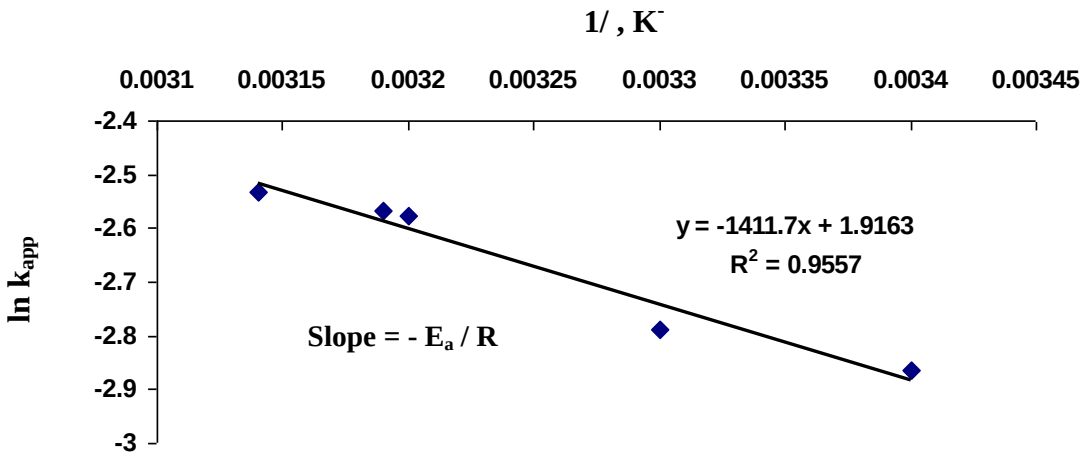

Figure (3-44): Arrhenius plot of rate constant versus reciprocal of reaction temperature for degradation of MV

Table (3-17): Thermodynamic parameters for the photocatalytic degradation of MV

T (K)	E_a (kJ mol^{-1})	$\Delta G^{\#}$ (kJ mol^{-1})	$\Delta H^{\#}$ (kJ mol^{-1})	$\Delta S^{\#}$ (JK^{-1} mol^{-1})
293	**11.7**	**78.6**	**8.06**	**-240.7**
298		**79.7**	**8.02**	**-240.5**
303		**81**	**7.98**	**-240.9**
308		**82**	**7.93**	**-240.4**
313		**83**	**7.89**	**-239.9**
318		**85**	**7.85**	**-242.6**

3.9 Comparison and evaluation of photocatalytic degradation of Eriochrom Black T (EBT) and Methyl Violet (MV) dyes

The comparison of photocatalytic degradation efficiency of EBT and MV dyes, at optimum conditions revealed different effects of pH on EBT and MV. EBT was degradated at acidic (pH=3) since it is anionic dye and consequently, lowering pH below pH_{zpc} = 6.9, would increase the positive charge onto TiO_2 surface and thus promotes the adsorption of anionic EBT dye onto positively charged TiO_2, which eventually accelerates the degradation. While, in the case of cationic dye the optimum adsorption and degradation occure at higher pH (neutral or basic pH). At the pH above pH_{zpc}=6.9 the negative charge on TiO_2 surface increases and thus promotes the adsorption of cationic MV dye onto negatively charged TiO_2 and accelerates the rate of the photocatalytic bleaching of the cationic dye [131,132]. Also note that the results show that both dye pollutants responded positively toward photocatalytic decomposition using neat TiO_2 and under visible light. This indicates that both dyes have propensity for in situ or self

sensitization of the laboratory synthesized nano anatase TiO_2 powder. Shorter illumination time was needed for the MV to be totally photodegraded in comparison with EBT. It is suggested that photodegradation efficiency of each dye is related with its initial concentration. Because of the higher E_{max} value (67709.5 $L.mol.^{-1}$ cm^{-1}) of MV than of EBT (9412.15$L.mol.^{-1}$ cm^{-1}), lower initial MV concentration was employed. Accordingly shorter complete photocatalysis time was required. The expectation is concerted with our experimental results of the lower rate and longer half life (0.099 min^{-1}, 7min) for EBT relatively to that of MV (0.077 min^{-1},9 min) despite of the higher adsorption coefficient of EBT ($K_{ads.}$=0.0199 μM^{-1}) onto TiO_2. Also from thermodynamic perspective, the relatively higher Ea for EBT results in intermediates with slower rates and probably higher heat of formation [133,134,135] and consequently lower apparent degradation rate.

3.10 Immobilization of TiO_2 nanoparticles

3.10.1 Dispersibility of nanoparticles

Anatase TiO_2 photocatalysis has been proven to be an effective process in water purification by the degradation of toxic organic contaminants [136]. Conventional photocatalytic studies are usually conducted with TiO_2 dispersions in aqueous solutions [137]. Unfortunately, the aqueous suspension of TiO_2 powder was limited for industrial applications due to the high cost of the catalyst filtration process which is considered as one of the major drawbacks and further, the loss of photocatalyst upon decantation process [138]. Accordingly, the immobilization strategy has been adopted as an approach to overcome this discrepancy, because

reactors utilizing the TiO_2 catalyst as immobilized on supports have shown a unique advantage over reactors exploiting suspended TiO_2 powder [139]. Furthermore, the immobilization of TiO_2 on a solid support permits its reuse without loses and improves its stability which in turns relies largely upon the dispersibility of the suspension, immobilization procedure and the properties of the substrate [140]. When the pH value of the suspension was adjusted to 3, the as-prepared TiO_2 nanoparticles were dispersed well in solution for at least 24 hours as shown in Figure (3-45), and beyond this period of time, a little precipitate was observed. However, the suspension could be readily redispersed in solution by either ultrasonication or stirring .When the aqueous solution was adjusted to pH 7, TiO_2 nanoparticles precipitated over this period of time. When the pH value was further increased to 9, TiO_2 nanoparticles were stably dispersed again. This suspension phenomenon could be ascribed to the electrostatic repulsion forces among colloidal particles [141]. Moreover, small amounts (0.5 g) of cetyltrimethyl ammonium bromide (CTAB) were added into the aqueous solution for further stabilization of the colloid.

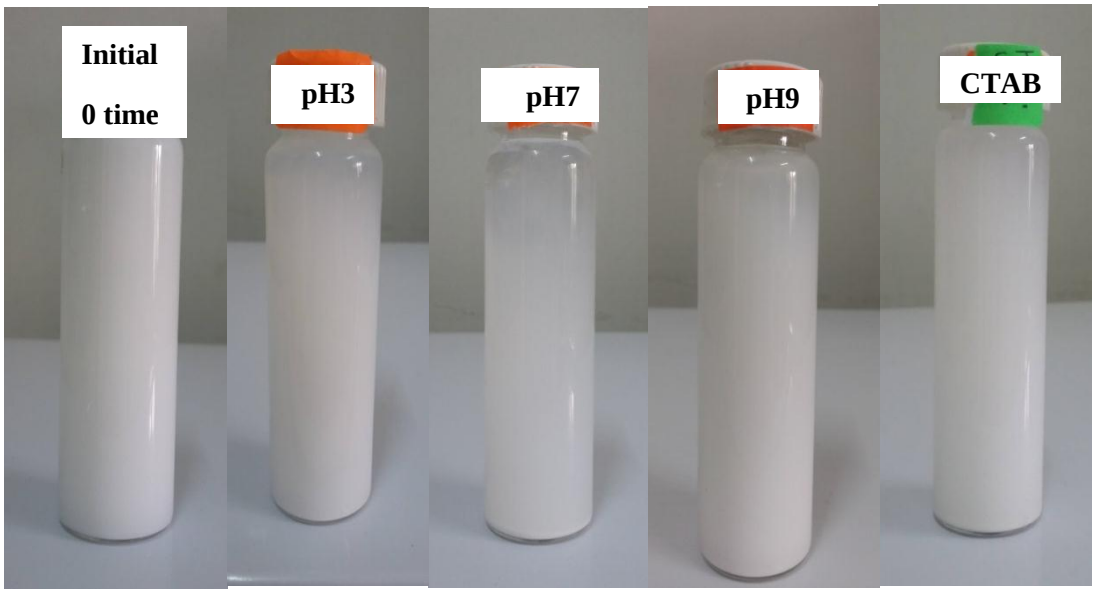

Figure (3-45): Photographs of dispersibility of as-prepared nano TiO_2 suspension in different media after 24 hours, used for the thin film coating of stainless steel slides.

These results suggested that the as prepared nano anatase TiO_2 suspensions were stable in water at about pH 3 or 9.

3.10.2 Immobilization methodologies

The aim of this part of study was to evaluate different recipes for immobilization of nano TiO_2 powder onto stainless steel slides and to find a suitable recipe to be applied in a prototype reactor later on. As prepared TiO_2 in anatase form has been immobilized in this research work onto stainless steel substrate by three techniques namely; Rotation, R, Dipping, D, and Swirling, S, in order to develop immobilized thin catalyst films for water decontamination. The first series of samples was coated to find a stable and suitable TiO_2 immobilization technique that could be applied afterwards in the photocatalytic prototype reactor. Multi TiO_2 coatings which were prepared by various recipes loaded several layers of TiO_2 on the surface of stainless steel slide following the R, D and S methodologies and their photocatalytic effects on the decomposition of EBT are shown in Figure (3-46). The photocatalytic decomposition yield of EBT increases with increasing the number of TiO_2 coatings via repetition of the immobilization procedure. Also from Figure (3-46) and Tables 3-18, 3-19 and 3-20, we observe the degradation percent of EBT reaches the highest values of 61%, 45% and 22% after 180 minutes of visible light illumination for R, D and S, respectively, for one, three and five TiO_2 coatings. Cherif et al. [142] reported that the catalyst film is porous and it consequently can provide a large surface area for the degradation of contaminant molecules upon increasing of the repetitions.

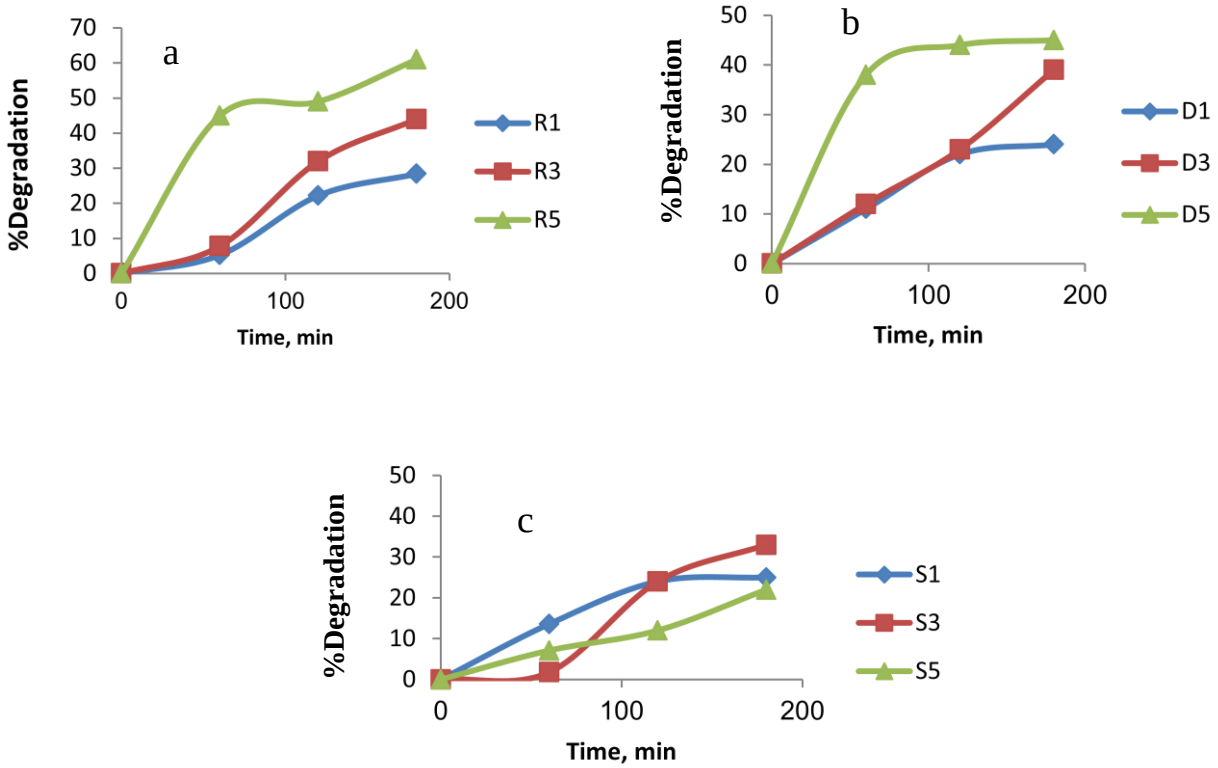

Figure (3-46): Effect of (a) Rotation; (b) Dipping; (c) Swirling immobilization techniques and the number of immobilizations on the photodegradation of EBT

Table (3-18): Percent degradation of EBT with rotating method

Time, min	R_1 %deg	R_3%deg	R_5%deg
0	0	0	0
60	5.26	7.2	45
120	22.2	32	49
180	28.4	44	61

Table (3-19): Percent degradation of EBT with dipping method

Time, min	%deg of D_1	%deg of D_3	%deg of D_5
0	0	0	0
60	11	12	38
120	22	23	44
180	24	39	45

Table (3-20): Percent degradation of EBT with swirling method

Time, min	%deg of S_1	%deg of S_3	%deg of S_5
0	0	0	0
60	13.6	1.78	7.1
120	24	24	12
180	25	33	22

Based on the above results one could report here that the rate of photocatalytic decomposition and the removal efficiency are sensitive to the variation of immobilized catalyst dosages. In other words, the number of TiO_2 particles that can be involved in the photocatalytic reaction increases with the number of coatings of TiO_2, which likely, to a good extent, could be interpreted in terms of increase in the generation of OH radicals.

Hu et al. [143] stated that the increase in the number of TiO_2 loaded layer will consequently increase the surface active sites of the catalyst, leading afterwards to higher pollutant removal efficiency. However, when the number of coatings was further increased to 7 loaded layers of TiO_2, no further improvement was observed and on contrast, the dye degradation yield was declined (see Figure (3-47)). This finding is in accordance with other reported data [139,143, 144]. Chen and Dionysiou [139] stated, in their work on the immobilization of Degussa P-25 TiO_2, that the increase in the TiO_2 loading on the slide causes an increase in;

i) the amount of crystalline material retained on the support; (ii) the number of grains and (iii) the number of pores on the slide. However,

Hu et al. [143] have very recently reported that partial aggregation of TiO_2 could be a result of multilayer coatings. Whereas, Feng and

coworkers [144] concluded that at high coating layers the outer TiO_2 molecules may block the inner ones and form TiO_2 agglomerate which consequently accelerates the recombination of the generated electrons and holes, thus lower the efficiency of light quantization and also declining removal efficiency. Accordingly, we believe that the active surface area of TiO_2 particles, beyond a certain limit, decreases gradually since only the outer surface can have contact with the EBT solution and correspondingly we conclude that five repetitions of the as prepared TiO_2 rotational (R5) immobilization procedure appeared to be optimal.

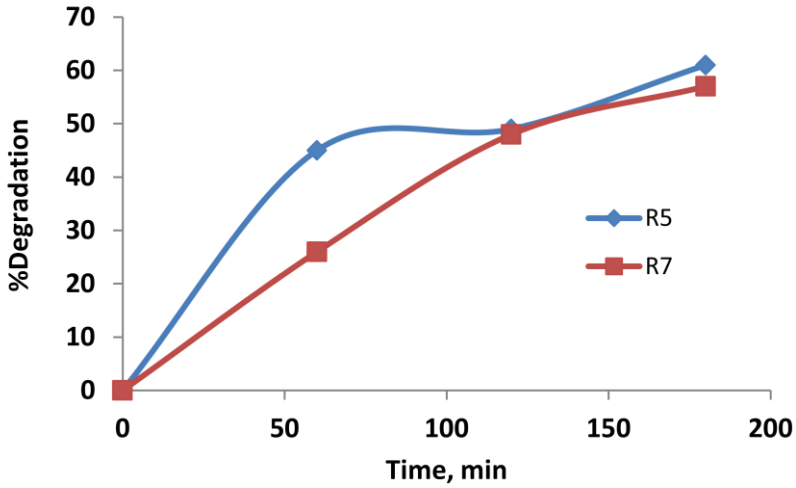

Figure (3-47): Photodegradation yield of EBT at R_5 and R_7 coatings

Figure (3-48) shows the optical microscopic images of the TiO_2 coatings onto stainless steel slides for the three immobilization methods (R, D, S) with different number of layer loadings. Figure (3-48 R_5) presents better coverage and distribution in comparison to R_3 and R_1. Figure (3-48 D_3) indicates that the second coat did not cover the entire surface; therefore, additional coats were needed to complete coverage (see Figure (3-48 D_5)). Swirling coats reveal poor distribution of TiO_2 particles and this is

concerted with the random results appears in Table (3-20). The interesting observation in Figure (3-48 R_7) is the explicit prevailing of TiO_2 aggregates which resembles randomly distributed colonies onto the slide. Hence, this result agrees well with the outputs of Figure (3-47).

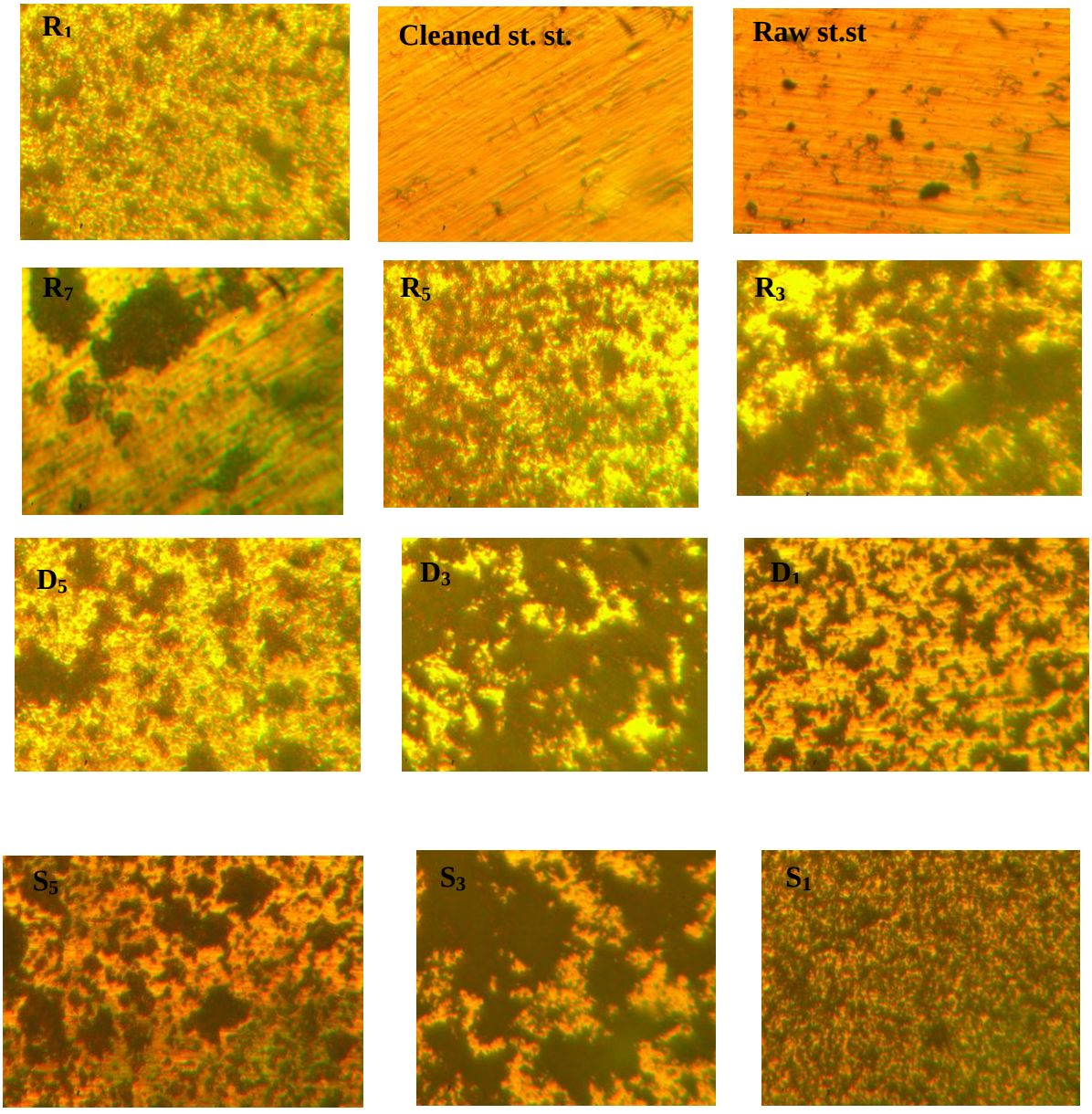

Figure (3-48): Optical microscopic images of the TiO_2 coatings onto stainless steel slides for three methods of immobilization

For further scrutinization, the R_5 coated slide was also employed in the photodegradation of the cationic MV dye under visible illumination. At optimum conditions of MV (pH 7, 4 ppm initial concentration) there was 58 % decrease in the concentration of dye after 3 hrs of visible light illumination, Figure (3-49).

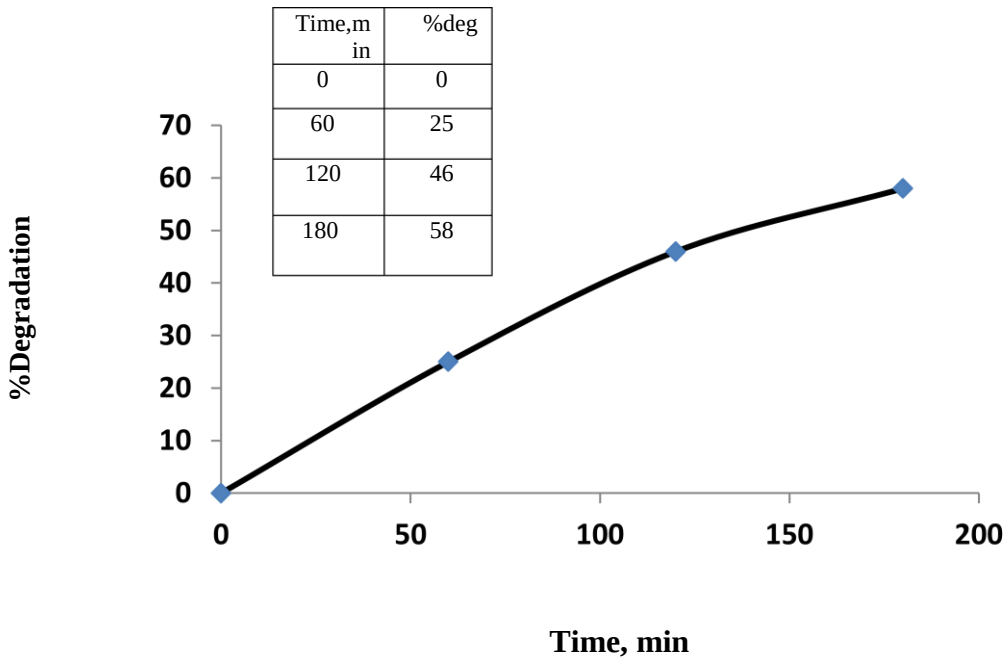

Fig (3-49): Percentage degradation of MV using R_5 immobilized TiO_2

3.10.3 Prototype immobilized TiO_2 assembly

Titanium dioxide generates normally electron–hole pairs and consequently degrades organic moieties only under UV irradiation. Therefore, many efforts have been paid to enhance the photoresponse of TiO_2 to longer wavelengths because UV radiation accounts for 4-7 % energy of the incoming sunlight, while the visible light ($\lambda > 400$ nm) constitutes around 43 % of solar energy [145,46]. In order to leverage the effectiveness of the rotational (R_5) approach, exhibited under visible light

on a laboratory scale, for the photocatalytic degradation of EBT and MV, we escalated the photocatalylsis unit, as shown previously in Figure (2-8), housing a st. st. 316L plate with coating repetitions of 1, 3 and 5 times and oriented in away facing the sun light at angle of 45 degrees. Figure (3-50) shows the optical microscope and photographic images for the one, three and five rotational technique coatings for a stationary phase immobilized TiO_2 onto st. st. plate constituted in the prototype assembly. The photocatalytic degradation process, in a continuous mode, using solar light as an irradiation source, and immobilized TiO_2 as a photocatalyst, has been applied on the photobleaching of EBT and MV using the laboratory built prototype assembly.

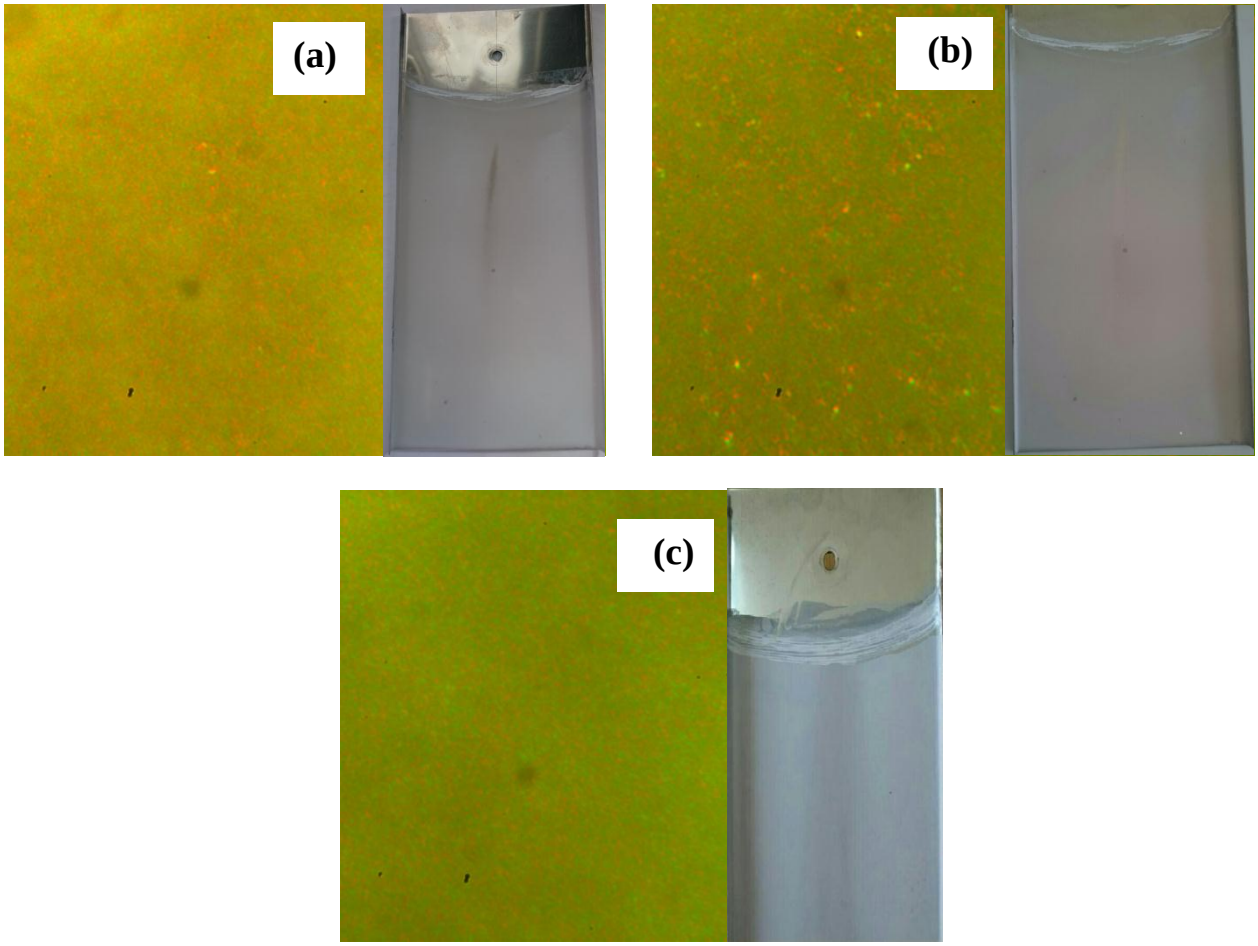

Figure (3-50): Optical microscope images for the TiO_2 film creation onto prototype plate following; (a) one; (b) three; (c) five rotational approach coating repetitions. Insets show the photographs of the coated plate.

Figure (3-51) shows the optical microscope images for the immobilized TiO_2 film onto prototype unit post solar light degradation of EBT and MV. Further, the insets represent the coated plates after continuous solar assisted degradation for each dye. We observe that the amount of stationary TiO_2 which is adherent to stainless steel slides is still persisting after a full photobleaching process.

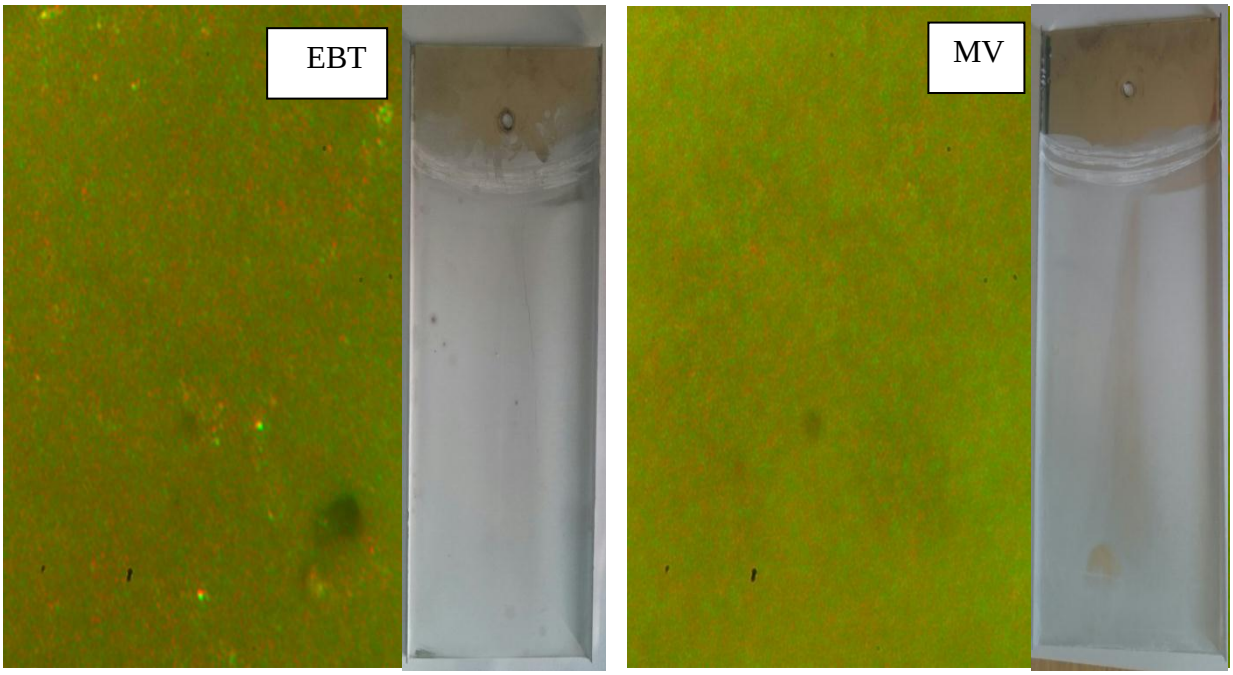

Figure (3-51): Optical microscope images for the immobilized TiO_2 film onto prototype unit post solar light degradation of EBT and MV. Insets represent the coated plates after continuous solar assisted degradation.

It was noticed that 91% and 97% photodegradation was achieved for EBT, MV within 180 and 120 minutes, respectively, as it is obviously presented in Figure (3-52). One of the interesting observations was that the faster degradation rate under sun light irradiation using immobilized TiO_2, in comparison to the pure visible light for laboratory runs, and this

is certainly attributed to the existence of about 5% UV light within the solar light. The higher degradation rates and yields for UV illumination over visible irradiation for the photodecomposition of EBT were also observed in our previous experiments as it is explicitly revealed in Figure (3-53) and Figure (3-54), respectively. Some authors [40,146] reported that the TiO_2 photocatalyst is able to utilize solar light to produce many reactive species, including the powerful and non-selective oxidant hydroxyl radicals, to destroy organic compounds exploiting the following initiation reactions;

$$TiO_2 \xrightarrow{\text{Sunlight}} h^+ + e^- \quad (3.27)$$

$$e^- + O_2 \rightarrow {}^{\cdot}O_2^- \quad (3.28)$$

$$h^+ + {}^-OH \rightarrow {}^{\cdot}OH \quad (3.29)$$

On the other hand, the decolorization of dye through photosensitization process was related to the adsorbability of dye on TiO_2 and the absorbance of dye under solar irradiation. Also Kuo and Ho [146] have stated that in a solar photocatalytic system immobilized with TiO_2 film, both the maximum absorbance wavelength of the dye and the adsorbability of the dye on TiO_2 film play significant roles on the rate and efficiency of color removal of the dye solutions.

Based on our findings and alongside the literature data , we report here that the photocatalytic degradation process using solar light as an irradiation source, and immobilized TiO_2 as a photocatalyst, showed potential application for the decolorization of EBT and MV dyes in aqueous media. In addition, solar light can be used as an alternative irradiation source for photocatalytic systems. However, the reported data

related to decoloring efficiency of dye on TiO_2 film especially with solar irradiation are quite limited [146].

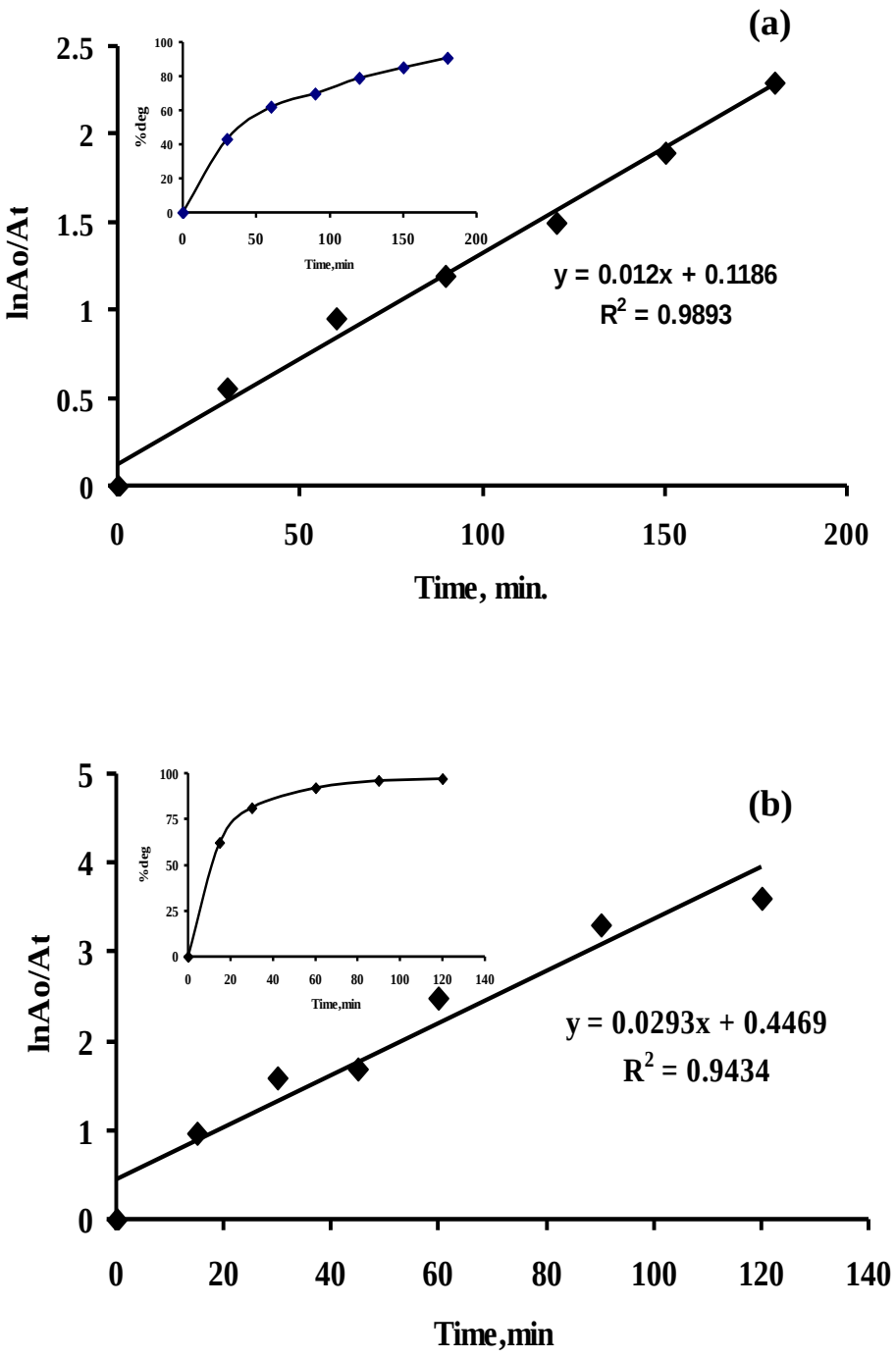

Figure (3-52): Photocatalytic degradation of (a) EBT and (b) MV employing prototype assembly under solar illumination. Insets represent degradation yields versus solar irradiation time.

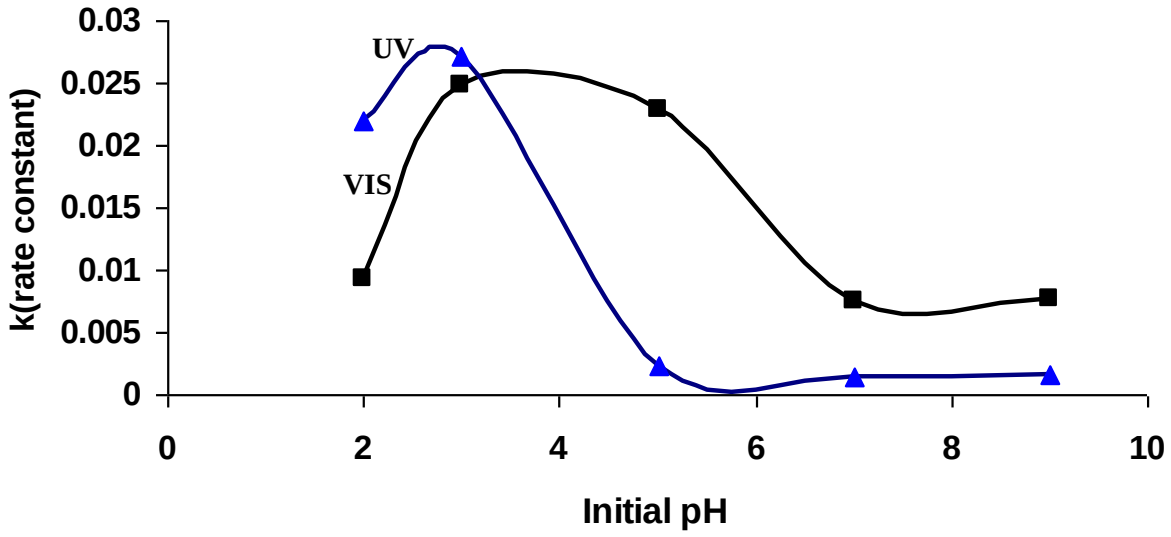

Figure (3-53): Comparison of reaction rates of EBT photodecomposition at different initial pHs under UV and VIS illumination.

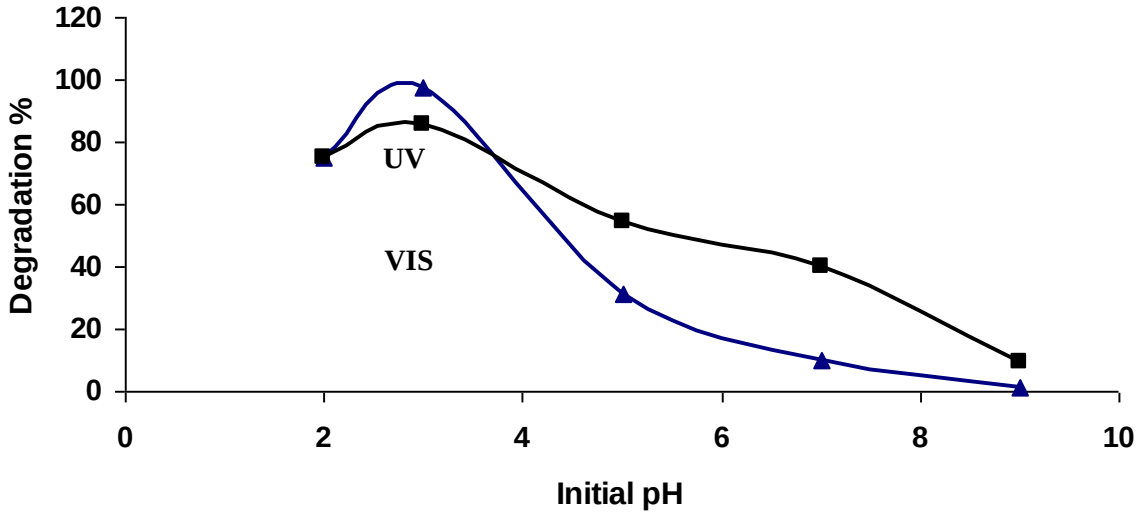

Figure (3-54): Comparison of photodegradation yield of EBT at different initial pHs under UV and VIS illumination.

REFERENCES

References

[1] A. AL-Kdasi, A. Idris, K. Saed, C. T. Guan, "Treatment of textile wastewater by advanced oxidation processes –A review" Global Nest J. 6 (2004) 222-230.

[2] S. Kaur, "Adsorption and photocatalytic degradation of Eriochrome Black-T by TiO_2 of different shapes" M.Sc. thesis School of Chem. and Biochem. Thapar University, July 2013.

[3] A. Biati, S. M. Khezri, A. M. Bidokhti, "Determination of optimum exposure time and pH for dye adsorption using an adsorbent made of sewage sludge" Int. J. Environ. Res. 8 (2014) 653-658.

[4] A. Dixit, A. J. Tirpude, A.K. Mungray, M. Chakraborty, "Degradation of 2, 4 DCP by sequential biological–advanced oxidation process using UASB and UV/TiO_2/H_2O_2" Desalination 272 (2011) 265–269.

[5] A. L. N. Mota, L. F. Albuquerque, L. T. C. Beltrame, O. Chiavone-Filho, A. M. Jr., C. A. O. Nascimento, "Advance oxidation processes and their application the petroleum industry: A review" Bra. J. Pet. Gas.2 (2008) 122-142.

[6] A. A. Hussain, " photocatalytic oxidation of phenolic compounds on nanocrystalline TiO_2 particles" M.Sc. thesis, AL-Nahrain university (2014) pp.1, 27.

[7] M. A. Rauf, S. S. Ashraf, "Radiation induced degradation of dyes- An overview" J. Hazard. Mater. 166 (2009) 6–16.

[8] M. Mohajerani, M. Mehrvar, F. E. Mozaffari, "An over view of the integration of advanced oxidation technologies and other processes for water treatment" Int. J. Eng. 3 (2009) 121-146.

[9] R. Munter, "Advanced oxidation processes-current status and prospects" Proc. Estonian Acad. Sci. Chem. 50 (2001) 59–80.

[10] S. Lathasreea, A. Nageswara Raoa, B. SivaSankarb, V. Sadasivamb, K. Rengaraj, "Heterogeneous photocatalytic mineralisation of phenols in aqueous solutions" J. Mol. Catal. A: Chem. 223 (2004) 101–105.

[11] M. Pelaez, N. T. Nolan, S. C. Pillai, M. K. Seery, P. Falaras, A. G. Kontos, P. S. M. Dunlop, J. W. J. Hamilton, J. A. Byrne, K. O'Shea, M. H. Entezari, D. D. Dionysiou, "A review on the visible light active titanium dioxide photocatalysts for environmental applications" Appl. Catal., B Environ. 125 (2012) 331-349.

[12] W. Y. Teoh, J. A. Scott, R. Amal, "Progress in heterogeneous photocatalysis: from classical radical chemistry to engineering nanomaterials and solar reactors" J. Phys. Chem. Lett. 3 (2012) 629-639.

[13] A. O. Ibhadon, P. Fitzpatrick, "Heterogeneous photocatalysis: recent advances and applications" Catal. 3 (2013) 189-218.

[14] D. I. Kondarides, "Catalysis-photocatalysis" a chapter in "Encyclopedia of life support systems (EOLSS)", UNESCO, 2007.

[15] K. Pirkanniemi, M. Sillanpaa, "Heterogeneous water phase catalysis as an environmental application: a review" Chemosphere 48 (2002) 1047–1060.

[16] R. A. Al-Rasheed, saline water conversion cooperation acquired experience symposium, Jeddah, Saudi Arabia, 2005.

[17] R. G. Saratale, G. D. Saratale, J.S. Chang, S.P. Govindwar, "Bacterial decolorization and degradation of azo dyes: A review" J. Taiwan Inst. Chem. Eng. 42 (2011) 138–157.

[18] G. Z. Kyzas, J. Fu, K. A. Matis, "The change from past to future for adsorbent materials in treatment of dyeing wastewaters" Materials 6 (2013) 5131-5158.

[19] B. Janveja, K. Kant, J. Sharma, "A study of activated rice husk charcoal as an adsorpent of congo red dye present in textile industrial waste" J. Punjab Acad. Foren. Medic. Toxicol. 8 (2008) 12-15.

[20] M. Günay, " Dyeing Process and Environmental Impact" a chapter in "Eco-Friendly Textile Dyeing and Finishing" Brazil 2013.

[21] Ch. S. Keng, Z. Zainal, A. H. Abdullah, "Removal of cationic and anionic dye by immobilized titanium dioxide loaded activated carbon" Malaysian J. Anal. Sci. 12 (2008) 451-457.

[22] G. Sumbali, R. S. Mehrotra, "Microscopy and staining" a chapter in "Principles of Microbiology" New delhi (2009).

[23] Z. Sun, Y. Chena, Q. Ke, Y. Yanga, J. Yuan, "Photocatalytic degradation of cationic azo dye by TiO_2/bentonite nanocomposite" J. Photochem. Photobiol. A: chem. 149 (2002) 169–174.

[24] S. T. Ramesh, R. Gandhima, T. E. Elavarasi, K. Sowmya, P. V. Nidheesh, "Comparison of methylene blue adsorption from aqueous solution using spent tea dust and raw coir pith" Global Nest J. 16 (2014) 146-159.

[25] H. S. Hilal, L. Z. Majjad, N. Zaatar, A. El-Hamouz, "Dye-effect in TiO_2 catalyzed contaminant photo-degradation: Sensitization vs. charge-transfer formalism" Solid State Sciences 9 (2007) 9-15.

[26] B. Basheer, D. Mathew, B. K. George, C. P. R. Nair, "An overview on the spectrum of sensitizers:The heart of dye sensitized solar cells" Sol. Energy 108 (2014) 479-507.

[27] S. Kohtani , A. Kudo, T. Sakata, "Spectral sensitization of a TiO_2 semiconductor electrode by CdS microcrystals and its photoelectrochemical properties" Chem. Phys. Lett. 206 (1993) 166-170.

[28] J. F. G. Gómez, P. E. Martínez, N. Pérez, M. V. Rodríguez, L. H. Reyes, A. H. Ramírez, "Sensitization of TiO_2 with novel Cu(II) and Ni(II)

polyaza complexes: evaluation of its photocatalytic activity" Ceram. Int. 40 (2014) 14207-14214.

[29] J. Grzechulska, A. W. Morawski, "Photocatalytic decomposition of azo-dye acid black 1 in water over modified titanium dioxide" Appl. Catal., B: Environ. 36 (2002) 45-51.

[30] H. Park, Y. Park, W. Kim, W. Choi, "Surface modification of TiO_2 photocatalyst for environmental applications" J. Photochem. Photobiol., C: Photochem. 15 (2012) 1-20.

[31] D. Pei, J. Luan, "Development of visible light-responsive sensitized photocatalysts" Int. J. of Photoenergy (2012) 1-13.

[32] D. Chatterjee , Sh. Dasgupta, "Visible light induced photocatalytic degradation of organic pollutants" J. Photochem. Photobiol.,C: Photochem. 6 (2005) 186–205.

[33] G. Calzaferri, W. Spahni, "Self-sensitization of photo-chlorine evolution in aqueous dispersions of silver zeolites" J. Photochem. 32 (1986) 151–155.

[34] C. Nasr, K. Vinodgopal, S. Hotchandani, A. K. Chattopadhyay, P. V. Kamat, "Excited states and reduced and oxidized forms of a textile diazo dye, naphthol blue black. Spectral characterization using laser flash photolysis and pulse radiolysis studies" Radiat. Phys. Chem. 49 (1997) 159-166.

[35] Ch. Bauer, P. Jacques, A. Kalt, "Photooxidation of an azo dye induced by visible light incident on the surface of TiO_2" J. Photochem. Photobiol., A: Chem. 140 (2001) 87–92.

[36] K. Nagaveni, G. Sivalingam, M.S. Hegde, Giridhar Madras, "Solar photocatalytic degradation of dyes: high activity of combustion synthesized nano TiO_2" Appl. Catal., B: Environ. 48 (2004) 83–93.

[37] Ch. Gadiyar, B. Boruah, C. Mascarenhas, V. Shetty K, "Immobilized nano TiO2 for photocatalysis of acid yellow-17 dye in fluidized bed reactor" Int. J. Current Eng. Technol. Sept ISSN 2277 – 4106 (2013) 1-4.

[38] J. Kumar, A. Bansal, "Immobilization of nanoparticles of titanium dioxide for photocatalytic degradation" (Proc. of the Intl. Conf. on Future Trends in Structural, Civil, Environmental and Mechanical Engineering -- FTSCEM 2013).

[39] M. Fathinia, A.R. Khataee, M. Zarei, S. Aber, "Comparative photocatalytic degradation of two dyes on immobilized TiO_2 nanoparticles: Effect of dye molecular structure and response surface approach" J. Mol. Catal. A: Chem. 333 (2010) 73–84.

[40] D. Mukherjee, Sh. Barghi, A. K. Ray, "Preparation and characterization of the TiO_2 immobilized polymeric photocatalyst for degradation of aspirin under UV and solar light" Processes 2 (2014) 12-23.

[41] T. Kanki, Sh. Hamasaki, N. Sano, A. Toyoda, K. Hirano, "Water purification in a fluidized bed photocatalytic reactor using TiO_2-coated ceramic particles" Chem. Eng. J. 108 (2005) 155–160.

[42] S. Mozia, P. B.˙zek, J. P. orski, B. Tryba, A. W. Morawski, "Immobilized TiO_2 for phenol degradation in a pilot-scale photocatalytic reactor" Journal of Nanomaterials 16 (2012) 1-10.

[43] M. A. Lazar, Sh. Varghese, S. S. Nair, "Photocatalytic water treatment by titanium dioxide: recent updates" Catalysts 2 (2012) 572-601.

[44] S. Matsuzawa, C. Maneerat, Y. Hayata, T. Hirakawa, N. Negishi, T. Sano, "Immobilization of TiO_2 nanoparticles on polymeric substrates by using electrostatic interaction in the aqueous phase" Appl.Catal., B: Environ. 83 (2008) 39–45.

[45] A. Y. Shan, T. I. M. Ghazi, S. A. Rashid, "Immobilisation of titanium dioxide onto supporting materials in heterogeneous photocatalysis: A review" Appl. Catal., A: General 389 (2010) 1–8.

[46] A. S. El-Kalliny, S. F. Ahmed, L. C. Rietveld, P. W. Appel, "Immobilized photocatalyst on stainless steel woven meshes assuring efficient light distribution in a solar reactor" Drink. Water Eng. Sci. 7 (2014) 41–52.

[47] E. N. Oguegbulu, J. Okumiahor, "Evaluation of the adsorption isotherm of activated charcoal used in pharmaceutical medicine from some Nigerian plant parts, corn cobs, the wooden parts of mangifera indica and azandirachta indica" Advancement in Medicinal Plant Research 1 (2013) 72-76.

[48] G. Pandhare, S. D. Dawande, " Neem leaves powder as a low-cost adsorbent and ITS characteristics" Int. J. Advanc. Eng. Technol. 4 (2013) 61-62.

[49] C. H. Giles, T. H. Macewans, N. Nakhwa, D. Smith, "A system of classication of solution adsorption isotherms, and its use in diagnosis of adsorption mechanisms and in measurement of specific surface areas of solids" J. Chem. Soc. (1960) 3973-3993.

[50] M. Králik, "Adsorption, chemisorption, and catalysis, review" J. Chem. 68 (2014) 1625–1638.

[51] P. A. Webb, "Introduction to chemical adsorption analytical techniques and their applications to catalysis" MIC Technical Publications January (2003).

[52] M. T. Yagub, T. K. Sen, SH. Afroze, H.M. Ang, "Dye and its removal from aqueous solution by adsorption: A review" Adv. Colloid Interface Sci. 209 (2014) 172–184.

[53] L. Al-Khatib, F. Fraige, M. Al-Hwaiti, O. Al-Khashman, "Adsorption from aqueous solution onto acid activated bentonite" Am. J. Environ. Sci. 8 (2012) 510-522**.**

[54] Sh. Rasalingam, R. Peng, R. T. Koodali, "An insight into the adsorption and photocatalytic degradation of rhodamine B in periodic mesoporous materials" Appl. Catal., B: Environ. 174 (2015) 49–59.

[55] E. Longhinotti, F. Pozza, L. Furlan, M. de N. de M. Sanchez, M. Klug, M. C.M. Laranjeira, V. T. Fávere, "Adsorption of anionic dyes on the biopolymer chitin" J. Braz. Chem. Soc. 9 (1998) 435-440.

[56] P. N. Dave, S. Kaur, E. Khosla, "Removal of Eriochrom Black T by adsorption on to eucalyptus bark using green technology" Indian J. Chem. Technol. 18 (2011) 53-60

[57] J. Shu, Z. Wang, Y. Huang, N. Huang, C. Ren, W. Zhang, "Adsorption removal of congo red from aqueous solution by polyhedral Cu_2O nanoparticles: kinetics, isotherms, thermodynamics and mechanism analysis" J. Alloys Compd. 633 (2015) 338–346.

[58] R. Ansari, Z. Mosayebzadeh, M. B. keivani, A. M. khah, "Adsorption of cationic dyes from aqueous solutions using polyaniline conducting polymer as a novel adsorbent" J. Adv. Sci. Res 2 (2011) 27-34.

[59] J. H. Chen, X. Sun, W. Weng, H. X. Guo, S. R. Hu, Y. S.He, F. M. Li, W. B. Wu, "Recovery and investigation of Cu(II) ions by tannin immobilized porous membrane adsorbent from aqueous solution" Chem. Eng. J. 273 (2015) 19–27.

[60] C. G. Hatchard, C. A. Parker, "A new sensitive chemical actinometer. II. potassium ferrioxalate as a standard chemical actinometer" Math. Phys. Sci. 235 (1956) 518-536.

[61] H. M. Hadi, " Photocatalysis of azo compounds on doped titanium dioxide" M.Sc. thesis, AL-Nahrain university (2015) pp. 38.

[62] J. Jiu, S. Isoda, M. Adachi, F. Wang, "Preparation of TiO_2 nanocrystalline with 3–5 nm and application for dye-sensitized solar cell", J. Photochem. Photobiol., A: Chem. 189 (2007) 314–321.

[63] G. Mamba, X.Y. Mbianda, A.K. Mishra, "Enhanced visible light photocatalytic degradation of Eriochrome Black T and eosin blue shade in water using tridoped titania decorated on SWCNTs and MWCNTs: Effect of the type of carbon nanotube Incorporated" Mat. Chem. Phy. 149-150 (2015) 734-742.

[64] O. Thomas, C. Burgess, "The Basics of spectrophotometric measurement " a chapter in " UV-Visible spectrophotometry of water and wastewater", Sherbrooke 2007.

[65] **S. Samira, A. Raja P, M. C, J. M. Modak, "**Photocatalytic degradation of crystal violet (C.I. basic violet 3) on nano TiO_2 Containing anatase and rutile phases (3:1)" J. Thermodynam Cat. 3 (2012) 1-6.

[66]http://www.flinnsci.com/media/1030075/cf_7644s_kinetics_of_crystal_violet_fading-r.pdf

[67] O. Carp, C.L. Huisman, A. Reller, "Photoinduced reactivity of Titanium dioxide" Prog. Solid State Chem. 32 (2004) 33–177.

[68] J. C. Yu, L. Zhang, W. Ho, "Enhancing effects of water content and ultrasonic irradiation on the photocatalytic activity of nano-sized TiO2 powders", J. photochem. Photobiol. A: Chem. 148 (2002) 263-271.

[69] M. E. Preethi, J. A. Priya, S. Thiriveni, "Solar light driven degradation of eriochrome black T by photocatalysis" J. Appl. Chem. 8 (2015) 55-62.

[70] S. Parra, J. Olivero, C. Pulgarin, "Relationships between physicochemical properties and photoreactivity of four biorecalcitrant phenylurea herbicides in aqueous TiO2 suspension" Appl. Catal. B: Environ. 36 (2002) 75–85.

[71] B. Neppolian, H. C. Choi, S. Sakthivel, B. Arabindoo, V. Murugesan, "Solar light induced and TiO_2 assisted degradation of textile dye reactive blue 4" Chemo. 46 (2002) 1173–1181.

[72] F. Moeinpour, A. Alimoradi, M. Kazemi "Efficient removal of Eriochrome Black-T from aqueous solution using $NiFe_2O_4$ magnetic nanoparticles" J. Environ. Health Sci. Eng. 12 (2014)112-118.

[73] B. K. Nandi, A. Goswami, M. K. Purkait "Removal of cationic dyes from aqueous solutions by kaolin: Kinetic and equilibrium studies" Appl. Clay Sci. 42 (2009) 583–590.

[74] R. Sivaraj, C. Namasivayam, K. Kadirvelu, "Orange peel as an adsorbent in the removal of acid violet 17 (acid dye) from aqueous solutions" Waste Manag. 21 (2001) 105-110.

[75] M. D. G. de Luna, E. D. Flores, D. A. D. Genuino , C. M. Futalan , M.W. Wan "Adsorption of Eriochrome Black T (EBT) dye using activated carbon prepared from waste rice hulls—Optimization, isotherm and kinetic studies" J. Taiwan Inst. Chem. Eng. 44 (2013) 646–653.

[76] K. Dong, F. Qiu, X. Guo, J. Xu, D. Yang, K. He "Adsorption behavior of azo dye Eriochrome Black T from aqueous solution by β-cyclodextrins/polyurethane foam material" Polymer-Plastics Technol. Eng. 52 (2013) 452–460.

[77] D. Ma, J. Zhang, J. Bai, H. Zhang, "Thermodynamic characteristics of adsorption-desorption of methane in 3# coal seam of sihe" Natur. Res. 5 (2014) 782-794.

[78] G. S. Dawood "Removal Orange (G) dye from aqueous solution by adsorption on Bentonite" Tikrit J. Pure Sci. 15 (2010) 231-235.

[79] A.S. Kovo, S.C. Olu, E.S. Gwatana " Adsorption of Chromium (IV) by a low cost adsorbent prepared from neem leaves" Iranica J. Energy Environ. 5 (2014) 277-286.

[80] M. Alkan, O. Demirbas, M. Dogan "Adsorption kinetics and thermodynamics of an anionic dye onto sepiolite"; Micropor. Mesopor. Mater. 101 (2007) 388–396.

[81] A. A. Ahmad, B. H. Hameed, N. Aziz "Adsorption of direct dye on palm ash: Kinetic and equilibrium modeling"; J. Hazard. Mater. 141 (2007) 70–76.

[82] S. Azizian "Kinetic models of sorption: a theoretical analysis" J. Coll. Int. Sci. 276 (2004) 47–52.

[83] A. Srinivasan, T. Viraraghavan "Decolorization of dye wastewaters biosorbents: A review" J. Environ. Manag. 91 (2010)1915-1929.

[84] M. A. Mahmoud "Removal of uranium (VI) from aqueous solution using low cost and eco-friendly adsorbents" J. Chem. Eng. Process Technol. 4 (2013) 1-4.

[85] M. A. Rauf, M. A. Meetani, S. Hisaindee, "An overview on the photocatalytic degradation of azo dyes in the presence of TiO_2 doped with selective transition metals" Desalination 276 (2011) 13–27.

[86] M. Montazerozohori, S. M. Jahromi, " Photocatalytic decolorization of ethyl orange at various buffer solutions using nano-titanium dioxide: a kinetic investigation" Desalination and Water Treat. 48 (2012) 261–266.

[87] A. Mills, S. Le Hunte, "An overview of semiconductor photocatalysis" J. Photochem. Photobiol., A: Chem. 108 (1997) 1-35.

[88] I. K. Konstantinou, T. A. Albanis, "TiO_2-assisted photocatalytic degradation of azo dyes in aqueous solution: kinetic and mechanistic investigations A review" Appl. Catal., B: Environ. 49 (2004) 1–14.

[89] M. F. Abid, A. A. Abdul-Rahman, N. H. Hamza, "Removal of Methyl Violet Dye from Synthetic Wastewater Using a Hybrid Detoxification Process" J. Eng. Technol. 32 (2014) 1544-1561.

[90] S. Senthilkumaar, K. Porkodi, "Heterogeneous photocatalytic decomposition of Crystal Violet in UV-illuminated sol–gel derived nanocrystalline TiO_2 suspensions" J. Colloid Interface Sci. 288 (2005) 184–189.

[91] O. Bibak, M. Aliabadi, "Photocatalytic degradation of malachite green in aqueous solution using TiO2 nanocatalyst" J. Biodiversity Environ. Sci. 5 (2014) 301-310.

[92] M. Shamsipur, H. R. Rajabi, "Study of photocatalytic activity of ZnS quantum dots as efficient nanoparticles for removal of methyl violet: Effect of ferric ion doping" Spectrochim. Acta, Part A: Mol. Biomol. Spectrosc. 122 (2014) 260–267.

[93] K. H. Wang, Y. H. Hsieh, L. J. Chen,"The heterogeneous photocatalytic degradation, intermediates and mineralization for the aqueous solution of cresols and nitrophenols", J. Hazar. Mater. 59 (1998) 251-260.

[94] http://en.wikipedia.org/wiki/Methyl_Violet#cite_note-4.

[95] J. Wang, T. Ma, Z. Zhang, X. Zhang, Y. Jiang, Z. Pan, F. Wen, P. Kang, P. Zhang, "Investigation on the sonocatalytic degradation of methyl orange in the presence of nanometer anatase and rutile TiO_2 powders and comparison of their sonocatalytic activities" Desalination 195 (2006) 294–305.

[96] A. K. Mohammed, K. T. Mckenzie, "Photocatalytic degradation of

Chicago sky blue 6B and Benzopurpurin 4B using titanium dioxide thin film" J. Environ. Sci. 17 (2005) 869-872.

[97] M. Stylidi, D. I. Kondarides, X. E. Verykios, "Pathways of solar light-induced photocatalytic degradation of azo dyes in aqueous TiO2 suspensions" Appl. Catal., B: Environ. 40 (2003) 271–286.

[98] M. R. Hoffmann, S. T. Martin, W. Choi, D. W. Bahnemann, "Environmental applications of semiconductor photocatalysis" Chem. Rev. 95 (1995) 69-96.

[99] J. Suna, L. Qiao, S. Sun, G. Wang, "Photocatalytic degradation of Orange G on nitrogen-doped TiO2 catalysts under visible light and sunlight irradiation" J. Hazard. Mater. 155 (2008) 312–319.

[100] N. Guetta, H. A. Amar, "Photocatalytic oxidation of methyl orange in presence of titanium dioxide in aqueous suspension. Part I: Parametric study" Desalination 185 (2005) 427–437.

[101] S. Yang, Y. Xu, Y. Huang, G. Zhou, Z. Yang, Y. Yang, G. Wang, "Photocatalytic degradation of methyl violet with $TiSiW_{12}O_{40}$/TiO2" Int. J. Photoenergy ID 191340 (2013) 1-5.

[102] S. Lakshmi, R. Renganathan, S. Fujita, "Study on TiO_2-mediated photocatalytic degradation of methylene Blue" J. Photochem. Photobiol., A: Chem. 88 (1995) 163-167.

[103] F. Sabin, Th. Tiirk, A. Vogler, "Photo-oxidation of organic compounds in the presence of titanium dioxide: determination of the efficiency" J. Photochem. PhofobioL A: Chem., 63 (1992) 99-106.

[104] J. Saien, A. R. Soleymani, "Degradation and mineralization of Direct Blue 71 in a circulating upflow reactor by UV/TiO2 process and employing a new method in kinetic study" J. Hazard. Mater. 144 (2007) 506–512.

[105] M. Nikazar, K. Gholivand, K. Mahanpoor, "Photocatalytic

degradation of azo dye Acid Red 114 in water with TiO2 supported on clinoptilolite as a catalyst" Desalination 219 (2008) 293–300.

[106] U. I. Gayaa, A. H. Abdullah, "Heterogeneous photocatalytic degradation of organic contaminants over titanium dioxide: A review of fundamentals, progress and problems" J. Photochem. Photobiol., C: Photochem. Reviews 9 (2008) 1–12.

[107] R.C. Meena, R. B. Pachwarya, V. K. Meena, S. Arya, "Degradation of textile dyes ponceau-s and sudan iv using recently developed photocatalyst, immobilized resin dowex-11" Am. J. Environ. Sci. 5 (2009) 444-450.

[108] S. Munesh, R. C. Meena, "Photocatalytic degradation of textile dye through an alternative photocatalyst methylene blue immobilized resin dowex 11 in presence of solar light " Archives Appl. Sci. Research, 4 (1): (2012) 472-479.

[109] J. Q. Chen, D. Wang, M. X Zhu, C. J. Gao, "Photocatalytic degradation of dimethoate using nanosized TiO_2 powder" Desalination 207 (2007) 87–94.

[110] E. M. Saggioro, A. S. Oliveira, T. Pavesi, C. G. Maia, L. F. V. Ferreira, J. C. Moreira, "Use of titanium dioxide photocatalysis on the remediation of model textile wastewaters containing azo dyes" Molecul. 16 (2011) 10370-10386.

[111] C. Mathivathana, V. Balasubramanian, K. Pandian, "The influence of the oxidizing agents on the rates of degradation of Rose bengal using Titanium oxide nanoparticles" Elixir Dye Chem. 56 (2013) 13510-13518.

[112] M. V. Shankar, B. Neppolian, S. Sakthivel, B. Arabindoo, M. Palanichamy, V. Murugesan, "Kinetics of photocatalytic degradation of textile dye reactive red 2" Ind. J. Eng. Mater. Sci. 8 (2001) 104-109.

[113] T. Cordero, C. Duchamp, J. M. Chovelon, C. Ferronato, J. Matos,

"Influence of L-type activated carbons on photocatalytic activity of TiO2 in 4-chlorophenol photodegradation" J. Photochem. Photobiol., A: Chem. 191 (2007) 122–131.

[114] M. S. T. Gonqalves, A. M. F.O. Campos, E. M. M. S. Pinto, P. M. S. Plasncia, M. J. R. P. Queiroz, "Photochemical treatment of solution of azo dyes containing TiO_2" Chemosphere 39 (1999) 781-786.

[115] R. S. Juang, S. H. Lin, P. Y. Hsueh, "Removal of binary azo dyes from water by UV-irradiated degradation in TiO_2 suspensions" J. Hazard. Mater.182 (2010) 820–826.

[116] D. Chen, A. K. Ray, "Photodegradation kinetics of 4- nitrophenol in TiO_2 suspension" Wat. Res. 32 (1998) 3223-3234.

[117] Y. Liu, X. Chen, J. Li, C. Burda, "Photocatalytic degradation of azo dyes by nitrogen-doped TiO_2 nanocatalysts" Chemosphere 61 (2005) 11–18.

[118] R. Molinari, F. Pirillo, M. Falco, V. Loddo, L. Palmisano, "Photocatalytic degradation of dyes by using a membrane reactor" Chem. Eng. Proc. 43 (2004) 1103–1114.

[119] A. Bianco-Prevot, C. Baiocchi, M. C. Brussino, E. Pramauro, P. Savarino, V. Augugliaro, G. Marci, L. Palmisano, "Photocatalytic degradation of acid blue 80 in aqueous solutions containing TiO_2 suspensions", Environ. Sci. Technol. 35 (2001) 971-976.

[120] S. Khezrianjoo, H. Revanasiddappa "Langmuir-hinshelwood kinetic expression for the photocatalytic degradation of metanil yellow aqueous solutions by ZnO catalyst" Chem. Sci. J. Vol. 2012: CSJ-85.

[121] H. S.Wahab, A. D. Koutselos "Computational modeling of the adsorption and ˙OH initiated photochemical and photocatalytic primary oxidation of nitrobenzene" J. Molec. Model. 15 (2009) 1237.

[122] J. C. Colmenares, R. Luque, J. M. Campelo, F. Colmenares, Z.

Karpiński, A. A. Romero, "Nanostructured photocatalysts and their applications in the photocatalytic transformation of lignocellulosic biomass: an overview" Mater. 2 (2009) 2228-2258.

[123] D. M. Fouad, M. B. Mohamed "Comparative study of the photocatalytic activity of semiconductor nanostructures and their hybrid metal nanocomposites on the photodegradation of malathion" J. Nanomater. Article ID 524123 (2012) 1-8.

[124] M. Ksibi, A. Zemzemi, R. Boukchina, "Photocatalytic degradability of substituted phenols over UV irradiated TiO_2" J. Photochem. Photobiol. A: Chemistry 159 (2003) 61-70.

[125] K. Naeem, P. Weiqian, F. Ouyang, "Thermodynamic parameters of activation for photodegradation of phenolics" Chem. Eng. J. 156 (2010) 505-509.

[126] F. Barbieri, D. Cauzzi, F. De Smet, M. Devillers, P. Moggi, G. Predieri, P. Ruiz, "Mixed-oxide catalysts involving V, Nb and Si obtained by a non-hydrolytic sol–gel route: preparation and catalytic behaviour in oxydative dehydrogenation of propane" Catal. Today 61 (2000) 353–360.

[127] T. Lonhienne, C. Gerday, G.Feller, "Psychrophilic enzymes: revisiting the thermodynamic parameters of activation may explain local fexibility" Biochim. Biophys. Acta 1543 (2000) 1-10.

[128] S. Zhu, X. Yang, W. Yang, L. Zhang, J. Wang, M. Huo, "Application of porous nickel-coated TiO_2 for the photocatalytic degradation of aqueous quinoline in an internal airlift loop reactor" Int. J. Environ. Res. Public Health 9 (2012) 548-563.

[129] A. F. Alkaima, T. A. Kandielc, F. H. Hussein, R. Dillert, D. W. Bahnemanna, "Solvent-free hydrothermal synthesis of anatase TiO_2 nanoparticles with enhanced photocatalytic hydrogen production activity" Appl. Catal. A: General 466 (2013) 32– 37.

[130] S. Malato, P. F. Ibanez, M.I. Maldonado, J. Blanco, W. Gernjak, "Decontamination and disinfection of water by solar photocatalysis: Recent overview and trends" Catal. Today 147 (2009) 1-59.

[131] P. T. Tanev, L. T. Vlaev, "An attempt at a more precise evaluation of the approach to mesopore size distribution calculation depending on the degree of pore blocking" J. Col. Int. Sci. 160 (1993) 110-116.

[132] O. P. Panwar, A. Kumar, M. Paliwal, R. Ameta, S. C. Ameta, "Use of zirconium phosphate as photocatalyst in photobleaching of some dyes" Bull. Catal. Soc. 7 (2008) 105-110.

[133] H. S. Wahab, "Molecular modeling of the adsorption and initial photocatalytic oxidation step for para-nitrophenol on nano-sized TiO_2 surface" Surf. Sci. 206 (2012) 624-633.

[134] H. S. Wahab, A. D. Koutselos "A computational study on the adsorption and $^{\cdot}OH$ initiated photochemical and photocatalytic primary oxidation of aniline" Chem. Phys. 238 (2009) 171-176.

[135] S. A. Abo-Farha "Photocatalytic degradation of monoazo and diazo dyes in wastewater on nanometer-sized TiO_2" Researcher 2 (2010) 1-20.

[136] T. Wu, X. Zhou, H. Zhang, X. Zhong, "Bi2S3 nanostructures: a new photocatalyst" Nano Res 3 (2010) 379-386.

[137] S. E. A. Sharaf El-Deen, Fu-Shen Zhang, "Immobilisation of TiO2-nanoparticles on sewage sludge and their adsorption for cadmium removal from aqueous solutions" J. Experiment. Nanosc. (2015) 1-20.

[138] A. H. Amar, "Development of a simple dip coating method for immobilization of TiO_2 onto solid supports using direct TiO_2 powder" M.Sc. thesis, University Sains Malaysia (2007) p14.

[139] Y. Chen, D. D. Dionysiou, " TiO_2 photocatalytic films on stainless steel: The role of Degussa P-25 in modified sol–gel methods" Appl.

Catal. B: Environ. 62 (2006) 255–264.

[140] J. Lin, Y. Liu, S. Chen, X. Le, X. Zhou, Z. Zhao, Y. Ou, J. Yang, " Reversible immobilization of laccase onto metal-ion-chelatedmagnetic microspheres for bisphenol A removal" Inter. J. Biol. Macromolecul. 84 (2016) 189–199.

[141] J. Xu, L. Li, Y. Yan, H. Wang, X. Wang, X. Fu, Guangshe Li, " Synthesis and photoluminescence of well-dispersible anatase TiO2 nanoparticles" J. Colloid Interface Sci.318 (2008) 29–34.

[142] L. Y. Cherif, I. Yahiaoui, F. Aissani-Benissad, K. Madi, N. Benmehdi, F. Fourcade, A. Amrane, "Heat attachment method for the immobilization of TiO2 on glass plates: application to photodegradation of basic yellow dye and optimization of operating parameters, using response surface methodology" Ind. Eng. Chem. Res. 53 (2014) 3813−3819.

[143] L. Hu, G. Zeng, G. Chen, H. Dong, Y. Liu, J. Wan, A. Chen, Z. Guo, M. Yan, H. Wu, Z. Yu, "Treatment of landfill leachate using immobilized Phanerochaete chrysosporium loaded with nitrogen-doped TiO_2nanoparticles" J. Hazard. Mater. 301 (2016) 106–118.

[144] D. Feng, Sh. Xu, G. Liu, "Application of immobilized TiO_2 photocatalysis to improve the inactivation of Heterosigma akashiwo in ballast water by intense pulsed light" Chemosphere 125 (2015) 102–107.

[145] A. T. Miah, B. Malakar, P. Saskia, "Gold over ceria–titania mixed oxides: solar light induced catalytic activity for nitrophenol reduction, DOI 10.1007/s10562-015-1644-y" Catal. Lett. (2015) 1-13.

[146] W. S. Kuo, P. H. Ho, "Solar photocatalytic decolorization of dyes in solution with TiO2 film" Dyes Pigmen. 71 (2006) 212-217.

جمهورية العراق
وزارة التعليم العالي والبحث العلمي
جامعة النهرين
كلية العلوم
قسم الكيمياء

التحطيم الضوئي للصبغات الملوثة بأستخدام ثنائي اوكسيد التيتانيوم النانوي المثبت كعامل مساعد

رسالة

مقدمة الى كلية العلوم / جامعة النهـرين

كجزء من متطلبات نيل شهادة الماجستيرفي علوم الكيمياء

من قبل

اسراء نـهاد اسماعيل

بكالوريوس كيمياء 2013

باشراف

الاستاذ الدكتور

هــلال شهاب وهــاب

رجب **1437**

نيسان **2016**